Edited by Philip Garrou,
Christopher Bower and Peter Ramm

WILEY-VCH

Handbook of 3D Integration

Technology and Applications of 3D Integrated Circuits

Volume 1

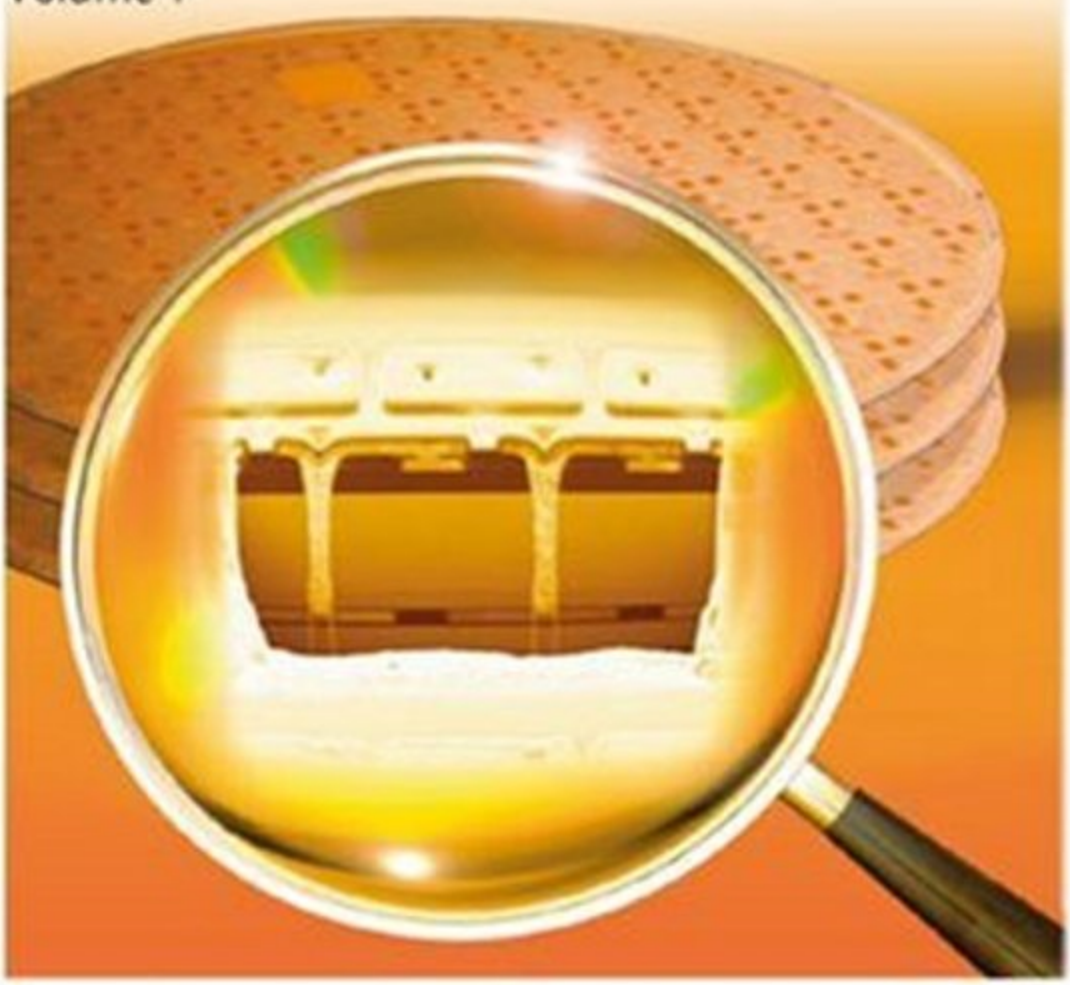

SINGLE CARRIER FDMA

Single Carrier FDMA: A New Air Interface for Long Term Evolution Hyung G. Myung and David J. Goodman
 ISBN: 978-0-470-72449-1

Wiley Series on Wireless Communications and Mobile Computing

Series Editors: Dr Xuemin (Sherman) Shen, *University of Waterloo, Canada*
Dr Yi Pan, *Georgia State University, USA*

The 'Wiley Series on Wireless Communications and Mobile Computing' is a series of comprehensive, practical and timely books on wireless communication and network systems. The series focuses on topics ranging from wireless communication and coding theory to wireless applications and pervasive computing. The books offer engineers and other technical professional, researchers, educators, and advanced students in these fields invaluable insight into the latest developments and cutting-edge research.

Other titles in this series

Mišić and Mišić: *Wireless Personal Area Networks: Performance, Interconnections and Security with IEEE 802.15.4,* January 2008 987-0-470-51847-2

Takagi and Walke: *Spectrum Requirement Planning in Wireless Communications: Model and Methodology for IMT-Advanced,* April 2008 987-0-470-98647-9

Pérez-Fontán and Mariño Espiñeira: *Modeling the Wireless Propagation Channel: A Simulation Approach with MATLAB®,* August 2008 987-0-470-72785-0

Ippolito: *Satellite Communications Systems Engineering: Atmospheric Effects, Satellite Link Design and System Performance,* September 2008 978-0-470-72527-6

Lin and Sou: *Charging for Mobile All-IP Telecommunications,* September 2008 987-0-470-77565-3

Hart, Tao, Zhou: *IEEE 802.16j Multi-hop Relay,* March 2009 978-0-470-99399-6

Qian, Muller, Chen: *Security in Wireless Networks and Systems,* May 2009 978-0-470-51212-8

Wang, Kondi, Luthra, Ci: *4G Wireless Video Communications,* May 2009 978-0-470-77307-9

Shen, Cai, Mark: *Multimedia for Wireless Internet — Modeling and Analysis,* May 2009 978-0-470-77065-8

Stojmenovic: *Wireless Sensor and Actuator Networks: Algorithms and Protocols for Scalable Coordination and Data Communication,* August 2009 978-0-470-17082-3

SINGLE CARRIER FDMA

A NEW AIR INTERFACE FOR LONG TERM EVOLUTION

Hyung G. Myung

Qualcomm/Flarion Technologies, USA

David J. Goodman

Polytechnic University, USA

WILEY

A John Wiley and Sons, Ltd, Publication

This edition first published 2008.

Registered office
John Wiley & Sons Ltd, The Atrium, Southern Gate, Chichester, West Sussex, PO19 8SQ, United Kingdom

Library of Congress Cataloging-in-Publication Data

Myung, Hyung G.
Single carrier FDMA : a new air interface for long term evolution / Hyung G. Myung, David J. Goodman.
p. cm.
Includes bibliographical references and index.
ISBN 978-0-470-72449-1 (cloth)
1. Wireless communication systems. 2. Mobile communication systems. I. Goodman, David J., 1939– II. Title.
TK5103.2.H983 2008
621.384–dc22

2008027441

A catalogue record for this book is available from the British Library.

ISBN 978-0-470-72449-1 (HB)

Typeset in 11/13pt Times by Aptara Inc., New Delhi, India.
Printed in Singapore by Markono Print Media Pte Ltd, Singapore.

Contents

Preface

Commercial cellular telecommunications date from the early 1980s when the first car telephone arrived on the market. Public acceptance grew rapidly and the technology progressed through a sequence of "generations" that begin with each new decade. The first generation systems in 1980 used *frequency* division multiple access (FDMA) to create physical channels. Digital transmission arrived in the early 1990s with the most popular systems employing *time* division multiple access (TDMA) and others relying on *code* division (CDMA). Third generation technology dating from 2000 uses *code* division whereas the next generation promises a return to *frequency* division. As the preferred form of multiple access migrates through the time-frequency-code space, the bandwidth of the transmission channels steadily increases. The first systems transmitted signals in 25 or 30 kHz bands. Second generation Global System for Mobile (GSM) uses 200 kHz and the CDMA channels occupy 1.25 MHz. The channel spacing of third generation wideband CDMA is 5 MHz and the next generation of cellular systems will transmit signals in bandwidths up to 20 MHz.

In 2008, two FDMA technologies are competing for future adoption by cellular operating companies. WiMAX, standardized by the IEEE (Institute of Electrical and Electronic Engineers), was first developed to provide broadband Internet access to stationary terminals and later enhanced for transmission to and from mobile devices. The other emerging technology, referred to as "long term evolution" (LTE), is standardized by 3GPP (Third Generation Partnership Project). WiMAX and LTE both use Orthogonal FDMA for transmission from base stations to mobile terminals and WiMAX also uses OFDMA for uplink transmission. On the other hand, the LTE standard for uplink transmission is based on Single Carrier FDMA (SC-FDMA), the principal subject of this book.

We aim to introduce SC-FDMA to an audience of industry engineers and academic researchers. The book begins with an overview of cellular technology evolution that can be appreciated by novices to the subject and non-technical readers. Subsequent chapters become increasingly specialized.

The first half of the book is a tutorial that introduces SC-FDMA and compares it with related techniques including single carrier modulation with frequency domain equalization, orthogonal frequency division modulation (used for example in wireless LANs and digital video broadcasting), and orthogonal FDMA.

The second chapter describes the wireless channel characteristics with the strongest impact on the performance of FDMA. The third chapter presents the signal processing operations of SC-FDMA and the time-domain and frequency-domain properties of SC-FDMA signals. Chapter 4 covers the physical layer of the LTE uplink, providing details of the SC-FDMA implementation standardized by 3GPP. The purpose of the standard is to ensure compatibility between conforming base stations and terminal equipment. However, the standard also allows for considerable operational flexibility in practical equipment and networks. Many of the implementation decisions fall in the category of "scheduling", the subject of Chapter 5. Scheduling, also an important aspect of OFDMA, involves apportioning the channel bandwidth among terminals by means of subcarrier mapping, adaptive modulation, and power control. In addition to a general description of scheduling issues, Chapter 5 presents research results obtained by the authors and our colleagues at Polytechnic University, comparing the effects of various scheduling techniques on system performance.

The final three chapters are also derived from our research. The subject of Chapter 6 is the application of multiple input multiple output (MIMO) transmission and reception to SC-FDMA systems, and Chapter 7 presents the peak power characteristics of SC-FDMA signals. A salient motivation for employing SC-FDMA in a cellular uplink is the fact that its peak-to-average power ratio (PAPR) is lower than that of OFDMA. Chapter 7 uses mathematical derivations and computer simulation to derive the probability model of instantaneous power for a wide variety of SC-FDMA system configurations. It also examines the possibility of clipping the transmitted signal amplitude to reduce the PAPR at the expense of increased binary error rate and increased out-of-band emissions. Finally, Chapter 8 describes the use of MATLAB® to perform link-level and PAPR simulations of SC-FDMA and related techniques.

We are pleased to acknowledge the contribution of Dr Junsung Lim, now at Samsung Corporation, who introduced us to the subject of SC-FDMA. In the course of his Ph.D. studies, Dr Lim collaborated with us in a large portion of the research described in the second half of this book. We were joined in this effort by Kyungjin Oh, who wrote an M.S. dissertation at Polytechnic University on the impact of imperfect channel state information on SC-FDMA. We are also grateful for the encouragement and advice

we received from the staff of John Wiley & Sons, Ltd, publisher of this book. We convey special thanks to Sarah Hinton and Emily Dungey, our main contacts at Wiley as we wrote the book. Our special thanks also go to Mark Hammond who was instrumental in the initial process of this book's writing. We are also grateful to Katharine Unwin and Alex King at Wiley who contributed to the quality of this book.

The material in this book is partially based upon work supported by the National Science Foundation under Grant No. 0430145.

1

Introduction

In less than three decades, the status of cellular telephones has moved from laboratory breadboard via curious luxury item to the world's most pervasive consumer electronics product. Cellular phones have incorporated an ever-growing array of other products including pagers, cameras, camcorders, music players, game machines, organizers, and web browsers. Even though wired telephony is 100 years older and the beneficiary of "universal service" policies in developed countries, the number of cellular phones has exceeded wired phones for a few years and the difference keeps growing. For hundreds of millions of people in developing countries, cellular communications is the only form of telephony they have experienced.

First conceived as a marriage of mature telephony and mature radio communications, cellular communications is now widely recognized as its own technical area and a driver of innovation in a wide range of technical fields including – in addition to telephony and radio – computing, electronics, cryptography, and signal processing.

1.1 Generations

The subject of this book, Single Carrier Frequency Division Multiple Access (SC-FDMA), is a novel method of radio transmission under consideration for deployment in future cellular systems. The development of SC-FDMA represents one step in the rapid evolution of cellular technology. Although technical progress is continuous and commercial systems frequently adopt new improvements, certain major advances mark the transition from one generation of technology to another. First generation systems, introduced in the early 1980s, were characterized by analog

Single Carrier FDMA: A New Air Interface for Long Term Evolution Hyung G. Myung and David J. Goodman
 ISBN: 978-0-470-72449-1

speech transmission. Second generation technology, deployed in the 1990s, transmits speech in digital format. Equally important, second generation systems introduced advanced security and networking technologies that make it possible for a subscriber to initiate and receive phone calls throughout the world.

Even before the earliest second generation systems arrived on the market, the cellular community turned its attention to third generation (3G) technology with the focus on higher bit rates, greater spectrum efficiency, and information services in addition to voice telephony. In 1985, the International Telecommunication Union (ITU) initiated studies of Future Public Land Telecommunication Systems [1]. Fifteen years later, under the heading IMT-2000 (International Mobile Telecommunications-2000), the ITU issued a set of recommendations, endorsing five technologies as the basis of 3G mobile communications systems. In 2008, cellular operating companies are deploying two of these technologies, referred to as WCDMA (wideband code division multiple access) and CDMA2000, where and when they are justified by commercial considerations. Meanwhile, the industry is looking beyond 3G and considering SC-FDMA as a leading candidate for the "long term evolution" (LTE) of radio transmissions from cellular phones to base stations. It is anticipated that LTE technology will be deployed commercially around 2010 [2].

With respect to radio technology, successive cellular generations have migrated to signals transmitted in wider and wider radio frequency bands. The radio signals of first generation systems occupied bandwidths of 25 and 30 kHz, using a variety of incompatible frequency modulation formats. Although some second generation systems occupied equally narrow bands, the two that are most widely deployed, GSM and CDMA, occupy bandwidths of 200 kHz and 1.25 MHz, respectively. The third generation WCDMA system transmits signals in a 5 MHz band. This is the approximate bandwidth of the version of CDMA2000 referred as 3X-RTT (radio transmission technology at three times the bandwidth of the second generation CDMA system). The version of CDMA2000 with a large commercial market is 1X-RTT. Its signals occupy the same 1.25 MHz bandwidth as second generation CDMA, and in fact it represents a graceful upgrade of the original CDMA technology. For this reason, some observers refer to 1X-RTT as a 2.5G technology [3]. Planners anticipate even wider signal bands for the long term evolution of cellular systems. Orthogonal Frequency Division Multiplexing (OFDM) and SC-FDMA are attractive technologies for the 20 MHz signal bands under consideration for the next generation of cellular systems.

1.2 Standards

The technologies employed in cellular systems are defined formally in documents referred to as "compatibility specifications". A compatibility specification is one type of technical standard. Its purpose is to ensure that two different network elements interact properly. In the context of cellular communications, the two most obvious examples of interacting equipment types are cellular phones and base stations. As readers of this book are aware, standards organizations define a large number of other network elements necessary for the operation of today's complex cellular networks.

In addition to cellular phones and base stations, the most familiar cellular network elements are mobile switching centers, home location registers, and visitor location registers. In referring to standards documents, it is helpful to keep in mind that the network elements defined in the documents are "functional" elements, rather than discrete pieces of equipment. Thus, two different network elements, such as a visitor location register and a mobile switching center, can appear in the same equipment and the functions of a single network element (such as a base transceiver station) can be distributed among dispersed devices.

Figure 1.1 shows the network elements and interfaces in one 3G system [4]. The network elements (referred to in the standards as "entities") are contained in four major groups enclosed by dotted boxes. The core network (CN) is at the top of the figure. Below the core network is the radio access network with three sets of elements; a Base Station System (BSS) exchanges radio signals with mobile stations (MS) to deliver circuit switched services, and a corresponding Radio Network System (RNS) exchanges radio signals with mobile stations to deliver packet switched services. This book focuses on the radio signals traveling across the air interfaces. The Um interface applies to circuit switched services carrying signals between mobile stations and Base Transceiver Stations (BTS). Uu applies to packet switched services carrying signals between a mobile station and a base station system.

1.3 Cellular Standards Organizations 3GPP and 3GPP2

Two Third Generation Partnership Projects publish 3GPP cellular standards. The original Partnership Project, 3GPP, is concerned with descendents of the Global System for Mobile (GSM). The 3G technologies standardized by 3GPP are often referred to collectively as WCDMA (wideband code division multiple access). 3GPP uses two other acronyms

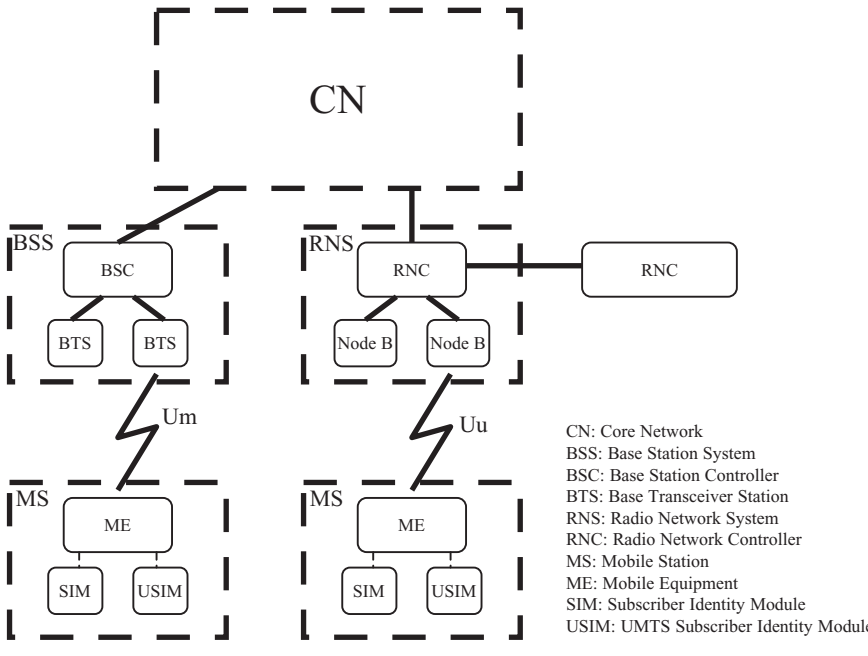

Figure 1.1 Basic configuration of a public land mobile network (PLMN) supporting circuit switched (CS) and packet switched (PS) services and interfaces [4]. *Source:* ETSI (European Telecommunications Standards Institute) © 2007. 3GPP™ TSs and TRs are the property of ARIB, ATIS, CCSA, ETSI, TTA and TTC who jointly own the copyright in them. They are subject to further modifications and are therefore provided to you "as is" for information purposes only. Further use is strictly prohibited.

to describe its specifications: UMTS (Universal Mobile Telecommunications System) applies to the entire cellular network contained in hundreds of 3GPP specifications; and UTRAN (Universal Terrestrial Radio Access Network) refers to the collection of network elements, and their interfaces, used for transmission between mobile terminals and the network infrastructure. The other project, 3GPP2, is concerned with advanced versions of the original CDMA cellular system. The technologies standardized by 3GPP2 are often referred to collectively as CDMA2000.

The Partnership Projects consist of "organizational partners", "market representation partners", and "individual members". The organizational partners are the regional and national standards organizations, listed in Table 1.1, based in North America, Europe, and Asia. The market representation partners are industry associations that promote deployment of specific technologies. The individual members are companies associated with one

Table 1.1 Organizational members of the Partnership Projects

Organizational member	Nationality	Affiliation
Association of Radio Industries and Businesses	Japan	3GPP and 3GPP2
Alliance for Telecommunication Industry Solutions	United States	3GPP
China Communications Standards Association	China	3GPP and 3GPP2
European Telecommunication Standards Institute	Europe	3GPP
Telecommunications Industry Association	North America	3GPP2
Telecommunications Technology Association	Korea	3GPP and 3GPP2
Telecommunication Technology Committee	Japan	3GPP and 3GPP2

or more of the organizational partners. In October 2006 there were 297 individual members of 3GPP and 82 individual members of 3GPP2.

The technologies embodied in WCDMA and CDMA2000 appear in hundreds of technical specifications covering all aspects of a cellular network. In both Partnership Projects, responsibility for producing the specifications is delegated to Technical Specification Groups (TSG), each covering one category of technologies. In 3GPP, the TSGs are further subdivided into Work Groups (WG). The publication policies of the two Partnership Projects are different. 3GPP periodically "freezes" a complete set of standards, including many new specifications. Each set is referred to as a "Release". Each Release is complete in that it incorporates all unchanged sections of previous standards that are still in effect as well as any new and changed sections. 3GPP also publishes preliminary specifications that will form part of a future Release. By contrast, each TSG in 3GPP2 publishes a new or updated specification whenever the specification obtains necessary approvals.

Release 5 of WCDMA was frozen in 2002, Release 6 in 2005, and Release 7 in 2007 [5]. In 2008, LTE specifications are being finalized as Release 8. Two of the innovations in Release 5 are High Speed Downlink Packet Access (HSDPA) and the IP Multimedia Subsystem (IMS). In Release 6, the innovations are High Speed Uplink Packet Access (HSUPA), the Multimedia Broadcast/Multicast Service (MBMS), and Wireless LAN/cellular interaction, and in Release 7, Multiple Input

Multiple Output (MIMO) and higher order modulation. Release 8 deliberations focus on the Long Term Evolution (LTE) of WCDMA. In the Radio Access Network (RAN), the LTE goals are data rates "up to 100 Mbps in full mobility wide area deployments and up to 1 Gbps in low mobility, local area deployments" [6]. For best effort packet communication, the long term spectral efficiency targets are 5–10 b/s/Hz in a single (isolated) cell; and up to 2–3 b/s/Hz in a multi-cellular case [6]. In this context, SC-FDMA is under consideration for transmission from mobile stations to a Base Station Subsystem or a Radio Network System.

1.4 IEEE Standards

In addition to the two cellular Partnership Projects, the Institute of Electrical and Electronic Engineers (IEEE) has published standards used throughout the world in products with a mass market. Within the IEEE LAN/MAN standards committee (Project 802), there are several working groups responsible for wireless communications technologies. The one with the greatest influence to date is IEEE 802.11, responsible for the "WiFi" family of wireless local area networks. Two of the networks conforming to the specifications IEEE 802.11a and IEEE 802.11g employ OFDM technology for transmission at bit rates up to 54 Mb/s [7,8]. The other working group standardizing OFDM technology is IEEE 802.16, responsible for wireless metropolitan area networks. Among the standards produced by this working group, IEEE802.16e, referred to as "WiMAX" and described in the next section, most closely resembles technology under consideration by 3GPP for cellular long term evolution.

1.5 Advanced Mobile Wireless Systems Based on FDMA

Three standards organizations, IEEE, 3GPP, and 3GPP2, have work in progress on advanced mobile broadband systems using frequency division transmission technology. The following subsections describe key properties of Mobile WiMAX (developed by the IEEE), Ultra Mobile Broadband (developed by 3GPP2), and 3GPP Long Term Evolution (LTE). SC-FDMA, the subject of this book, is a component of LTE.

1.5.1 IEEE 802.16e-Based Mobile WiMAX

Following in the footsteps of the highly successful IEEE 802.11 family of wireless local area network (WLAN) standards, the IEEE 802.16 Working Group on Broadband Wireless Access (BWA) began its work of

Table 1.2 Evolution of the IEEE 802.16 standard

Standards	Publication date	Highlights
802.16	Apr. 2002	Line-of-sight fixed operation in 10 to 66 GHz band.
802.16a	Apr. 2003	Air interface support for 2 to 11 GHz band.
802.16-2004 (802.16d)	Oct. 2004	Minor improvements and fixes to 802.16a.
802.16e	Feb. 2006	Support for vehicular mobility and asymmetrical link.
802.16m	In progress	Higher peak data rate, reduced latency, and efficient security mechanism.

developing the IEEE 802.16 wireless metropolitan area network (WMAN) standards in July 1999. Initially, IEEE 802.16 primarily focused on a point-to-multipoint topology with a cellular deployment of base stations, each tied into core networks and in contact with fixed wireless subscriber stations.

Since the first publication of the standard in 2002, the IEEE 802.16 standard has evolved through various amendments and IEEE 802.16e, published in February 2006, specifies physical and medium access control layers for both fixed and mobile operations [9]. Currently, 802.16m is being developed for the next generation system. Table 1.2 summarizes the IEEE 802.16 evolution.

Mobile WiMAX is an IEEE 802.11e-based technology maintained by the WiMAX Forum [10], which is an organization of more than 400 operators and communications component/equipment companies. Its charter is to promote and certify the compatibility and interoperability of broadband wireless access equipment that conforms to the IEEE 802.16 specifications. The WiMAX Forum Network Working Group (NWG) develops the higher-level networking specifications for Mobile WiMAX systems beyond what is defined in the IEEE 802.16 specifications, which address the air interface only.

Key features of the 802.16e-based Mobile WiMAX are:

- Up to 63 Mb/s for downlink and up to 28 Mb/s for uplink per sector throughput in a 10 MHz band.
- End-to-end IP-based Quality of Service (QoS).

- Scalable OFDMA and spectrum scalability.
- Robust security: Extensible Authentication Protocol (EAP)-based authentication, AES-CCM-based authenticated encryption, and CMAC/HMAC-based control message protection schemes.
- Optimized handoff scheme and low latency.
- Adaptive modulation and coding (AMC).
- Hybrid automatic repeat request (HARQ) and fast channel feedback.
- Smart antenna technologies: beamforming, space-time coding, and spatial multiplexing.
- Multicast and broadcast service (MBS).

1.5.2 3GPP2 Ultra Mobile Broadband

3GPP2 developed Ultra Mobile Broadband (UMB) based on the frameworks of CDMA2000 1xEV-DO revision C [11], IEEE 802.20 [12], and Qualcomm Flarion Technologies' FLASH-OFDM [13]. The UMB standard was published in April 2007 by the 3GPP2 and the UMB system is expected to be commercially available in early 2009.

The key features of UMB include [11]:

- OFDMA-based air interface.
- Multiple Input Multiple Output (MIMO) and Space Division Multiple Access (SDMA).
- Improved interference management techniques.
- Up to 280 Mb/s peak data rate on forward link and up to 68 Mb/s peak data rate on reverse link.
- An average of 16.8 msec (32-byte, round trip time) end-to-end network latency.
- Up to 500 simultaneous VoIP users (10 MHz FDD allocations).
- Scalable IP-based flat or hierarchical architecture.
- Flexible spectrum allocations: scalable, noncontiguous, and dynamic channel (bandwidth) allocations and support for bandwidth allocations of 1.25 MHz, 5 MHz, 10 MHz, and 20 MHz.
- Low power consumption and improved battery life.

1.5.3 3GPP Long Term Evolution

3GPP's work on the evolution of the 3G mobile system started with the Radio Access Network (RAN) Evolution workshop in November 2004

[14]. Operators, manufacturers, and research institutes presented more than 40 contributions with views and proposals on the evolution of the Universal Terrestrial Radio Access Network (UTRAN), which is the foundation for UMTS/WCDMA systems. They identified a set of high level requirements at the workshop: reduced cost per bit, increased service provisioning, flexibility of the use of existing and new frequency bands, simplified architecture and open interfaces, and reasonable terminal power consumption. With the conclusions of this workshop and with broad support from 3GPP members, a feasibility study on the Universal Terrestrial Radio Access (UTRA) and UTRAN Long Term Evolution started in December 2004. The objective was to develop a framework for the evolution of the 3GPP radio access technology towards a high-data-rate, low-latency, and packet-optimized radio access technology. The study focused on means to support flexible transmission bandwidth of up to 20 MHz, introduction of new transmission schemes, advanced multi-antenna technologies, signaling optimization, identification of the optimum UTRAN network architecture, and functional split between radio access network nodes.

The first part of the study resulted in an agreement on the requirements for the Evolved UTRAN (E-UTRAN). Key aspects of the requirements are as follows [15]:

- Up to 100 Mb/s within a 20 MHz downlink spectrum allocation (5 b/s/Hz) and 50 Mb/s (2.5 b/s/Hz) within a 20 MHz uplink spectrum allocation.
- Control-plane capacity: at least 200 users per cell should be supported in the active state for spectrum allocations up to 5 MHz.
- User-plane latency: less than 5 msec in an unloaded condition (i.e., single user with single data stream) for small IP packet.
- Mobility: E-UTRAN should be optimized for low mobile speeds 0–15 km/h. Higher mobile speeds between 15 and 120 km/h should be supported with high performance. Connections shall be maintained at speeds 120–350 km/h (or even up to 500 km/h depending on the frequency band).
- Coverage: throughput, spectrum efficiency, and mobility targets should be met for 5 km cells and with a slight degradation for 30 km cells. Cells ranging up to 100 km should not be precluded.
- Enhanced multimedia broadcast multicast service (E-MBMS).
- Spectrum flexibility: E-UTRA shall operate in spectrum allocations of different sizes including 1.25 MHz, 1.6 MHz, 2.5 MHz, 5 MHz, 10 MHz, 15 MHz, and 20 MHz in both uplink and downlink.

- Architecture and migration: packet-based single E-UTRAN architecture with provision to support systems supporting real-time and conversational class traffic and support for an end-to-end QoS.
- Radio Resource Management: enhanced support for end-to-end QoS, efficient support for transmission of higher layers, and support of load sharing and policy management across different radio access technologies.

The wide set of options initially identified by the early LTE work was narrowed down in December 2005 to a working assumption that the downlink would use Orthogonal Frequency Division Multiplex (OFDM) and the uplink would use Single Carrier Frequency Division Multiple Access (SC-FDMA). Supported data modulation schemes are QPSK, 16QAM, and 64QAM. The use of Multiple Input Multiple Output (MIMO) technology with up to four antennas at the mobile side and four antennas at the base station was agreed. Re-using the expertise from the UTRAN, they agreed to the same channel coding type as UTRAN (turbo codes), and to a transmission time interval (TTI) of 1 msec to reduce signaling overhead and to improve efficiency [16,17].

The study item phase ended in September 2006 and the LTE specification is due to be published in 2008.

1.5.4 Summary and Comparison of Mobile WiMAX, LTE and UMB

In summary, the upcoming systems beyond 3G overviewed in the previous sections have the following features in common:

- Up to 20 MHz transmission bandwidth.
- Multi-carrier air interface for robustness against frequency-selective fading and for increased spectral efficiency: OFDM/OFDMA and its variant forms are the basic modulation and multiple access schemes.
- Advanced multi-antenna techniques: various MIMO techniques are integrated to the system to increase spectral efficiency and to make the link more reliable.
- Fast time-frequency resource scheduling.
- Flat all-IP network architecture: reduced network overhead by eliminating network layers.
- Multicast and broadcast multimedia service.

Table 1.3 compares the air interfaces of the three beyond-3G systems.

Table 1.3 Summary and comparison of Mobile WiMAX, LTE and UMB

	Mobile WiMAX	3GPP LTE	3GPP2 UMB
Channel bandwidth	5, 7, 8.75, and 10 MHz	1.4, 3, 5, 10, 15, and 20 MHz	1.25, 2.5, 5, 10, and 20 MHz
DL multiplex	OFDM	OFDM	OFDM
UL multiple access	OFDMA	SC-FDMA	OFDMA and CDMA
Duplexing	TDD	FDD and TDD	FDD and TDD
Subcarrier mapping	Localized and distributed	Localized	Localized and distributed
Subcarrier hopping	Yes	Yes	Yes
Data modulation	QPSK, 16-QAM, and 64-QAM	QPSK, 16-QAM, and 64-QAM	QPSK, 8-PSK, 16-QAM, and 64-QAM
Subcarrier spacing	10.94 kHz	15 kHz	9.6 kHz
FFT size (5 MHz bandwidth)	512	512	512
Channel coding	Convolutional coding and convolutional turbo coding: block turbo coding and LDPC coding optional	Convolutional coding and turbo coding	Convolutional coding, turbo coding, and LDPC coding
MIMO	Beamforming, space-time coding, and spatial multiplexing	Multi-layer precoded spatial multiplexing, space-time/ frequency block coding, switched transmit diversity, and cyclic delay diversity	Multi-layer precoded spatial multiplexing, space-time transmit diversity, spatial division multiple access, and beamforming

1.6 Figures of Merit

Standards organizations, in principle, provide a venue for interested parties to establish the technologies that provide the best tradeoff among a variety of performance objectives. In practice, the aim for excellence is modulated by the need for industry participants to advance the interests of

their employers. In balancing these conflicting interests, the organizations measure possible solutions with respect to several figures of merit. The figures of merit most relevant to the systems covered in this book are spectral efficiency, throughput, delay, and power consumption in mobile portable devices.

SC-FDMA, which utilizes single carrier modulation, DFT-precoded orthogonal frequency multiplexing, and frequency domain equalization, is a technique that has similar performance and essentially the same overall complexity as OFDMA. One prominent advantage over OFDMA is that the SC-FDMA signal has better peak power characteristics because of its inherent single carrier structure. SC-FDMA has drawn great attention as an attractive alternative to OFDMA, especially in the uplink communications where better peak power characteristics greatly benefit the mobile terminal in terms of transmit power efficiency and manufacturing cost. SC-FDMA has been adopted for the uplink multiple access scheme in 3GPP LTE.

A major purpose of this book is to show how the details of an SC-FDMA transmission scheme influence the tradeoffs among these figures of merit.

1.7 Frequency Division Technology in Broadband Wireless Systems

Frequency division was a mature radio technology, and therefore the earliest cellular systems used it to separate different analog speech transmissions: frequency division multiplexing in the forward (downlink) direction and frequency division multiple access in the reverse (uplink) direction. Second generation systems use either code division technology or a hybrid of time division and frequency division to convey speech and other signals in digital form. Although the two 3G systems are based on code division technologies, all of the advanced broadband systems are reverting to frequency division. As explained in Chapter 2, frequency division technology is well-suited to transmission through mobile radio channels subject to frequency-selective fading due to multipath propagation. Orthogonal frequency division techniques, which effectively transmit a high-speed data signal as a composite of a large number of low-speed signals, each occupying a narrow frequency band, have been employed in digital audio and digital television broadcasting, wireless metropolitan area networks, and wireless local area networks. The same reasons that make them effective in those environments, also make frequency division techniques attractive for the long term evolution of cellular networks. In establishing standards for LTE, 3GPP recognized that OFDMA places significant implementation

burdens on mobile terminals. From the point of view of implementation, SC-FDMA can be viewed as a modification of OFDMA with extended battery life in mobile terminals due to low peak power characteristics.

Chapter 2 describes the propagation characteristics of broadband mobile radio signals that make frequency division techniques attractive for high-speed data transmission. It also provides a summary of the main characteristics of OFDM and OFDMA, the predecessors of SC-FDMA. Finally, before presenting details of SC-FDMA in the remainder of this book, Chapter 2 describes in general terms single carrier high-speed data transmission with frequency domain equalization.

References

[1] International Telecommunication Union, "About Mobile Technology and IMT-2000," http://www.itu.int/osg/spu/imt-2000/technology.html.

[2] Toskala, A., Holma, H., Pajukoski, K., *et al*., "UTRAN Long Term Evolution in 3GPP," *Proc. International Symposium on Personal, Indoor and Mobile Radio Communications (PIMRC) '06*, Helsinki, Finland, Sep. 2006.

[3] Smith, C. and Collins, D., *3G Wireless Networks*, McGraw Hill, 2002, pp. 201–213.

[4] 3rd Generation Partnership Project, *3GPP TS 23.002 – Technical Specification Group Services and Systems Aspects; Network Architecture (Release 8)*, June 2007, Section 5.1.

[5] Holma, H. and Toskala, A., *WCDMA for UMTS – HSPA Evolution and LTE*, John Wiley & Sons, Ltd, 4th edition, 2007, p. 5.

[6] 3rd Generation Partnership Project, *3GPP TR 21.902 – Technical Specification Group Services and System Aspects; Evolution of 3GPP system; (Release 7)*, June 2007.

[7] Institute of Electrical and Electronics Engineers, *IEEE Std 802.11a – Part 11: Wireless LAN Medium Access Control (MAC) and Physical Layer (PHY) Specifications; High-Speed Physical Layer in the 5 GHz Band*, 1999.

[8] Institute of Electrical and Electronics Engineers, *IEEE Std 802.11g – Part 11: Wireless LAN Medium Access Control (MAC) and Physical Layer (PHY) Specifications*, 2003.

[9] Balachandran, K., Calin, D., Cheng, F-C., *et al*., "Design and Analysis of an IEEE 802.16e-based OFDMA Communication System," *Bell Labs Tech. Jour.*, vol. **11**, no. 4, Mar. 2007, pp. 53–73.

[10] WiMAX Forum, "Mobile WiMAX - Part I: A Technical Overview and Performance Evaluation," http://www.wimaxforum.org/technology/downloads/Mobile_WiMAX_Part1_Overview_and_Performance.pdf, Aug. 2006.

[11] Das, S., Li, S., Monogioudis, P., *et al*., "EV-DO Revision C: Evolution of the cdma2000 Data Optimized System to Higher Spectral Efficiencies and Enhanced Services," *Bell Labs Tech. Jour.*, vol. **11**, no. 4, Mar. 2007, pp. 5–24.

[12] Institute of Electrical and Electronics Engineers, *IEEE 802.20 Mobile Broadband Wireless Access (MBWA)*, 2008, http://www.ieee802.org/20/.

[13] Laroia, R., Uppala, S., and Li, J., "Designing a Mobile Broadband Wireless Access Network," *IEEE Sig. Proc. Mag.*, vol. **21**, no. 5, Sep. 2004, pp. 20–28.

[14] 3rd Generation Partnership Project, "UTRA-UTRAN Long Term Evolution (LTE) and 3GPP System Architecture Evolution (SAE)," http://www.3gpp.org/Highlights/LTE/LTE.htm.

[15] 3rd Generation Partnership Project, *3GPP TR 25.913 – Technical Specification Group Radio Access Network; Requirements for Evolved UTRA and Evolved UTRAN (Release 7)*, Mar. 2006.

[16] Ekström, H., Furuskär, A., Karlsson, J., *et al*., "Technical Solutions for the 3G Long-Term Evolution," *IEEE Commun. Mag*., vol. **44**, no. 3, Mar. 2006, pp. 38–45.

[17] Bachl, R., Gunreben, P., Das, S., *et al*., "The Long Term Evolution towards a New 3GPP Air Interface Standard," *Bell Labs Tech. Jour.*, vol. **11**, no. 4, Mar. 2007, pp. 25–51.

2

Channel Characteristics and Frequency Multiplexing

2.1 Introduction

In the previous chapter, Section 1.6 identifies the figures of merit for uplink transmission techniques in cellular systems as high spectral efficiency, high throughput, low delay, and long battery life in portable devices. The challenge of radio system design is to optimize these figures of merit in the presence of impairments in communication channels. In order to increase spectral efficiency and achieve increasingly high transmission rates, successive generations of cellular systems have moved to signals with higher and higher bandwidth. As indicated in Table 1.3, the technologies developed by 3GPP for long term cellular evolution (LTE) will use signals with bandwidths as high as 20 MHz.

To set the stage for the presentation of the SC-FDMA system under consideration by 3GPP in the remainder of this book, this chapter provides background information on radio signal propagation. It then describes two approaches to frequency-domain signal processing in the transmission of individual signals: orthogonal frequency division multiplexing (OFDM) and single carrier transmission with frequency-domain equalization (SC/FDE).

2.2 Radio Channel Characteristics

Radio signal propagation in cellular systems is the subject of a huge body of theoretical and experimental research and a thorough exposition of important issues would fill a volume larger than this book. The purpose of

Single Carrier FDMA: A New Air Interface for Long Term Evolution Hyung G. Myung and David J. Goodman
 ISBN: 978-0-470-72449-1

the following paragraphs is to describe briefly the main transmission impairments encountered by cellular signals, emphasizing the impairments that have the strongest effects on the design and performance of broadband transmission technologies including SC-FDMA.

The impairments can be grouped into three categories according to the phenomena that cause them:

- impairments due to the physics of radio propagation from transmitter to receiver;
- impairments due to the presence of extraneous signals at the receiving antenna; and
- impairments due to the properties of transmitting and receiving equipment.

Table 2.1 is a list of the principal impairments in each category.

2.2.1 Physics of Radio Transmission

2.2.1.1 Attenuation

The energy radiated from an omnidirectional antenna fills a sphere, and therefore the fraction of the original energy incident on a receiving antenna varies inversely with the distance between the transmitting and receiving antennas. In free space the received energy would be inversely proportional

Table 2.1 Transmission impairments in cellular systems

Physics of radio propagation	Attenuation Shadowing Doppler shift Inter-symbol interference (ISI) Flat fading Frequency-selective fading
Extraneous signals	Co-channel interference Adjacent channel interference Impulse noise White noise
Transmitting and receiving equipment	White noise Nonlinear distortion Frequency and phase offset Timing errors

to the square of the distance (d meters). For terrestrial signals the received energy also varies inversely with distance (as $1/d^{\alpha}$) but various environmental factors result in the exponent $\alpha > 2$. In most cellular environments, $3.5 \leq \alpha \leq 4.5$. Signals transmitted from directional antennas have a similar relationship between received energy and distance but the constant of proportionality depends on the antenna gains determined by the nature of the transmitting and receiving antennas.

2.2.1.2 Shadowing

If attenuation were the only effect of distance on signal strength, a signal would be received with equal power at all points equally distant from a transmitter. However, due to differences in the path taken by the transmitted signal, there is noticeable variation in the power in received signals at different points on a circle surrounding a transmitter. Figure 2.1 illustrates this situation. It is a scatter plot of received signal power, measured in dBm – decibels relative to 1 mW – as a function of distance, plotted on a log scale at various locations in a cellular service area. The variability in received signal power at a given distance is usually referred to as "shadowing" or "shadow fading", because much of it is due to differences in obstacles along the line from transmitter to receiver at various points on the circle around the transmitter.

Extensive measurements indicate that the distribution of the signal power, measured in dB, due to shadow fading can be represented accurately

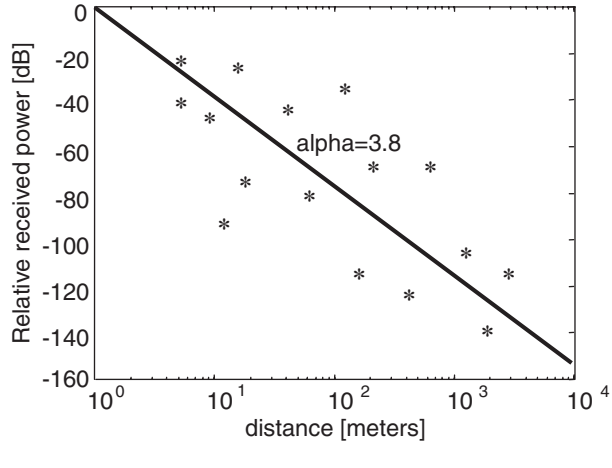

Figure 2.1 Received signal power as a function of distance between transmitter and receiver

as a Gaussian random variable. The expected value is given by the inverse exponential relationship between received signal power and distance ($1/d^{\alpha}$), the solid line in Figure 2.1. The standard deviation, σ dB, depends on the uniformity of the characteristics of the cellular service area. Usually, 6 dB $\leq \sigma \leq$ 10 dB, with higher standard deviations in urban areas and lower ones in flat rural environments. Shadowing effects change gradually as a terminal moves from one location to another, with significant correlation observed over tens of meters. Consequently, the term "slow fading" is a synonym for shadow fading. This spatial variation contrasts strongly with the phenomena that produce flat fading and frequency-selective fading, described later in this section. Those phenomena are correlated over distances on the order of a few centimeters.

2.2.1.3 Doppler

When the transmitted signal is a sine wave and the transmitter and/or receiver is moving, the frequency of a single ray within the received signal is different from the frequency of the transmitted signal. The difference is the *Doppler shift* and it is proportional to $f_d = v/\lambda$ Hz, where v m/s is the relative velocity of the transmitter and receiver and λ m is the wavelength of the transmitted sine wave. For example, the Doppler frequency of a 2 GHz sine wave at a cellular phone in a vehicle moving at 100 km/h is $f_d = 185.2$ Hz.

The frequency difference is also proportional to the cosine of the angle of incidence of the ray. In cellular systems, scattering causes the received signal to be a composite of many rays arriving at different angles incident on the received antenna. Therefore the received signal has components at a continuum of frequencies offset from the original by frequencies between $-f_d$ Hz and $+f_d$ Hz. The relative strength of these signal components is characterized by the *Doppler spectrum* of the radio channel, which represents power spectral density as a function of frequency. The *classical Doppler spectrum* derived mathematically for a transmitted sine wave is:

$$S(f) = \begin{cases} \dfrac{A}{\sqrt{1 - \left(\dfrac{f}{f_d}\right)^2}}, & |f| < f_d \\ 0, & |f| > f_d \end{cases} \tag{2.1}$$

Figure 2.2 shows $S(f)$ with $f_d = 185.2$ Hz and $A = 1$.

Because the broadband single carrier signals in SC-FDMA have sinusoidal components spanning up to 20 MHz, the Doppler effect is more complex when the mobile terminal is moving at any significant speed.

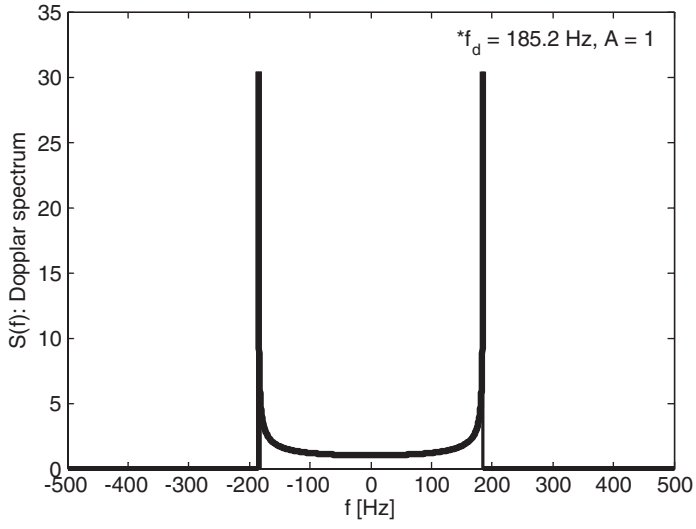

Figure 2.2 The classical Doppler spectrum

2.2.1.4 Inter-Symbol Interference

Multipath propagation is a pervasive phenomenon in cellular signal transmission. Due to the features of the operating environment, components of the transmitted signal arrive at the receiver after reflections from the ground and various natural features and manmade structures as shown in Figure 2.3. Therefore, the impulse response of the channel can be modeled as a set of impulses arriving with relative delays proportional to the path lengths of the different signal components.

At a receiver, a signal, representing a digital symbol of duration T seconds, has components arriving over a longer interval and therefore interfering with signals representing other symbols. The overall effect is *inter-symbol interference* (ISI) and its impact on transmission systems increases with the duration of the channel impulse response. The most common measure of inter-symbol interference is "rms delay spread", τ_{rms} seconds. It is a function of the magnitudes of the components of the impulse response and their time differences. The maximum anticipated delay spread, τ_{max} seconds, is the difference in delay between the shortest and longest signal path. It is proportional to the difference in path length. If the greatest path length difference is D_{max} km, then $\tau_{max} = D_{max}/0.3$ μs. D_{max} depends on the physical characteristics of the cellular service area.

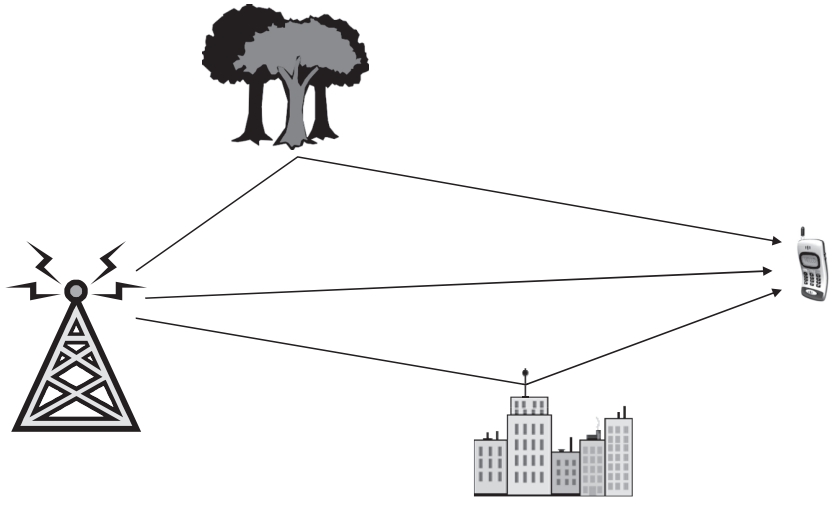

Figure 2.3 Multipath propagation

2.2.1.5 Flat Fading and Frequency-Selective Fading

Signal scattering and multipath propagation together produce rapid fluctuations in the strength of signals received at a base station as a cellular phone moves through its service area. These fluctuations are due to differences in received signal strength at locations spaced on the order of the wavelength of the carrier frequency of the transmitted signal. This phenomenon is usually referred to as *fast fading* to distinguish it from shadow fading. The differences in received signal strength associated with shadow fading are noticeable at locations spaced in the order of tens of meters whereas fast fading signals result from signal strength differences at locations spaced on the order of a few centimeters.

The effect of fast fading on received cellular signals depends on the relationship of signal bandwidth to the width of the frequency response of the channel. The frequency response is the Fourier transform of the impulse response and its width is inversely proportional to the rms delay spread of the multipath profile. When the signal bandwidth B_S Hz is small compared to the width of the frequency response, the fast fading is referred to as "flat" because all the frequency components of the transmitted signal are attenuated approximately equally. Otherwise the fast fading is "frequency-selective". Flat fading occurs when the product $B_S\tau_{rms}$ is small. Although the nature of the fading changes gradually with changes in $B_S\tau_{rms}$, it is customary to refer to the fading as flat when $B_S\tau_{rms} < 0.02$. At this value, the correlation between two signal components at extreme ends of the

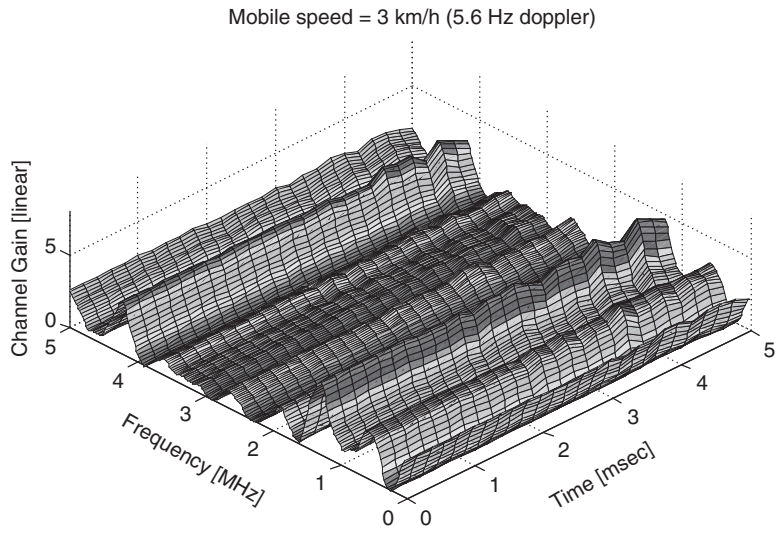

Figure 2.4 Time variation of 3GPP TU6 Rayleigh fading channel in 5 MHz band with 2 GHz carrier frequency and user speed = 3 km/h (Doppler frequency = 5.6 Hz)

frequency band occupied by the signal is at least 0.9 [1]. When $B_S\tau_{rms} > 0.02$, the fading is described as frequency selective.

Figures 2.4 and 2.5 show the variation of channel gain with time (over 5 msec) and frequency (over $B_S = 5$ MHz) for one channel model. In Figure 2.4 the mobile terminal speed is 3 km/h. In Figure 2.5 it is 60 km/h. For this channel model, $\tau_{rms} = 5$ μs and the fading is frequency selective because $B_S\tau_{rms} = 25 > 0.02$ for the 5 MHz band.

Figure 2.6 summarizes the fading channel manifestations and their mathematical descriptions [2].

2.2.2 Effects of Extraneous Signals

2.2.2.1 Co-Channel Interference

Co-channel interference is a well-known consequence of cellular reuse. In order to use the cellular radio spectrum efficiently, several base stations in a service area use the same physical channels simultaneously.

2.2.2.2 Adjacent Channel Interference

Adjacent channel interference also occurs in all cellular systems. Even though a signal occupies a nominal bandwidth that determines the

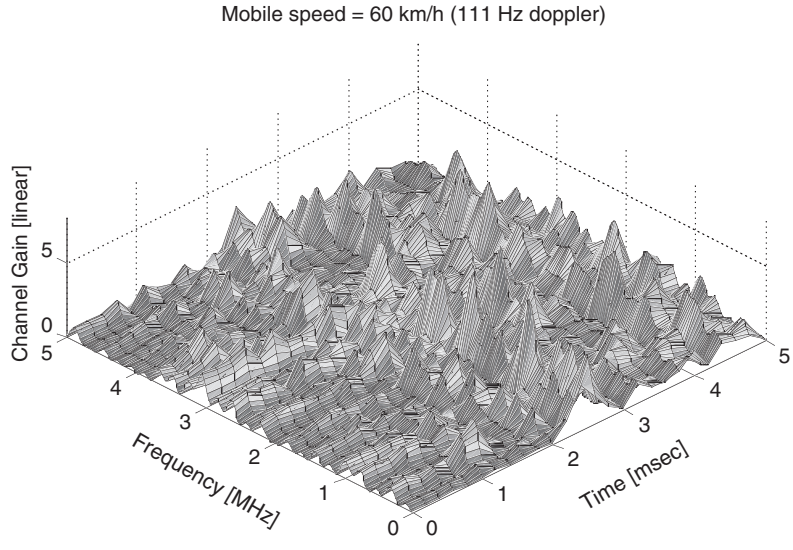

Figure 2.5 Time variation of 3GPP TU6 Rayleigh fading channel in 5 MHz band with 2 GHz carrier frequency and user speed = 60 km/h (Doppler frequency = 111 Hz)

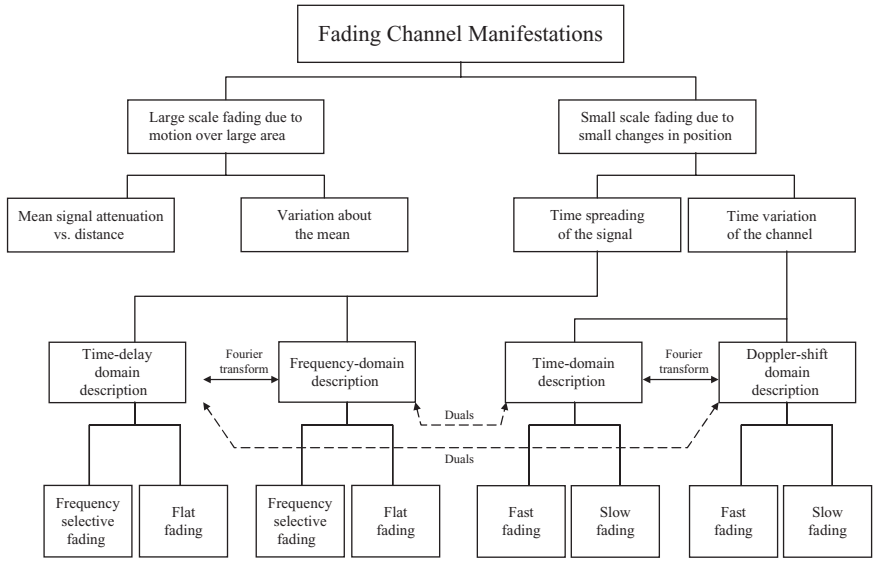

Figure 2.6 Fading channel manifestations [2]

differences in carrier frequency of different signals, the signal necessarily has energy at frequencies outside of the nominal bandwidth.

2.2.2.3 Noise

Co-channel interference and adjacent channel interference are effects of signals generated by a cellular system and therefore under the control of the cellular network operator. Even though network operators have licenses that give them exclusive rights to transmit energy in their assigned spectrum, there is energy radiated in the cellular bands by a host of natural and manmade sources outside the control of a network operator. Their effects on base station receivers are usually modeled as white noise or impulse noise. The most pervasive noise source is the thermal activity of the atmosphere. Atmospheric noise is modeled as white noise with power spectral density

$$N_0 = 1.3807 \times 10^{-23} \times T \text{ Joules} \tag{2.2}$$

where T is the ambient temperature in degrees Kelvin and the coefficient is Boltzmann's constant.

The unit of measurement, Joules, can also be expressed as watts/Hz. Thus, in a bandwidth of B_S Hz, the noise power is $N_0 B_S$ watts. For example, at an ambient temperature of 300 °K (27 °C) and a bandwidth 5 MHz, the atmospheric noise power is

$$N_W = 2.071 \times 10^{-14} \text{ W} \tag{2.3}$$

In cellular systems, power levels are usually measured in units of *dBm*, decibels relative to 1 mW. The noise power in Equation (2.3) can also be written as

$$N_{dBm} = -106.84 \text{ dBm} \tag{2.4}$$

2.2.3 Transmitting and Receiving Equipment

2.2.3.1 Noise

Thermal noise in device electronics enhances the atmospheric noise power in a radio receiver. The added noise is usually expressed as a receiver noise figure, which is the ratio of the total noise power in the receiver to the atmospheric noise in Equation (2.3).

2.2.3.2 Nonlinear Distortion

Nonlinearity in the transmitter power amplifier is the imperfection that most influences performance of frequency-division techniques. Technologies that require highly linear power amplifiers are relatively expensive and heavy and they operate with low power efficiency (measured as the ratio of radiated power to power consumed by amplifier electronics). In FDMA systems, vulnerability to amplifier nonlinearity increases with the high peak-to-average power ratio (PAPR) of the transmitted signal. A principal motivation for adopting SC-FDMA in future cellular systems is the fact that its PAPR is lower than that of alternative transmission techniques, especially OFDMA.

2.2.3.3 Frequency Offset

There are inevitable differences in the frequencies and phases of local oscillators at the transmitter and receiver of a communication system. Frequency-domain techniques are especially vulnerable to these offsets because at a receiver they destroy the orthogonality of the signals in the separate sub-bands. To minimize the frequency offsets, OFDM and SC-FDMA systems use some of the narrowband channels as *pilot tones* transmitting known signals to help the receiver generate a frequency reference that is closely matched to the transmitter's.

2.2.4 Radio Propagation Models

In the design and performance analysis of cellular transmission technologies, engineers refer to abstract channel models published by 3GPP (TS 25.101, TS 45.005) [3], [4]. The models are based on the assumption that the signals can be represented by wide sense stationary stochastic processes with uncorrelated scattering (WSSUS model). Each channel model consists of a probability density function of signal amplitude (either Rayleigh or Rice), a multipath delay profile, and a formula for the Doppler spectrum, with Doppler frequency f_d as a parameter. The Doppler frequency depends on the velocity of a mobile terminal and the frequency of the transmitted signal. The multipath delay profile for a specific channel has two data points for each of several propagation paths: relative delay measured in microseconds (TS 45.005) or nanoseconds (TS 25.101) and relative signal strength measured in decibels. Most of the models specify a Rayleigh probability density and the *classical* Doppler spectrum in Equation (2.1).

With one exception ("very small cells" with 2 paths), the multipath profiles originally specified for evaluation of GSM systems (TS 45.005) have

Table 2.2 Summary of salient parameters of propagation models for cellular signal transmissions

Transmission impairment	Parameter	Description	Range of values
Attenuation	α	Propagation exponent	$3.5 \leq \alpha \leq 4.5$
Shadow fading	σ dB	Standard deviation	$6 \leq \sigma \leq 10$ dB
Doppler	f_d Hz	Doppler frequency	$0 \leq f_d \leq 7500$ Hz
Intersymbol interference	τ_{rms} μs τ_{max} μs	Root mean square delay spread Maximum delay spread	$1\ \mu\text{s} \leq \tau_{max} \leq 191\ \mu\text{s}$
Noise (including receiver noise)	N_0 W/Hz	Noise power spectral density	$\sim 10^{-21}$ W/Hz

either 6 or 12 paths with delays up to 20 μs (6 km path length difference). They have nomenclatures corresponding to the physical environments of cellular systems such as "rural area", "hilly terrain", and "urban area". The multipath profiles specified for 3G systems have 2, 4, or 6 paths and are distinguished by the equipment velocity (3 km/h for pedestrians and 120 km/h for vehicles) and abstract type labels "A" and "B". In addition, 3GPP TS 25.101 specifies two families of multipath models with dynamically varying relative path delays. In each family there are two propagation paths in which the relative delays change continuously with time. One family is labeled "moving propagation conditions" with relative delays up to 6 μs (1.8 km path length difference) and the other "birth-death propagation conditions" with relative delays up to 191 μs (57.3 km path length difference).

Table 2.2 is a summary of some salient parameters of propagation models used to analyze cellular signal transmissions.

2.3 Orthogonal Frequency Division Multiplexing

The adoption of OFDM for downlink radio transmission by 3GPP for cellular long term evolution and SC-FDMA for uplink transmission follows the successful implementation of OFDM for a variety of other applications including digital subscriber loops, wide area broadcasting (digital audio and video), and local area networks.

OFDM is a multi-carrier system as shown in Figure 2.7. It multiplexes the data on multiple carriers and transmits them in parallel. OFDM uses orthogonal subcarriers, which overlap in the frequency domain. Figure 2.8 shows the spectrum of ten orthogonal signals with minimum frequency separation. Each signal is constant over one symbol period and the spectrum

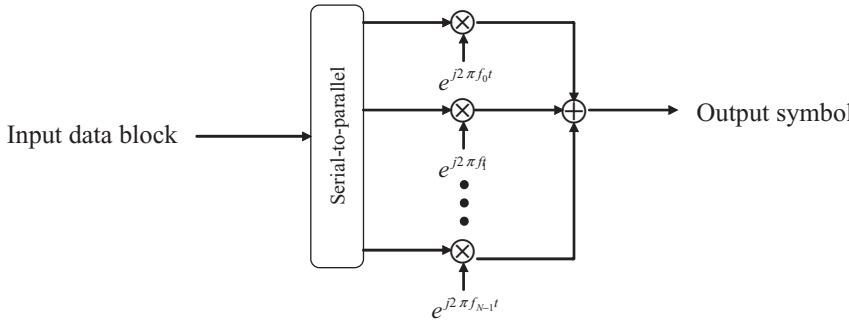

Figure 2.7 A general multi-carrier modulation system

has a *sin*(*x*)/*x shape*. Because it uses overlapping orthogonal subcarriers, the spectral efficiency is very high compared to conventional frequency division multiplexing (FDM), which requires guard bands between the adjacent sub-bands.

2.3.1 Signal Processing

The basic idea of OFDM is to divide a high-speed digital signal into several slower signals and transmit each slower signal in a separate frequency band. The slow signals are frequency multiplexed to create one waveform. If there are enough slow narrowband signals, the symbol duration in each

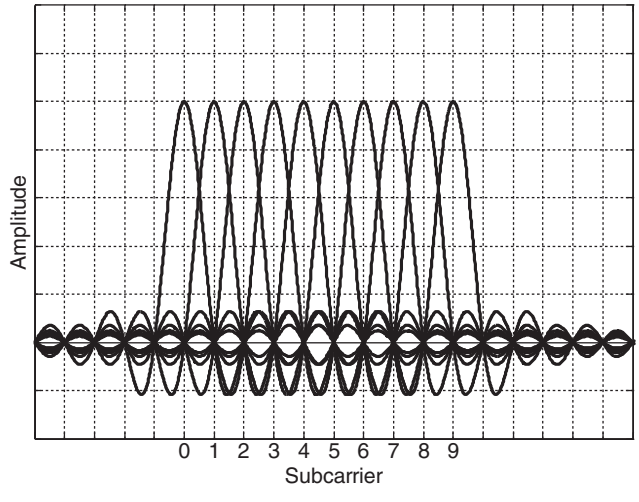

Figure 2.8 Orthogonal subcarriers in OFDM

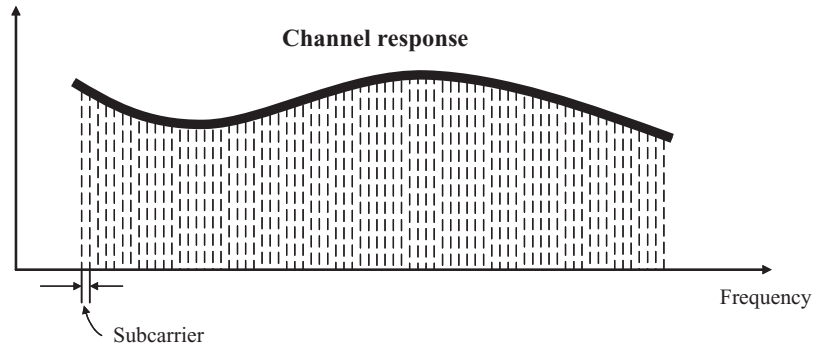

Figure 2.9 Channel response and the subcarriers in the frequency domain

one is long enough to essentially eliminate inter-symbol interference. Even though the fast fading is frequency-selective across the entire OFDM signal band, it is effectively flat in the band of each low-speed signal as shown in Figure 2.9.

This idea of using frequency division to eliminate inter-symbol interference was first applied in a military communication system, Kineplex, in the 1950s [5] using analog radio technology. The use of orthogonal signals to carry the different low-speed signals was introduced in the 1960s, and the roots of current implementations based on digital signal processing date from the early 1970s [5].

The discrete Fourier transform (DFT) and its inverse (IDFT) are the signal processing techniques at the heart of OFDM implementations. Usually they are realized as a fast Fourier transform (FFT) and an inverse FFT (IFFT). Figure 2.10 shows the essential elements of an OFDM transmitter and receiver using digital signal processing technology. The binary input to the OFDM modulator is the output of a channel coder that introduces an error correcting code and cyclic redundancy check to the information signal to be transmitted. The digital baseband modulator, typically performing quadrature amplitude modulation (QAM), transforms the binary input signal into a sequence of complex-valued multilevel modulation symbols. A signal processor then performs an IDFT on a sequence of N modulation symbols to produce one OFDM symbol, consisting of one transformed modulation symbol in each of N frequency *sub-bands*.

The N sub-band samples obtained from the IDFT are transmitted sequentially over a fading channel and the receiver performs a DFT to recover the N time-domain modulation symbols from the received frequency domain representation. The channel inversion operation compensates for the linear distortion introduced by multipath propagation. Finally a

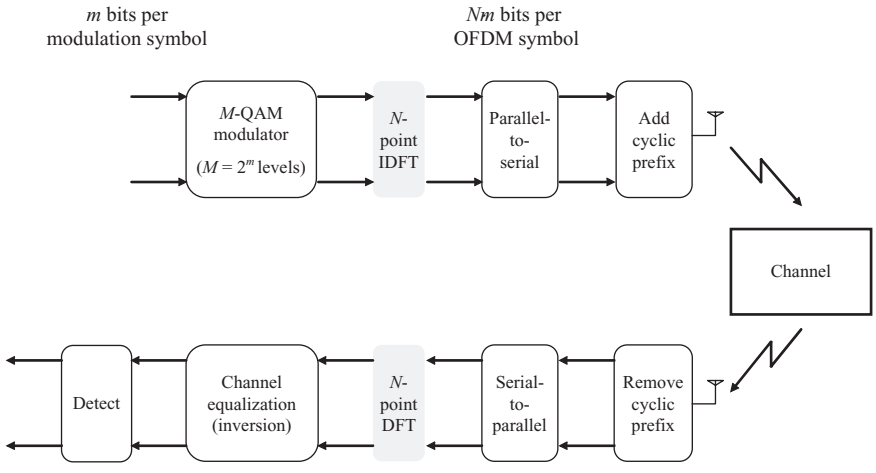

Figure 2.10 Essential OFDM signal processing

detector (demodulator) produces a binary signal corresponding to the original input to the OFDM transmitter. To eliminate interference between successive modulation symbols, the symbol duration in each sub-band, τ_{sub} seconds, should be greater than the maximum delay spread of the channel: $\tau_{sub} > \tau_{max}$. The sub-band symbol duration is proportional to the number of sub-bands: $\tau_{sub} = N \cdot \tau_{mod}$, where τ_{mod} seconds is the duration of a modulation symbol. Therefore the minimum number of sub-bands is $N > \tau_{max}/\tau_{mod}$. For a channel with a maximum rms delay spread of 10 μs and a transmission scheme with modulation symbols of duration 0.13 μs (used in 5 MHz channels in the 3GPP LTE specification), $N > 76$ sub-bands. The LTE specification calls for 512 subcarriers in 5 MHz channels. Therefore the system can operate without inter-symbol interference in channels with path duration up to $512 \times 0.13 = 66.7$ μs.

Although the operations shown in Figure 2.10 eliminate inter-symbol interference from the slow signals in the different frequency bands, the delay spread of the channel can still cause interference between successive OFDM symbols. To reduce this type of inter-symbol interference, the OFDM system introduces a *guard time*, τ_g seconds, between successive OFDM symbols. To be effective, it is necessary that $\tau_g \geq \tau_{max}$. This guard time corresponds to the transmission time of G modulation samples and during the guard time, at the beginning of each OFDM symbol transmission interval, the transmitter reproduces the final G transformed modulation signals generated by the IDFT processor. The G modulation samples transmitted during the guard time are referred to as the *cyclic prefix* (CP) of the

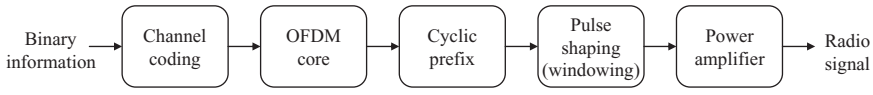

Figure 2.11 OFDM transmitter components

OFDM symbol. Figure 2.10 shows a frequency domain equalizer (channel inversion) operating on the output symbols in each frequency band. The channel inversions are simple because of the long time duration of each symbol in an OFDM system.

Figure 2.11 is a more complete picture of the signal processing operations that take place at an OFDM transmitter. In addition to the core OFDM system elements in Figure 2.10, it shows the channel coding, cyclic prefix, and power amplifier as well as a pulse-shaping (windowing) filter. The pulse-shaping filter attenuates signal energy outside of the nominal OFDM bandwidth. In a practical device, most of the operations in Figures 2.10 and 2.11 are digital. Digital-to-analog conversion and radio-frequency modulation take place after pulse shaping in Figure 2.11.

The components of an OFDM receiver invert the operations in the transmitter.

2.3.2 Advantages and Weaknesses

The principal advantage of OFDM in broadband radio systems is the strong reduction in inter-symbol interference, which would otherwise impose a heavy signal processing burden on a receiver. In summary, OFDM has the following advantages:

- For a given channel delay spread, the receiver complexity is much lower than that of a single carrier system with a time domain equalizer.
- Spectral efficiency is high because it uses overlapping orthogonal subcarriers in the frequency domain.
- Modulation and demodulation are implemented using IDFT and DFT, respectively, and fast Fourier transform (FFT) algorithms can be applied to make the overall system efficient.
- Capacity can be significantly increased by adapting the data rate per subcarrier according to the signal-to-noise ratio (SNR) of the individual subcarrier.

A principal weakness of OFDM is the high peak-to-average power ratio (PAPR). The transmitted signal is the sum of all the modulated subcarriers

and high amplitude peaks are inevitable because many of the subcarriers are in phase for some input sequences. The amplitude peaks impose a heavy burden on the power amplifier of a transmitter. Relative to time-domain transmission techniques, OFDM is also more vulnerable to frequency offset. It also requires an adaptive or coded scheme to overcome spectral nulls in the channel.

The decision of 3GPP to specify OFDM for downlink transmission in future cellular systems and SC-FDMA for uplink transmission places both the main transmitter burden (power amplifier) and the main receiver burden (compensation for inter-symbol interference) at base stations rather than at portable terminals.

2.4 Single Carrier Modulation with Frequency Domain Equalization

2.4.1 Frequency Domain Equalization

An equalizer compensates for linear distortion introduced by the multipath propagation channel. For broadband channels, conventional time domain equalizers are impractical because of the very long channel impulse response in the time domain. Frequency domain equalization (FDE) is more practical for such channels.

Channel equalization is essentially an inverse filtering of the linear distortion introduced to the channel by the multipath propagation. From a linear time invariant system perspective, linear filtering is a convolution operation in the time domain and a point-wise multiplication operation in the frequency domain. The Fourier transform, converts the time domain signal to a frequency domain signal, which can be equalized by dividing it point-by-point by an estimate of the channel frequency response. Figure 2.12 shows the basic operation of time domain equalization (convolution) and frequency domain equalization (point-wise multiplication).

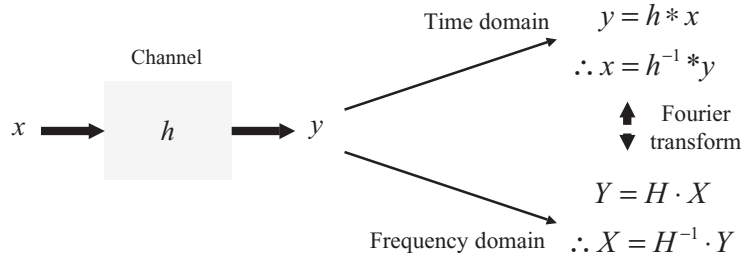

Figure 2.12 Basic idea behind FDE

Using DFT, the frequency domain equalization can be easily implemented using modern digital signal processors (DSP). Because the DFT size does not grow linearly with the length of the channel response, the complexity of FDE is much lower than that of the equivalent time domain equalizer for broadband channels.

Single carrier modulation with frequency domain equalization (SC/FDE) is a practical technique for mitigating the effects of frequency-selective fading. It delivers performance similar to OFDM with essentially the same overall complexity, even for a long channel impulse response [6],[7]. Figure 2.13 shows the block diagrams of an SC/FDE receiver and, for comparison, an OFDM receiver. We can see that both systems use the same communication component blocks and the only difference between the two diagrams is the location of the IDFT block. Thus, one can expect the two systems to have similar link level performance and spectral efficiency.

An SC/FDE modulator transmits modulation symbols sequentially. It divides the sequence of modulation symbols into blocks and adds a cyclic prefix (CP) to the beginning of each block. The CP is a copy of the last part of the block as shown in Figure 2.14. As in OFDM, the CP prevents inter-block interference. It also ensures that the convolution of the channel impulse response with the modulated symbols has the form of a circular convolution. This matches the signal processing performed by the channel with the signal processing performed by the FDE because multiplication in the DFT-domain is equivalent to circular convolution in the time domain.

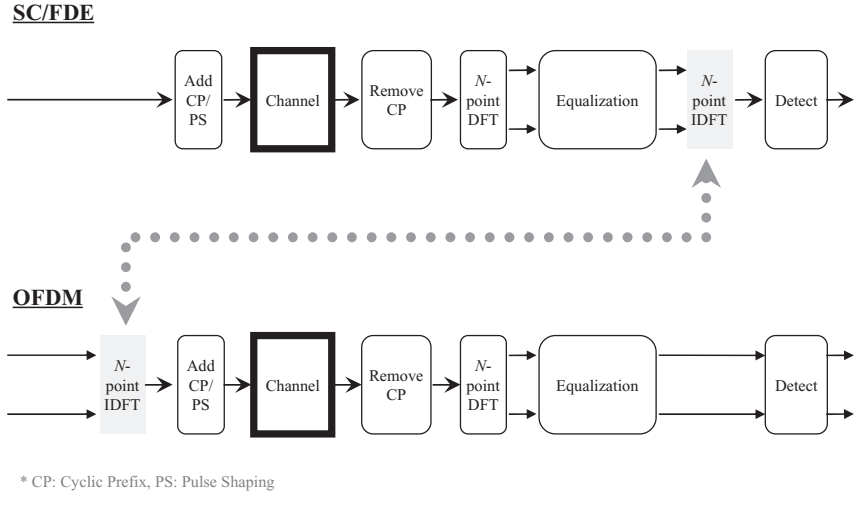

Figure 2.13 Block diagrams of SC/FDE and OFDM systems

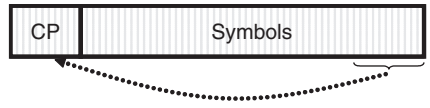

Figure 2.14 Cyclic prefix (CP)

It should be noted that the problem of aligning the signal processing in the receiver with the signal transformation performed by the channel is a general problem for frequency domain equalization using discrete transforms. When the data signal propagates through the channel, it linearly convolves with the channel impulse response. Because an equalizer attempts to invert the channel impulse response, it should perform the same type of convolution as the channel, either linear convolution or circular convolution. One way to resolve this problem is to add a CP in the transmitter that will make the channel filtering look like a circular convolution and match it to the DFT-based FDE. Another approach is not to use a CP but perform an "overlap and save" method [8] in the frequency domain equalizer to emulate the linear convolution.

As shown in Figure 2.13, an SC/FDE receiver transforms the received signal to the frequency domain by applying a DFT. It performs equalization in the frequency domain. Most of the well-known time domain equalization techniques, such as minimum mean-square error (MMSE) equalization, decision feedback equalization, and turbo equalization, can be applied to the FDE [9]–[13]. After the equalization, an IDFT transforms the single carrier signal back to the time domain and a detector recovers the original modulation symbols. In contrast, OFDM employs a separate detector for each subcarrier.

2.4.2 Comparison with OFDM

OFDM and SC/FDE are similar in many ways. However, there are distinct differences that make the two systems perform differently. The main differences are in the nature of the equalizers. SC/FDE employs both a DFT and an IDFT in the receiver, whereas OFDM has the IDFT at the transmitter and the DFT at the receiver.

In the receiver, OFDM performs data detection on a per-subcarrier basis in the frequency domain whereas SC/FDE performs data detection in the time domain after the additional IDFT operation, as shown in Figure 2.15. This difference means that OFDM is more sensitive to a null in the channel spectrum and it requires channel coding or power/rate control to overcome this vulnerability.

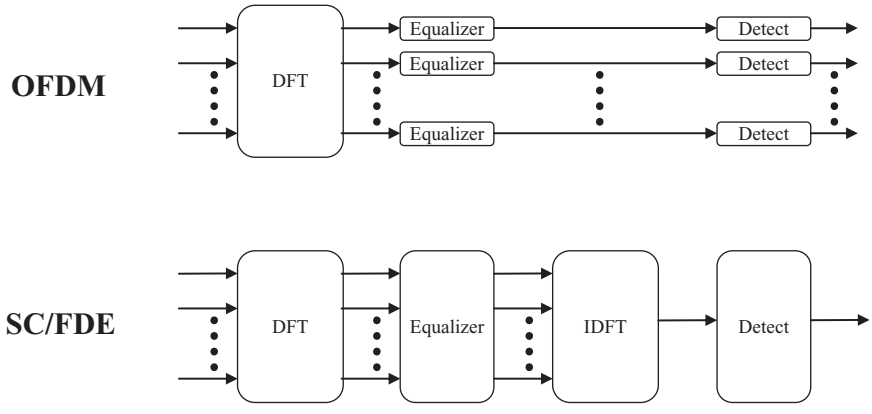

Figure 2.15 OFDM and SC/FDE receivers

Also, the duration of the modulated time symbols is expanded in the case of OFDM with parallel transmission of the data block during the elongated time period, as shown in Figure 2.16. Also, the system bandwidth B_s Hz is subdivided into smaller-bandwidth subcarriers and the individual data is conveyed on each subcarrier.

In summary, SC/FDE has advantages over OFDM as follows:

- low PAPR due to single carrier modulation at the transmitter;
- robustness to spectral null;

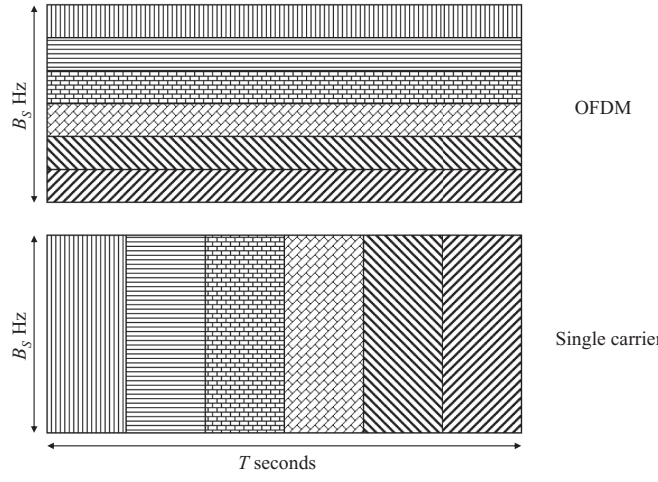

Figure 2.16 OFDM and SC/FDE symbols: there are six data symbols and the system bandwidth is B_s Hz

- lower sensitivity to carrier frequency offset;
- lower complexity at the transmitter that benefits the mobile terminal in cellular uplink communications.

The next chapter describes Single Carrier FDMA (SC-FDMA), which is an extension of SC/FDE to accommodate multi-user access.

2.5 Summary

In this chapter, we first surveyed the key characteristics of wireless radio channels. Among the impairments of the wireless channel, multipath propagation is a significant obstacle for broadband wireless systems. A multipath channel causes inter-symbol interference (ISI) in the time domain and frequency selectivity in the frequency domain.

There are two practical approaches to overcoming the effects of a multipath channel. One approach is to use a multi-carrier modulation, such as OFDM, and the other approach is to use frequency domain equalization (FDE). OFDM extends the symbol duration of the individual data and uses orthogonal subcarriers to convey the lower rate data in parallel, which mitigates the ISI. Also, with the system bandwidth divided into narrow sub-bands, each sub-band sees a flat fading channel, instead of a frequency selective channel. Single carrier modulation with frequency domain

Table 2.3 Comparison between OFDM and SC/FDE

	OFDM	SC/FDE
Similarities	DFT/IDFT-based implementation and use of cyclic prefix Frequency domain equalization Lower complexity than conventional time domain equalizer	
Dissimilarities	Multi-carrier transmission	Single-carrier transmission
	Parallel transmission of the data with low individual symbol rate	Sequential transmission of the data with high individual symbol rate
	High peak-to-average power ratio	Low peak-to-average power ratio
	Sensitive to frequency offset	Less sensitive to frequency offset
	Sensitive to spectral null	Robust to spectral null
	Frequency-selective adaptive bit/power loading possible	Frequency-selective adaptive bit/power loading *not* possible

equalization (SC/FDE) essentially has the same performance and structures as OFDM. It addresses the ISI and frequency-selectivity problem by means of frequency domain equalization along with cyclic prefix and discrete transforms (DFT/IDFT). Table 2.3 compares OFDM and SC/FDE.

References

[1] Rappaport, T.S., *Wireless Communications: Principles and Practice*, Prentice Hall PTR, 2nd edition, 2002.

[2] Sklar, B., "Rayleigh Fading Channels in Mobile Digital Communication Systems: Part I: Characterization," *IEEE Commun. Mag.*, vol. **35**, no. 7, July 1997, pp. 90–100.

[3] 3GPP, *3GPP TS 25.101 – Technical Specification Group Radio Access Network; User Equipment (UE) Radio Transmission and Reception (FDD) (Release 7)*, Sep. 2007.

[4] 3GPP, *3GPP TS 45.005 – Technical Specification Group GSM/EDGE Radio Access Network; Radio Transmission and Reception (Release 7)*, Sep. 2006.

[5] van Nee, R. and Prasad, R., *OFDM for Wireless Multimedia Communications*, Artech House, 2000.

[6] Sari, H., Karam, G., and Jeanclaude, I., "Transmission Techniques for Digital Terrestrial TV Broadcasting," *IEEE Commun. Mag.*, vol. **33**, no. 2, Feb. 1995, pp. 100–109.

[7] Falconer, D., Ariyavisitakul, S.L., Benyamin-Seeyar, A., *et al.*, "Frequency Domain Equalization for Single-Carrier Broadband Wireless Systems," *IEEE Commun. Mag.*, vol. **40**, no. 4, Apr. 2002, pp. 58–66.

[8] Oppenheim, A.V., Schafer, R.W., and Buck, J.R., *Discrete-Time Signal Processing*, Prentice Hall, 2nd edition, 1999.

[9] Kaleh, G.K., "Channel Equalization for Block Transmission Systems," *IEEE J. Select. Areas Commun.*, vol. **13**, no. 1, Jan. 1995, pp. 110–121.

[10] Clark, M.V., "Adaptive Frequency-Domain Equalization and Diversity Combining for Broadband Wireless Communications," *IEEE J. Sel. Areas Commun.*, vol. **16**, no. 8, Oct. 1998, pp. 1385–1395.

[11] Tüchler, M. and Hagenauer, J., "Linear Time and Frequency Domain Turbo Equalization," *Proc. IEEE 53rd Veh. Technol. Conf. (VTC)*, vol. **2**, May 2001, pp. 1449–1453.

[12] Benvenuto, N. and Tomasin, S., "Iterative Design and Detection of a DFE in the Frequency Domain," *IEEE Trans. Commun.*, vol. **53**, no. 11, Nov. 2005, pp. 1867–1875.

[13] Pancaldi, F. and Vitetta, G.M., "Block Channel Equalization in the Frequency Domain," *IEEE Trans. Commun.*, vol. **53**, no. 3, Mar. 2005, pp. 463–471.

3

Single Carrier FDMA

3.1 Introduction

Orthogonal Frequency Division Multiple Access (OFDMA) and Single Carrier Frequency Division Multiple Access (SC-FDMA) are modified versions of the OFDM and SC/FDE schemes described in Chapter 2. In contrast with the techniques described in Chapter 2, the multiple access techniques presented in this chapter transmit several signals simultaneously. All the orthogonal frequency division techniques employ a discrete set of orthogonal subcarriers distributed across the system bandwidth. They all include discrete transforms to move signals between the time domain and frequency domain. To transmit several signals simultaneously the multiple access techniques assign the signals to mutually exclusive sets of subcarriers. Because broadband channels experience frequency-selective fading, the FDMA techniques can employ channel dependent scheduling to achieve multi-user diversity, and because the fading characteristics of the terminals in different locations are statistically independent, the scheduling techniques can assign each terminal to subcarriers with favorable transmission characteristics at the location of the terminal.

The WiMAX cellular system uses OFDMA for transmission of signals both from the base station and from the mobile terminals. By contrast, 3GPP prescribes OFDMA for downlink transmission and SC-FDMA for uplink transmission in the long term evolution (LTE) of cellular systems in order to make the mobile terminal power-efficient. Anticipating future versions of present CDMA systems, the partnership project 3GPP2 is working on a variant of SC-FDMA using code spreading for the uplink of the Ultra Mobile Broadband (UMB) technique [1]. One disadvantage of OFDMA is the high peak-to-average power ratio (PAPR), which raises the cost and

Single Carrier FDMA: A New Air Interface for Long Term Evolution Hyung G. Myung and David J. Goodman
 ISBN: 978-0-470-72449-1

lowers the power efficiency of a transmitter's power amplifier. With a lower PAPR, the power amplifiers at mobile terminals employing SC-FDMA can be simpler and more power-efficient than they would be with OFDMA transmission. On the other hand, with its high signaling rate, the frequency domain equalizer of an SC-FDMA link is far more complicated than an OFDMA equalizer. With SC-FDMA transmission confined to the LTE uplink, complicated equalizers are required only at base stations and not at mobile terminals.

In this chapter, we introduce SC-FDMA signal processing operations in the next section. Section 3.3 describes the three approaches to assigning mobile terminals to subcarriers: localized FDMA (LFDMA), distributed FDMA (DFDMA), and interleaved FDMA (IFDMA), a special case of distributed FDMA. Section 3.4 presents the time-domain representations of SC-FDMA signals. Sections 3.5 and 3.6 describe the relationships of SC-FDMA to OFDMA and direct sequence CDMA with frequency domain equalization, respectively.

3.2 SC-FDMA Signal Processing

Figure 3.1 shows an SC-FDMA transmitter sending one *block* of data to a receiver. The input of the transmitter and the output of the receiver are complex modulation symbols. Practical systems dynamically adapt the modulation technique to the channel quality, using binary phase shift keying (BPSK) in weak channels and up to 64-level quadrature amplitude modulation (64-QAM) in strong channels. The data block consists of M complex modulation symbols generated at a rate R_{source} symbols/second. Figure 3.2 provides details of the three central elements of the transmitter in Figure 3.1. The M-point discrete Fourier transform (DFT) produces M frequency domain symbols that modulate M out of N orthogonal subcarriers spread over a bandwidth

$$W_{channel} = N \cdot f_0 \text{ [Hz]} \tag{3.1}$$

where f_0 Hz is the subcarrier spacing. The channel transmission rate is

$$R_{channel} = \frac{N}{M} \cdot R_{source} \text{ [symbols/second]} \tag{3.2}$$

If Q denotes the bandwidth spreading factor, i.e.,

$$Q = \frac{R_{channel}}{R_{source}} = \frac{N}{M} \tag{3.3}$$

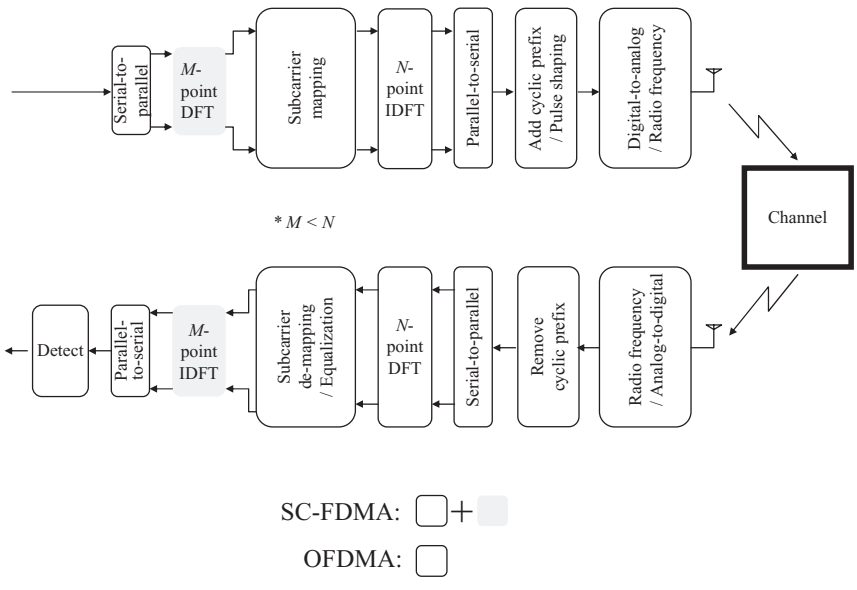

Figure 3.1 Transmitter and receiver structure of SC-FDMA and OFDMA systems

then, the SC-FDMA system can handle up to Q orthogonal source signals with each source occupying a different set of M orthogonal subcarriers. In the notation of Figure 3.2, x_m ($m = 0, 1, \ldots, M-1$) represents modulated source symbols and X_k ($k = 0, 1, \ldots, M-1$) represents M samples of the DFT of x_m. Y_l ($l = 0, 1, \ldots, N-1$) represents the frequency domain samples after subcarrier mapping and y_n ($n = 0, 1, \ldots, N-1$) represents the transmitted time domain channel symbols obtained from the inverse DFT (IDFT) of Y_l. The *subcarrier mapping* block in Figures 3.1 and 3.2 assigns frequency domain modulation symbols to subcarriers. The mapping

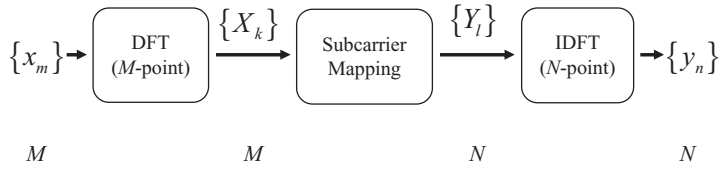

Figure 3.2 Generation of SC-FDMA transmit symbols; there are N subcarriers among which M ($< N$) subcarriers are occupied by the input data

process is sometimes referred to as *scheduling*. Because spatially dispersed terminals have independently fading channels, SC-FDMA and OFDMA can benefit from channel dependent scheduling. The inverse transform (IDFT) in Figures 3.1 and 3.2 creates a time domain representation, y_n, of the N subcarrier symbols. The parallel-to-serial converter places $y_0, y_1, \ldots, y_{N-1}$ in a time sequence suitable for modulating a radio frequency carrier and transmission to the receiver.

The transmitter in Figure 3.1 performs two other signal processing operations prior to transmission. It inserts a set of symbols referred to as cyclic prefix (CP) in order to provide a guard time to prevent inter-block interference (IBI) due to multipath propagation. The transmitter also performs a linear filtering operation referred to as pulse shaping in order to reduce out-of-band signal energy. The cyclic prefix is a copy of the last part of the block. It is inserted at the start of each block for two reasons. First, the CP acts as a guard time between successive blocks. If the length of the CP is longer than the maximum delay spread of the channel, or roughly, the length of the channel impulse response, then, there is no IBI. Second, since the CP is a copy of the last part of the block, it converts a discrete time linear convolution into a discrete time circular convolution. Thus, transmitted data propagating through the channel can be modeled as a circular convolution between the channel impulse response and the transmitted data block, which in the frequency domain is a point-wise multiplication of the DFT frequency samples. Then, to remove the channel distortion, the DFT of the received signal can simply be divided by the DFT of the channel impulse response point-wise.

One commonly used pulse-shaping filter is a raised-cosine filter. The frequency domain and time domain representations of the filter are as follows:

$$P(f) = \begin{cases} T, & 0 \le |f| \le \dfrac{1-\alpha}{2T} \\ \dfrac{T}{2}\left\{1 + \cos\left[\dfrac{\pi T}{\alpha}\left(|f| - \dfrac{1-\alpha}{2T}\right)\right]\right\}, & \dfrac{1-\alpha}{2T} \le |f| \le \dfrac{1+\alpha}{2T} \\ 0, & |f| \ge \dfrac{1+\alpha}{2T} \end{cases} \tag{3.4}$$

$$p(t) = \frac{\sin(\pi t/T)}{\pi t/T} \cdot \frac{\cos(\pi \alpha t/T)}{1 - 4\alpha^2 t^2/T^2} \tag{3.5}$$

where T is the symbol period and α is the roll-off factor.

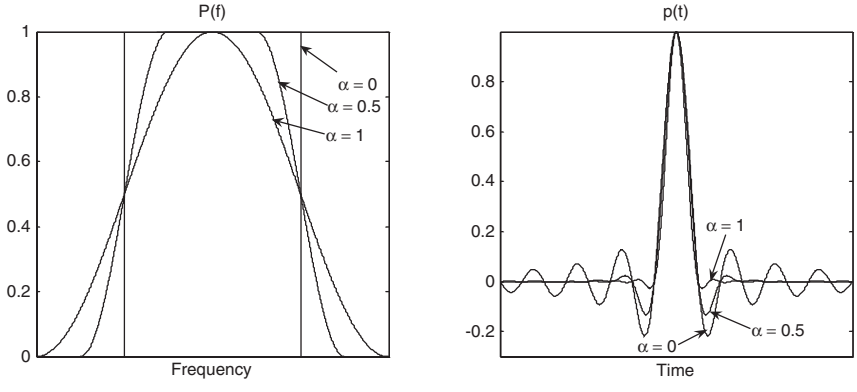

Figure 3.3 Raised-cosine filter

Figure 3.3 shows the raised-cosine filter graphically in the frequency domain and time domain. Roll-off factor α ranges from 0 to 1 and controls the amount of out-of-band radiation. With $\alpha = 0$, the filter is an ideal bandpass filter that suppresses all out-of-band radiation. As α increases, the out-of-band radiation increases. In the time domain, the side lobes of the filter impulse response increase as α decreases and this increases the peak power of the transmitted signal after pulse shaping. Therefore the choice of filter roll-off factor requires a compromise between the goals of low out-of-band radiation and low peak-to-average power ratio. We discuss the effect of pulse shaping on the peak power characteristics in Chapter 7.

The DFT in the receiver of Figure 3.1 transforms the received signal to the frequency domain in order to recover N subcarriers. The de-mapping operation isolates the M frequency domain samples of each source signal. Because SC-FDMA uses single carrier modulation, it encounters substantial linear distortion manifested as inter-symbol interference (ISI). The frequency domain equalizer cancels the ISI. The IDFT in the receiver of Figure 3.1 transforms equalized symbols back to the time domain where a detector produces the received sequence of M modulation symbols.

Figure 3.4 illustrates SC-FDMA receiver operation from a multiple user access perspective in the uplink. Before performing the basic SC-FDMA demodulation process, the base station separates the users in the frequency domain during the subcarrier de-mapping process.

Figure 3.1 indicates that SC-FDMA incorporates the signal processing elements of OFDMA and adds a DFT at the input of the transmitter and a corresponding IDFT at the output of the receiver. Because the SC-FDMA transmitter expands the signal bandwidth to cover the bandwidth of the channel, SC-FDMA is sometimes referred to as DFT-spread OFDMA. Section 3.5 compares OFDMA and SC-FDMA in further detail.

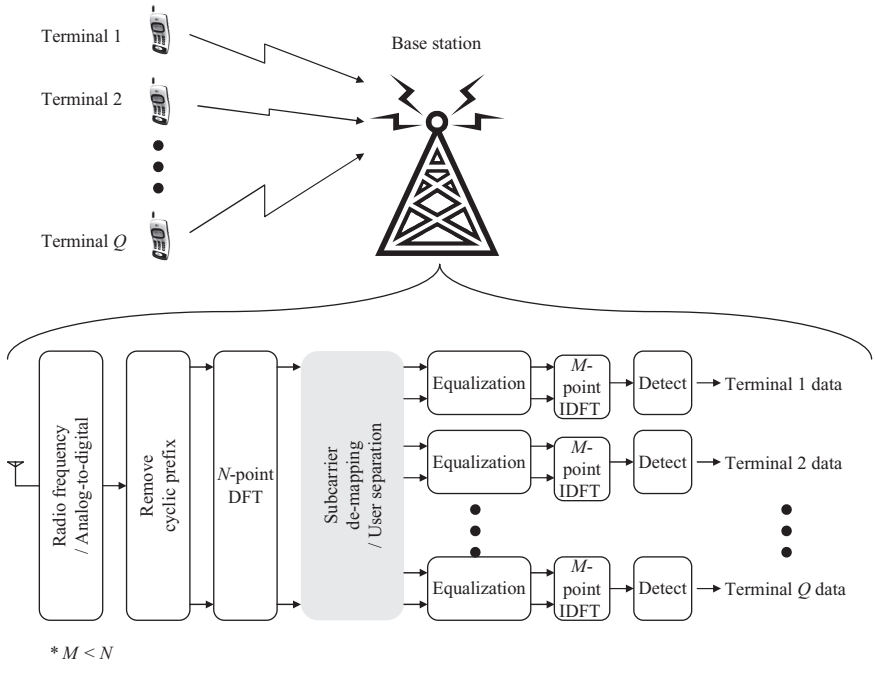

Figure 3.4 SC-FDMA receiver structure from a multiple user access perspective with Q terminals in the uplink

3.3 Subcarrier Mapping

Figure 3.5 shows two methods of assigning the M frequency domain modulation symbols to subcarriers: *distributed* subcarrier mapping and *localized* subcarrier mapping. In the localized subcarrier mapping mode, the modulation symbols are assigned to M adjacent subcarriers. In the distributed mode, the symbols are equally spaced across the entire channel bandwidth. In both modes, the IDFT in the transmitter assigns zero amplitude to the $N - M$ unoccupied subcarriers. We refer to the localized subcarrier mapping mode of SC-FDMA as localized FDMA (LFDMA) and distributed subcarrier mapping mode of SC-FDMA as distributed FDMA (DFDMA). The case of $N = Q \times M$ for the distributed mode with equidistance between occupied subcarriers is referred to as Interleaved FDMA (IFDMA) [2], [3]. IFDMA is a special case of SC-FMDA and it is very efficient in that the transmitter can modulate the signal strictly in the time domain without the use of DFT and IDFT. In Section 3.4, we show that for IFDMA, the combination of the DFT and IDFT reduces to a single complex multiplication, equivalent to a phase rotation of each modulation symbol at the input to the transmitter.

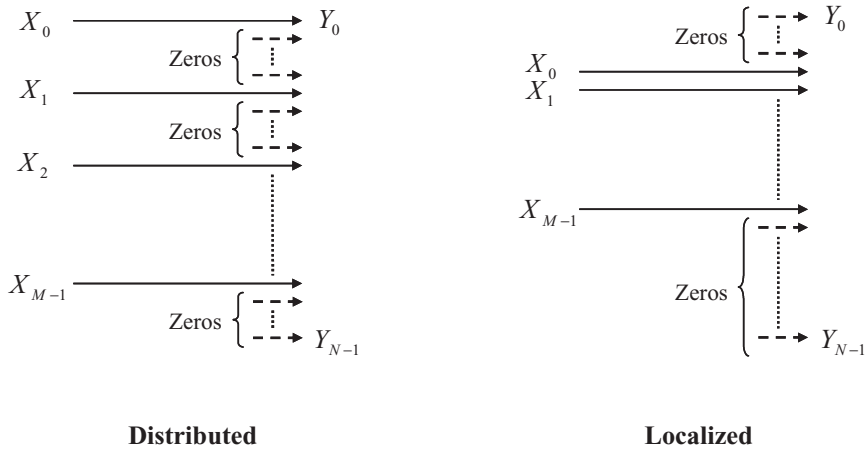

Figure 3.5 Subcarrier mapping modes; distributed and localized

Figure 3.6 illustrates three examples of SC-FDMA transmit symbols in the frequency domain for $M = 4$ symbols per block, $N = 12$ subcarriers, and $Q = N/M = 3$ terminals. In the localized mode, the four modulation symbols occupy subcarriers 0, 1, 2, and 3: $Y_0 = X_0$, $Y_1 = X_1$, $Y_2 = X_2$, $Y_3 = X_3$, and $Y_i = 0$ for $i \neq 0, 1, 2, 3$. In the distributed mode with modulation symbols equally spaced over all the subcarriers, $Y_0 = X_0$, $Y_2 = X_1$, $Y_4 = X_2$, $Y_6 = X_3$, and in the interleaved mode, $Y_0 = X_0$, $Y_3 = X_1$, $Y_6 = X_2$, $Y_9 = X_3$.

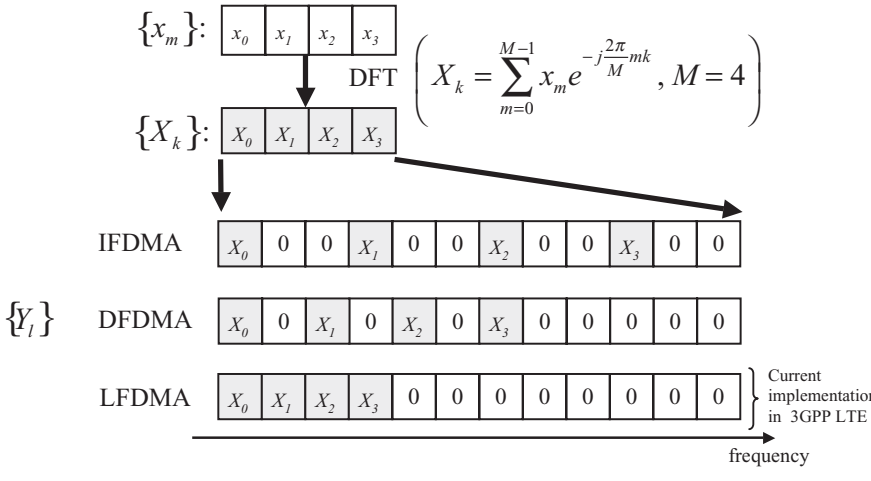

Figure 3.6 An example of different subcarrier mapping schemes for $M = 4$, $Q = 3$, and $N = 12$

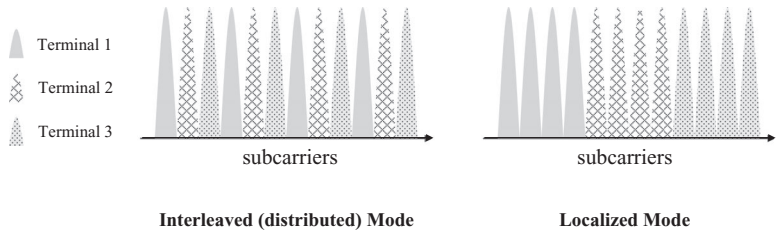

Figure 3.7 Subcarrier allocation methods for multiple users (3 users, 12 subcarriers, and 4 subcarriers allocated per user)

Figure 3.7 shows IFDMA and LFDMA demonstrating that the signals of the three different terminals arriving at a base station occupy mutually exclusive sets of subcarriers.

From a resource allocation point of view, subcarrier mapping methods are further divided into static scheduling and channel-dependent scheduling (CDS) methods. CDS assigns subcarriers to users according to the channel frequency response of each user. For both scheduling methods, distributed subcarrier mapping provides frequency diversity because the transmitted signal is spread over the entire bandwidth. With distributed mapping, CDS incrementally improves performance. By contrast, CDS is of great benefit with localized subcarrier mapping because it provides significant multi-user diversity. Chapter 5 contains a detailed description of channel dependent scheduling.

3.4 Time Domain Representation of SC-FDMA Signals

For IFDMA, LFDMA, and DFDMA, the three operations in Figure 3.2 can be viewed as one linear operation on the sequence of modulation symbols $\{x_m: m = 0, 1, 2, \ldots, M-1\}$. Therefore each element of the output sequence $\{y_n: n = 0, 1, 2, \ldots, N-1\}$ is a weighted sum of the elements of the input sequence, where the weights are complex numbers. In the case of IFDMA, the weights are zero for all but one element of the input sequence. The set of operations reduces to multiplying each input symbol by a complex number with unit magnitude and repeating the input sequence with proper phase rotation Q times, where Q is the bandwidth expansion factor.

Section 3.4.1 derives this property for the example $M = 4$ symbols per block, $N = 12$ subcarriers and $Q = 3$ terminals. Section 3.4.1 also shows graphically the spectrum and time sequence of an IFDMA signal block. The formulas for the time sequences of LFDMA and DFDMA are more complicated than for IFDMA. Sections 3.4.2 and 3.4.3 show the spectrum of each of these two subcarrier mapping techniques along with

the formulas for the elements of the time sequence. The detailed derivation of the time domain samples for IFDMA, LFDMA, and DFDMA can be found in [4].

3.4.1 Time Domain Symbols of IFDMA

For IFDMA, the combination of the DFT and IDFT in the transmitter of Figures 3.1 and 3.2 reduce to the simple signal processing operations of multiplying each input symbol by a complex number with unit magnitude and repeating the input sequence with proper phase rotation Q times, where Q is the bandwidth expansion factor. The multiplication is equivalent to a rotation of each complex modulation symbol in the transmission block. To verify that this is true, we observe two properties of the DFT and its inverse: (a) equally spaced nonzero samples in one domain correspond to a periodic sequence in the other domain; and (b) a shift of r in the frequency domain corresponds to a phase rotation of each time sample. The phase rotation is accomplished by multiplying each sample by $\exp(j2\pi rn/N)$, where N is the number of points in the inverse transform, r is the amount of the frequency shift, and n is the output sample number in the time domain. The following paragraph is a detailed mathematical demonstration of this property. Figure 3.8 is an illustration for our example of $M = 4$ symbols per block, $Q = 3$ terminals, and $N = Q \times M = 12$ subcarriers.

For one input signal, $\{Y_l\colon l = 0, 1, 2, \ldots, N-1\}$ is the spectrum of the transmitted SC-FDMA sequence representing the block of data $\{x_m\colon m = 0, 1, \ldots, M-1\}$. In IFDMA, the spectrum has M uniformly-spaced nonzero components, with adjacent samples separated by $Q-1$ samples in the frequency domain. The corresponding time domain signal $\{y_n\colon n = 0, 1, 2, \ldots, N-1\}$ is periodic with Q replicas distributed over times $n = 0, 1, 2, \ldots, M-1\ (= N/Q-1)$ and with phase rotation of $\exp(j\,2\pi rn/N)$. Consider the input signal $\{x_m\colon m = 0, 1, \ldots, M-1\}$ that occupies subcarriers $l = 0, Q, 2Q, \ldots, (M-1)\cdot Q$. The periodic transmitted time signal corresponding to the spread spectrum of this signal has the sequence $\{x_0/Q, x_1/Q, \ldots, x_{M-1}/Q\}$, repeated Q times (rotation of 0 radian). Now consider the signal from another terminal $\{u_m\colon m = 0, 1, \ldots, M-1\}$ that modulates the next set of equally spaced subcarriers $n = 1, Q+1, 2Q+1, \ldots, (M-1)\cdot Q+1$. The spectrum of this signal $\{V_l\colon l = 0, 1, 2, \ldots, N-1\}$ is similar to the spectrum of Y_l, but with nonzero components shifted by one subcarrier. This shift in the frequency domain corresponds to multiplication in the time domain by $\exp(j2\pi n/N)$. Therefore the transmitted time domain sequence is u_0/Q, $u_1\ \exp(j2\pi/N)/Q, \ldots, u_{M-1}\exp(j2\pi(M-1)/N)/Q$, repeated Q times with appropriate phase rotations. In general, we have for

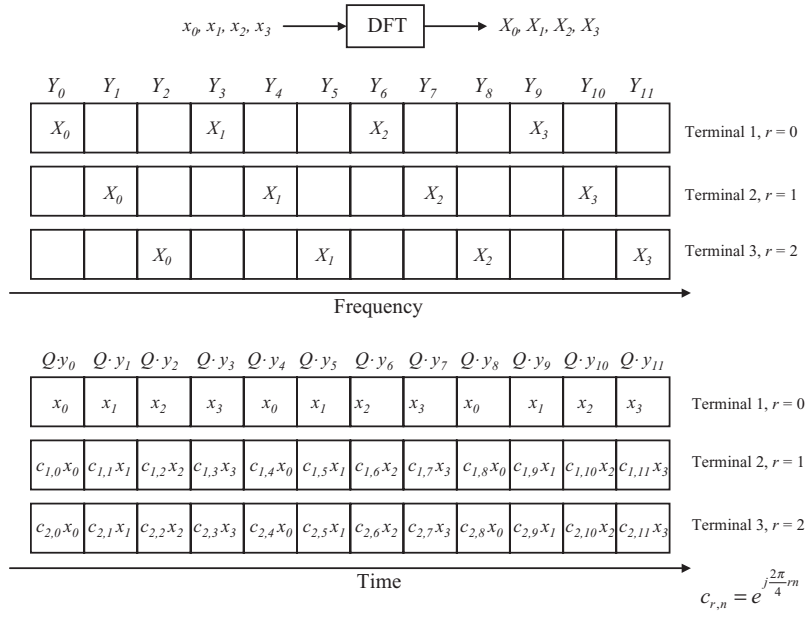

Figure 3.8 Illustration of IFDMA subcarrier mapping for $M = 4$ symbols per block, $Q = 3$ terminals, and $N = Q \times M = 12$ subcarriers

the input signal $\{x_m: m = 0, 1, \ldots, M - 1\}$ that modulates subcarriers $n = r, Q + r, 2Q + r, \ldots, (M - 1) + r$, the transmitted signal $\{x_m: m = 0, 1, \ldots, M - 1\}$ repeated Q times with phase rotation of $\exp(j2\pi rn/N)$.

The mathematical formulas corresponding to this description begin with frequency domain symbols Y_l

$$Y_l = \begin{cases} X_{l/Q}, & l = Q \cdot k \quad (0 \le k \le M - 1) \\ 0, & \text{otherwise} \end{cases} \tag{3.6}$$

where $0 \le l \le N - 1$ and $N = Q \cdot M$.

Let $n = M \cdot q + m$ $(0 \le q \le Q - 1, 0 \le m \le M - 1)$. Then,

$$\begin{aligned} y_n &= \left(y_{Mq+m}\right) \\ &= \frac{1}{N}\sum_{l=0}^{N-1} Y_l e^{j2\pi \frac{n}{N}l} = \frac{1}{N}\sum_{l=0}^{N-1} X_{l/Q} e^{j2\pi \frac{n}{N}l} = \frac{1}{Q}\cdot\frac{1}{M}\sum_{k=0}^{M-1} X_k e^{j2\pi \frac{n}{QM}Qk} \\ &= \frac{1}{Q}\cdot\frac{1}{M}\sum_{k=0}^{M-1} X_k e^{j2\pi \frac{Mq+m}{M}k} = \frac{1}{Q}\cdot\left(\frac{1}{M}\sum_{k=0}^{M-1} X_k e^{j2\pi \frac{m}{M}k}\right) \\ &= \frac{1}{Q}x_m = \frac{1}{Q}x_{(n) \bmod M} \end{aligned} \tag{3.7}$$

The resulting time symbols $\{y_n\}$ are simply a repetition of the original input symbols $\{x_m\}$ with a scaling factor of $1/Q$ in the time domain just as we described.

When the subcarrier allocation starts from the rth subcarrier ($0 < r \leq Q - 1$), then,

$$Y_l = \begin{cases} X_{l/Q-r}, & l = Q \cdot k + r \quad (0 \leq k \leq M - 1) \\ 0, & \text{otherwise} \end{cases} \tag{3.8}$$

Corresponding to Equation (3.7), the time symbols $\{y_n\}$ can be derived as

$$y_n = \frac{1}{Q} x_{(n) \bmod M} \cdot e^{j2\pi \frac{rn}{N}} \tag{3.9}$$

As can be seen from Equation (3.9), there is an additional phase rotation of $\exp(j2\pi rn/N)$ as noted earlier when the subcarrier allocation starts from rth subcarrier instead of subcarrier zero. This phase rotation will also apply to the other subcarrier mapping schemes.

3.4.2 Time Domain Symbols of LFDMA

Figure 3.9 is a diagram of the LFDMA subcarrier mapping. It shows the modulation symbols that occupy the 12 subcarriers $\{Y_l\}$ in the example.

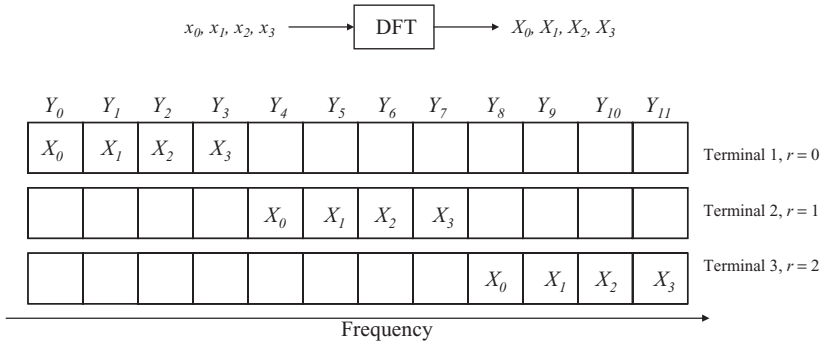

Figure 3.9 Illustration of LFDMA subcarrier mapping for $M = 4$ symbols per block, $Q = 3$ terminals, and $N = Q \times M = 12$ subcarriers

The time domain samples of the LFDMA signal can be expressed as follows [4]:

$$y_n = y_{Q\cdot m+q} = \begin{cases} \dfrac{1}{Q} x_{(n)_{\bmod M}}, & q = 0 \\ \dfrac{1}{Q} \cdot \left(1 - e^{j2\pi \frac{q}{Q}}\right) \cdot \dfrac{1}{M} \displaystyle\sum_{p=0}^{M-1} \dfrac{x_p}{1 - e^{j2\pi \left\{ \frac{(m-p)}{M} + \frac{q}{QM} \right\}}}, & q \neq 0 \end{cases} \tag{3.10}$$

Detailed derivations of Equation (3.10) are provided in Appendix A at the end of this book. As can be seen in Equation (3.10), the LFDMA signal in the time domain has exact copies of input time symbols with a scaling factor of $1/Q$ at sample positions that are integer multiples of Q. Intermediate values are weighted sums of all the time symbols in the input block.

3.4.3 Time Domain Symbols of DFDMA

Figure 3.10 is a diagram of the DFDMA subcarrier mapping. It shows the modulation symbols that occupy the 12 subcarriers, $\{Y_l\}$ in the example.

The time domain samples of the DFDMA signal can be expressed as follows [4]:

$$y_n = y_{Q\cdot m+q} = \begin{cases} \dfrac{1}{Q} \cdot x_{\left(\tilde{Q}(n)_{\bmod M}\right)_{\bmod M}}, & q = 0 \\ \dfrac{1}{Q}\left(1 - e^{j2\pi \frac{\tilde{Q}}{Q} q}\right) \cdot \dfrac{1}{M} \displaystyle\sum_{p=0}^{M-1} \dfrac{x_p}{1 - e^{j2\pi \left\{ \frac{(\tilde{Q}m-p)}{M} + \frac{\tilde{Q}q}{QM} \right\}}}, & q \neq 0 \end{cases} \tag{3.11}$$

where $\tilde{Q}$ $(1 \leq \tilde{Q} < Q)$ is the actual spreading factor. The time domain samples of DFDMA have the same structure as those of LFDMA. Detailed derivations of Equation (3.11) are provided in Appendix A.

3.4.4 Comparison of Subcarrier Mapping Schemes

Figure 3.11 shows the time domain samples for each subcarrier mapping described earlier. The IFDMA signal maintains the input time symbols in each sample whereas LFDMA and DFDMA have more complicated time samples because of the complex-weighted sum of the input symbols. This implies that higher peak power is expected for LFDMA and DFDMA

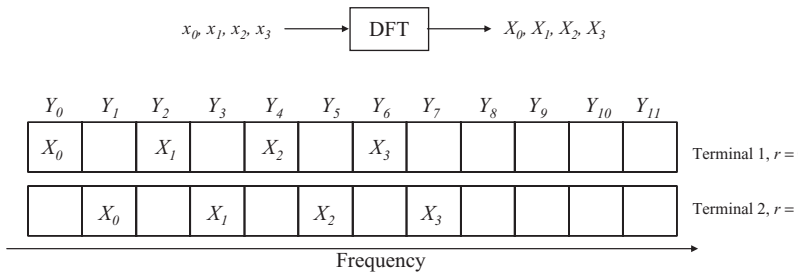

Figure 3.10 Illustration of DFDMA subcarrier mapping for $M = 4$ symbols per block, $Q = 3$ terminals, and $N = Q \times M = 12$ subcarriers

signals, which we will see through the numerical analysis of peak-to-average power ratio (PAPR) in Chapter 7.

Figure 3.12 shows one instance of the amplitude of the samples for each subcarrier mapping for $N = 64$ subcarriers, $M = 16$ subcarriers per block, $Q = 4$ spreading factor for IFDMA with four terminals, and $\tilde{Q} = 3$ spreading factor for DFDMA with three terminals. In Figure 3.12 there is no pulse shaping. For comparison Figure 3.12 also shows the corresponding OFDMA waveform. These particular input symbols for the SC-FDMA modulation used QPSK. For IFDMA, we can observe the constant amplitude that comes from maintaining the constant envelope property of QPSK. For LFDMA and DFDMA, we can see more fluctuation and higher peaks.

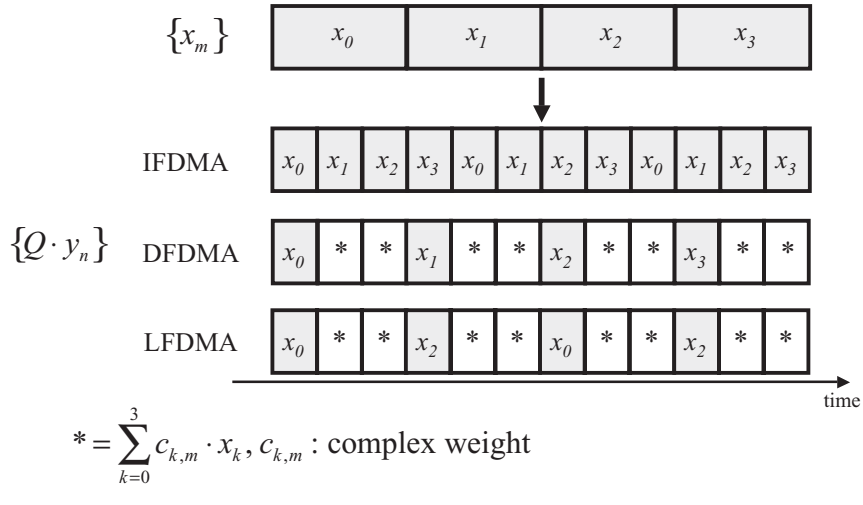

Figure 3.11 Time domain samples of different subcarrier mapping schemes

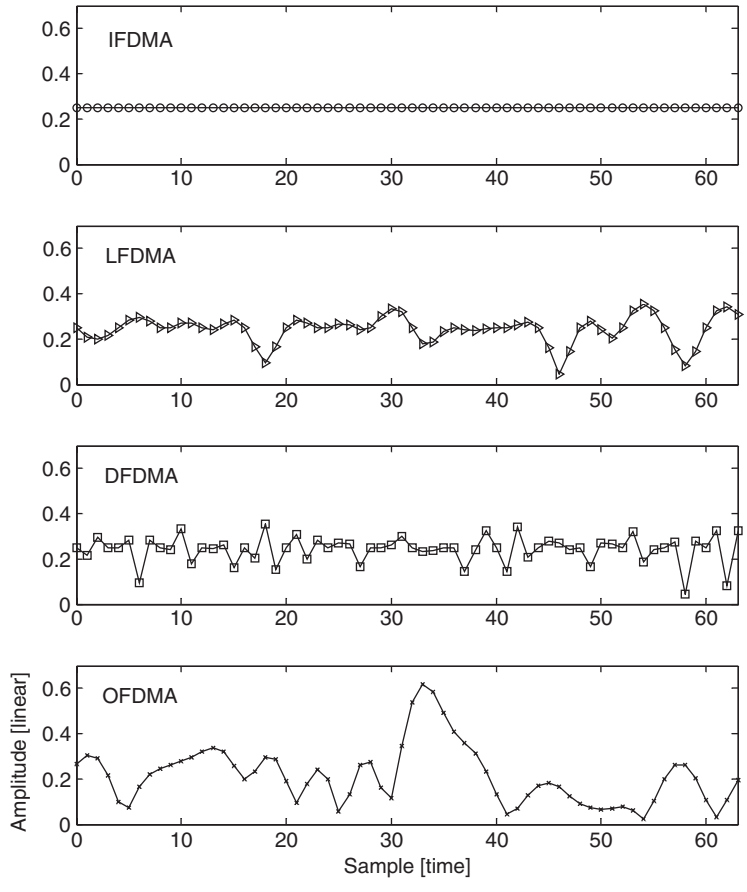

Figure 3.12 Amplitude of SC-FDMA and OFDMA samples for QPSK input modulation without pulse shaping with $N = 64$ subcarriers, $M = 16$ subcarriers per block, $Q = 4$ spreading factor for IFDMA with four terminals, and $\tilde{Q} = 3$ spreading factor for DFDMA with three terminals

Overall, all three single carrier subcarrier mapping schemes exhibit lower peak power than OFDMA.

3.5 SC-FDMA and Orthogonal Frequency Division Multiple Access

Section 2.4 describes the relationship between single carrier transmission and OFDM for the transmission of one signal occupying the entire system bandwidth. There is a similar relationship between OFDMA and SC-FDMA for the transmission of independent signals from dispersed

terminals to one base station. Figure 3.1 indicates that OFDMA and SC-FDMA transmitters and receivers perform many common signal-processing functions. The two techniques share the following properties:

- modulation and transmission of data in blocks consisting of M modulation symbols;
- division of the transmission bandwidth into sub-bands with information carried on discrete subcarriers;
- frequency domain channel equalization;
- the use of a cyclic prefix to prevent inter-block interference.

However, there are distinct differences that lead to different performance. The most obvious difference is that OFDMA transmits a multi-carrier signal whereas SC-FDMA transmits a single carrier signal. Because of this, SC-FDMA has a lower peak-to-average power ratio (PAPR) than OFDMA.

In the time domain, the duration of the modulated symbols is expanded in the case of OFDMA. When there are M symbols per block and N sub-carriers spread across the system bandwidth, both SC-FDMA and OFDMA can transmit signals from $Q = N/M$ terminals simultaneously. Figure 3.14 shows, for $M = 4$, $N = 12$, and $Q = 3$, that if the modulated symbol duration is T seconds, the OFDMA symbol duration is $M \times T$ seconds. This time expansion reduces inter-symbol interference (ISI), providing the main benefit of OFDMA. By contrast, SC-FDMA compresses the modulated symbols in time. The SC-FDMA symbol duration is T/Q seconds as in a TDMA system. SC-FDMA uses frequency domain equalization at the base station to cancel the ISI.

Figure 3.13 shows blocks of $M = 4$ modulated symbols from $Q = 3$ terminals each of duration T seconds occupying a bandwidth B_{source} Hz.

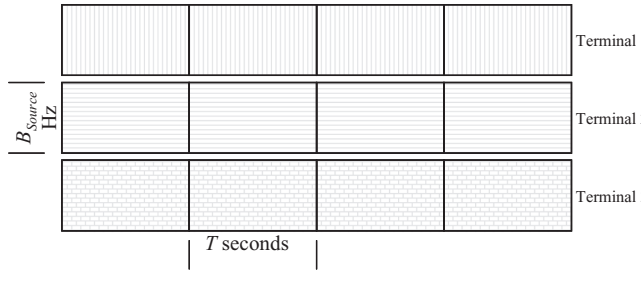

Figure 3.13 $M = 4$ modulation symbols from $Q = 3$ terminals; symbol duration is T seconds; source bandwidth is B_{Source} Hz

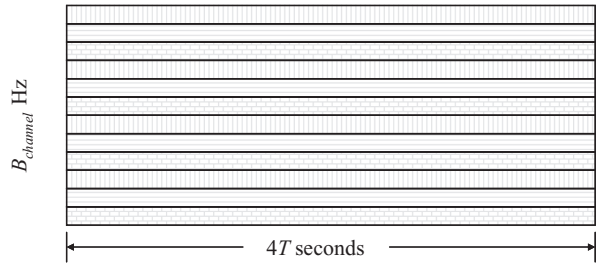

Figure 3.14 OFDMA compresses the individual data bandwidth to $B_{Source}/4$ Hz and expands the time to $4T$ seconds

Figure 3.14 shows an OFDMA signal with $N = 12$ subcarriers, each with bandwidth $B_{source}/4$ Hz. Each subcarrier carries one modulated symbol for $4T$ seconds. Figure 3.15 shows an SC-FDMA signal, using IFDMA scheduling. Here each modulated symbol occupies the entire bandwidth $B_{channel} = 3B_{source}$ Hz. Correspondingly, the symbol duration is reduced to $T/3$ seconds.

Figure 3.16 shows that OFDMA performs equalization and data detection separately for each subcarrier. By contrast, SC-FDMA performs equalization across the entire channel bandwidth. It then uses the IDFT to transform the signal from one terminal to the time domain prior to detection of the modulated symbols. The IDFT prior to symbol detection is necessary because, except for IFDMA, the transmitted signal consists of a weighted sum of all symbols in a block, as described in Section 3.4. The IDFT retrieves the original symbols from the composite signal. Because SC-FDMA effectively spreads each modulated symbol across the entire

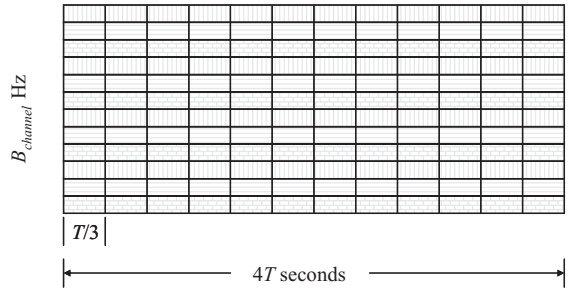

Figure 3.15 SC-FDMA expands the bandwidth to $B_{channel} = 3B_{Source}$; it compresses the symbol time to $T/3$ seconds

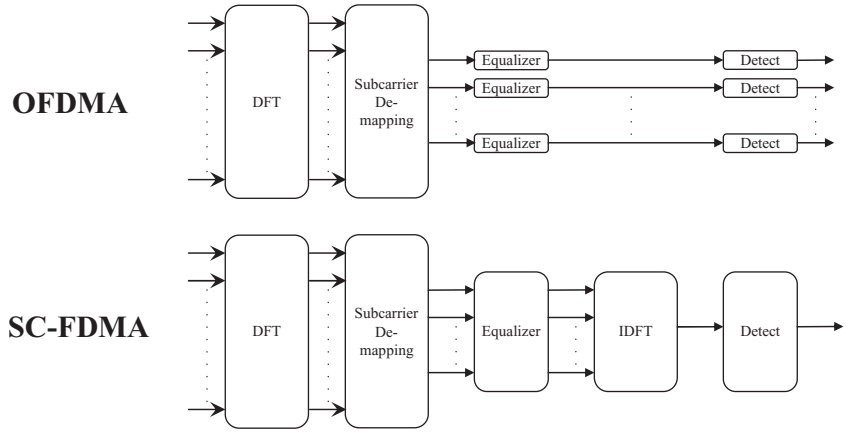

Figure 3.16 OFDMA and SC-FDMA; detection and equalization

channel bandwidth, it is less sensitive to frequency-selective fading than OFDMA, which transmits modulated symbols in narrow sub-bands.

One of the advantages of OFDMA over SC-FDMA is that channel-adaptive subcarrier bit and power loading is possible [5]. By adapting the symbol modulation and power for individual subcarriers, OFDMA is able to come close to the upper bound of the capacity limit for a given channel.

3.6 SC-FDMA and CDMA with Frequency Domain Equalization

Direct sequence code division multiple access (DS-CDMA) with frequency domain equalization (FDE) replaces the rake receiver, commonly used in the conventional DS-CDMA, with the frequency domain equalizer [6]. A rake receiver consists of a bank of correlators, each synchronized with one multipath component of the desired signal. As the number of multipaths increase, the frequency selectivity in the channel also increases and the complexity of the rake combiner increases. The use of FDE instead of rake combing can alleviate the complexity problem in DS-CDMA. Figure 3.17 is a block diagram of direct sequence CDMA with FDE.

The transmitter of DS-CDMA/FDE is the same as the conventional DS-CDMA except for the addition of a cyclic prefix. The spreading of the

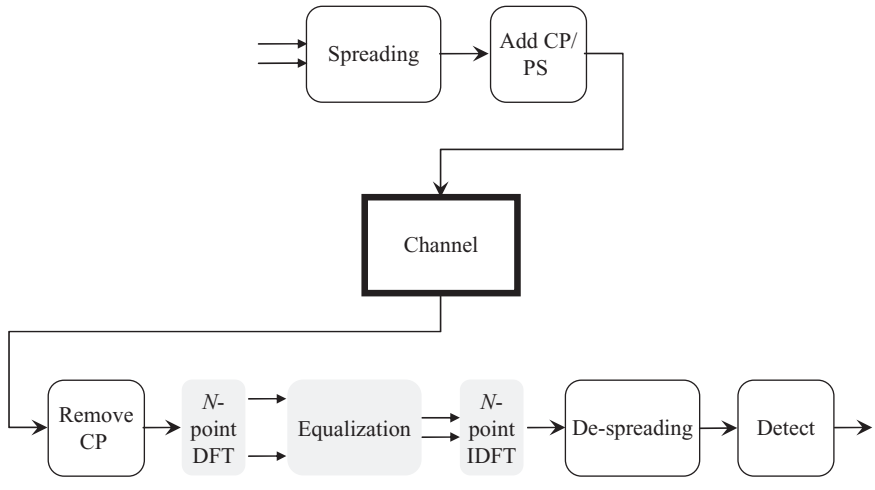

* CP: Cyclic Prefix, PS: Pulse Shaping

Figure 3.17 DS-CDMA with frequency domain equalization (FDE)

baseband digital signal produces a sequence of chips with bandwidth spread across the entire band of the channel. The FDE in the receiver cancels the inter-chip interference in the received signal. For small spreading factors, the performance of the rake receiver significantly degrades because of the inter-path interference and FDE has a much better performance. For large spreading factors, both have similar performance. More technical details of the DS-CDMA/FDE system can be found in [6].

SC-FDMA and DS-CDMA/FDE are similar in that both techniques achieve processing gain from spreading narrow-band data into a broader band. They both maintain low PAPR because of the single carrier transmission.

An interesting relationship between orthogonal DS-CDMA and IFDMA is that by exchanging the roles of spreading sequence and data sequence, DS-CDMA modulation becomes IFDMA modulation [7], [8]. An example of this observation is illustrated in Figure 3.18. We can see that the result of the spreading with exchanged roles is in the form of IFDMA modulated symbols.

One advantage of SC-FDMA over DS-CDMA/FDE is that channel dependent resource scheduling is possible to exploit frequency selectivity of the channel.

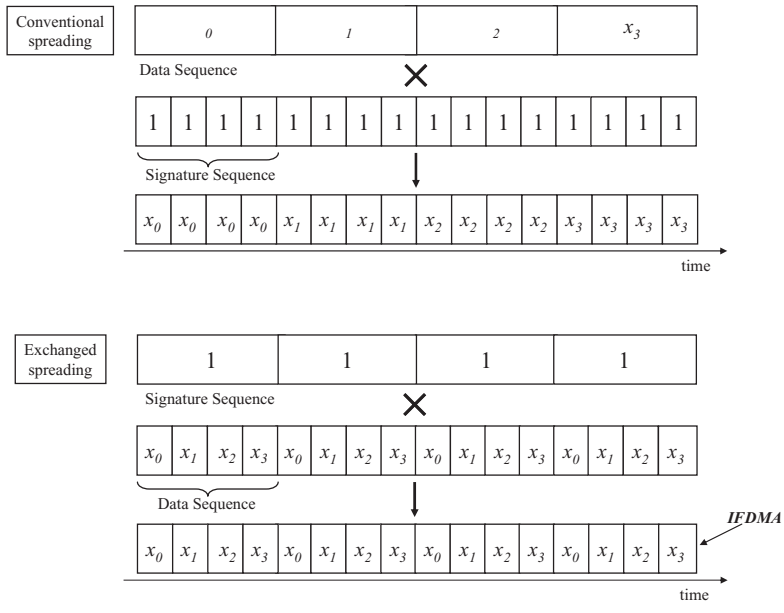

Figure 3.18 Spreading with the roles of data sequence and signature sequence exchanged for spreading signature of $\{1, 1, 1, 1\}$ with a data block size of 4

3.7 Single Carrier Code-Frequency Division Multiple Access (SC-CFDMA)

Conventional SC-FDMA cannot operate with some terminals using localized scheduling and others using distributed scheduling because it achieves orthogonality of sources by having each subcarrier occupied by no more than one terminal at any time. By using the orthogonal direct sequence spread spectrum technique prior to SC-FDMA modulation, both mappings can coexist with overlapping subcarriers as illustrated in Figure 3.19. We refer to this multiple access scheme as single carrier code-frequency division multiple access (SC-CFDMA), which can be viewed as a combination of DS-CDMA and SC-FDMA. This form of SC-FDMA is used in the 3GPP2 UMB uplink for control signaling.

Figure 3.20 shows the block diagram of an SC-CFDMA system and Figure 3.21 compares SC-FDMA and SC-CFDMA in terms of occupied subcarriers for the same number of users. In Figures 3.19 and 3.21, vertical lined-blocks refer to spreading code 1 and horizontal lined-blocks refer to spreading code 2. In SC-FDMA or OFDMA, the users are separated strictly in the frequency domain whereas SC-CFDMA separates different users in both the frequency domain and code domain.

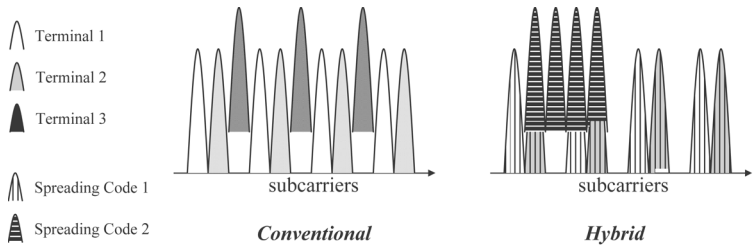

Figure 3.19 Conventional subcarrier mapping and hybrid subcarrier mapping; vertical lined-blocks refer to spreading code 1 and horizontal lined-blocks refer to spreading code 2

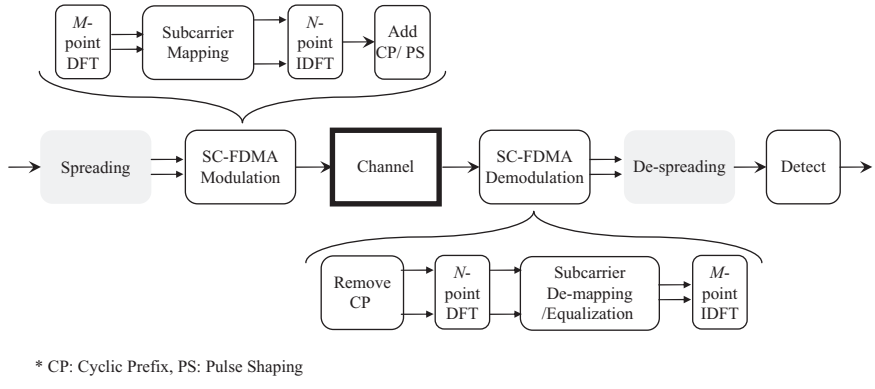

Figure 3.20 Block diagram of a single carrier code-frequency division multiple access (SC-CFDMA) system

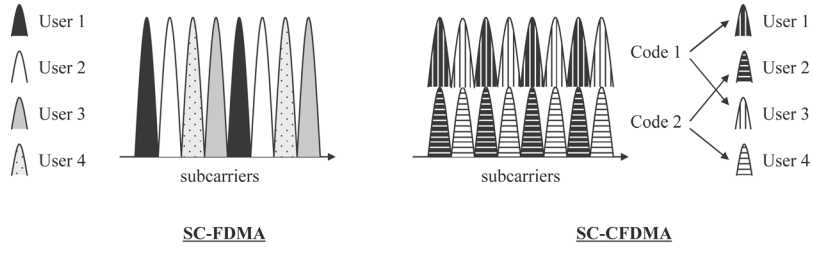

Figure 3.21 Comparison between SC-FDMA and SC-CFDMA in terms of occupied subcarriers for the same number of users; vertical lined-blocks refer to spreading code 1 and horizontal lined-blocks refer to spreading code 2

3.8 Summary

Single carrier FDMA (SC-FDMA) is a multiple access technique that utilizes single carrier modulation, orthogonal frequency multiplexing, and frequency domain equalization. It has similar performance and essentially the same overall complexity as orthogonal frequency division multiple access (OFDMA). One prominent advantage over OFDMA is that the SC-FDMA signal has better peak power characteristics because of its inherent single carrier structure. SC-FDMA has drawn great attention as an attractive alternative to OFDMA, especially in the uplink communications where better peak power characteristics greatly benefit the mobile terminal in terms of transmit power efficiency and manufacturing cost. Because of its merits, SC-FDMA has been chosen as the uplink multiple access scheme in 3GPP Long Term Evolution (LTE). Also, a modified form of SC-FDMA is used for the uplink control channel in 3GPP2 Ultra Mobile Broadband (UMB).

So why do we call this new multiple access scheme "Single Carrier" "FDMA"? As shown in Figure 3.22, SC-FDMA symbols are transmitted sequentially over a *single carrier* as opposed to the parallel transmission of OFDM/OFDMA over multiple carriers. Also, the users are orthogonally multiplexed and de-multiplexed in the *frequency domain*, which gives SC-FDMA an aspect of FDMA.

In this chapter, we first gave an overview of SC-FDMA and explained the transmission and reception operations in detail. SC-FDMA has two different approaches to subcarrier mapping: distributed and localized. In a distributed subcarrier mapping scheme, a user's data symbols occupy a set of subcarriers distributed over the entire frequency range of the channel and

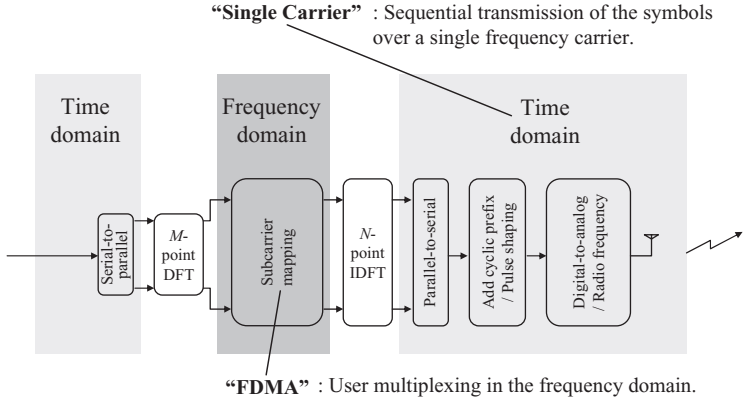

Figure 3.22 Why call it "Single Carrier" "FDMA"?

we achieve frequency diversity. In a localized subcarrier mapping scheme, a user's data symbols occupy a set of consecutive subcarriers and we can achieve multi-user diversity by means of channel-dependent scheduling. The two subcarrier mappings also affect the structure of the time domain signal and the peak power characteristics. The two approaches to subcarrier mapping give the network operator flexibility to adapt to the specific requirements of each operating environment.

SC-FDMA and other broadband multiple access schemes, namely OFDMA and direct sequence CDMA with frequency domain equalization (DS-CDMA/FDE), were compared in Sections 3.5 and 3.6. Figure 3.23 shows a summary of the comparisons. All three schemes use block-based processing, DFT-based frequency domain channel equalization, and cyclic prefix. SC-FDMA is similar to OFDMA in that users are multiplexed and de-multiplexed in the frequency domain via the subcarrier mapping and that frequency-selective channel-dependent scheduling is possible.

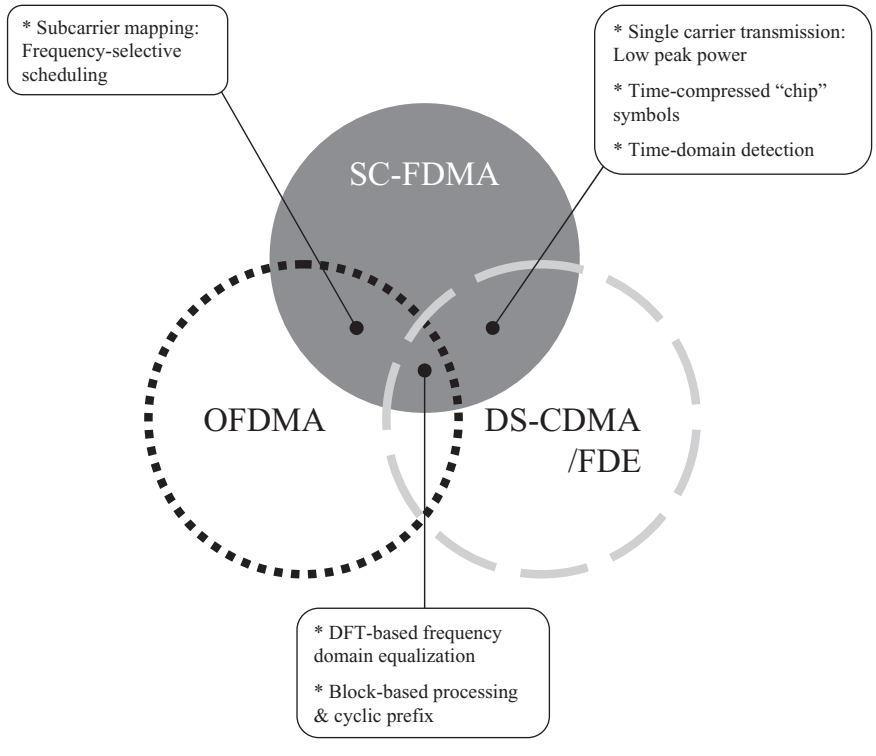

Figure 3.23 Similarities and dissimilarities among SC-FDMA, OFDMA, and DS-CDMA/FDE

SC-FDMA also bears similarities to DS-CDMA/FDE in terms of bandwidth spreading (time-compressed *chip* symbols), processing gain from spreading, low peak power, and time domain detection.

References

[1] Das, S., Li, S., Monogioudis, P., *et al*., "EV-DO Revision C: Evolution of the cdma2000 Data Optimized System to Higher Spectral Efficiencies and Enhanced Services," *Bell Labs Tech. Jour.*, vol. **11**, no. 4, Mar. 2007, pp. 5–24.

[2] Sorger, U., De Broeck, I., and Schnell, M., "Interleaved FDMA - A New Spread-Spectrum Multiple-Access Scheme," *Proc. IEEE ICC '98*, Atlanta, GA, Jun. 1998, pp. 1013–1017.

[3] Frank, T., Klein, A., and Costa, E., "IFDMA: A Scheme Combining the Advantages of OFDMA and CDMA," *IEEE Wireless Commun.*, vol. **14**, no. 3, June 2007, pp. 9–17.

[4] Myung, H.G., "Single Carrier Orthogonal Multiple Access Technique for Broadband Wireless Communications," Ph.D. Dissertation, Polytechnic University, Jan. 2007. Available online at http://hgmyung.googlepages.com/Hyung_G_Myung_PhD_thesis.pdf.

[5] Wong, C.Y., Cheng, R.S., Letaief, K.B., *et al*., "Multiuser OFDM with Adaptive Subcarrier, Bit, and Power Allocation," *IEEE J. Select. Areas Commun.*, vol. **17**, Oct. 1999, pp. 1747–1757.

[6] Adachi, F., Garg, D., Takaoka, S., *et al*., "Broadband CDMA Techniques," *IEEE Wireless Comm.*, vol. **12**, no. 2, Apr. 2005, pp. 8–18.

[7] Chang, C. and Chen, K., "Frequency-Domain Approach to Multiuser Detection in DS-CDMA Communications," *IEEE Comm. Letters*, vol. **4**, no 11, Nov. 2000, pp. 331–333.

[8] Chang, C. and Chen, K., "Frequency-Domain Approach to Multiuser Detection over Frequency-Selective Slowly Fading Channels," *IEEE International Symposium on Personal, Indoors and Mobile Radio Communications (PIMRC) 2002*, Lisboa, Portugal, Sep., 2002, pp. 1280–1284.

4

SC-FDMA in 3GPP Long Term Evolution

4.1 Introduction

4.1.1 3GPP Technical Specifications

Single carrier frequency division multiple access (SC-FDMA) has been adopted by the third generation partnership project (3GPP) [1] for uplink transmission in technology standardized for long term evolution (LTE) of cellular systems. 3GPP publishes standards for cellular systems that build on GSM, the second generation cellular system that has been adopted by hundreds of operating companies and used by billions of people throughout the world. GSM uses time division multiple access (TDMA) for radio transmission in 200 kHz bands. The third generation successor to GSM is referred to as Universal Terrestrial Radio Access (UTRA) and relies on wideband code division multiple access (W-CDMA) for radio transmission in 5 MHz bands. The letter G in GSM stands for "global" and the U in UTRA stands for "universal". LTE technology is referred to as E-UTRA (evolved UTRA), perhaps because 3GPP could not find an adjective more comprehensive than universal. It is anticipated that LTE technology will be ready for deployment in 2010. LTE uses orthogonal frequency division multiplexing (OFDM) for downlink radio transmission and SC-FDMA for uplink radio transmission. LTE anticipates transmissions in spectrum bands with widths ranging from 1.4 to 20 MHz. This choice of transmission technologies places the complex, power-hungry operations of frequency domain equalization (in SC-FDMA) and linear power amplification (in OFDM) at the base station, rather than in portable terminals. Both

Single Carrier FDMA: A New Air Interface for Long Term Evolution Hyung G. Myung and David J. Goodman
 ISBN: 978-0-470-72449-1

Table 4.1 LTE technical specifications

Specification index	Description of contents
TS 36.1xx	Equipment requirements: Terminals, base stations, and repeaters.
TS 36.2xx	Physical layer.
TS 36.3xx	Layers 2 and 3: Medium access control, radio link control, and radio resource control.
TS 36.4xx	Infrastructure communications (UTRAN = UTRA Network) including base stations and mobile management entities.
TS 36.5xx	Conformance testing.

UTRA and E-UTRA incorporate many core network standards formulated originally for GSM.

The specific application of SC-FDMA within E-UTRA appears in Technical Specifications (TS) and Technical Reports (TR) published by 3GPP. These documents all have numbers beginning with 36. Table 4.1 describes the scope of the technical specifications. The specifications do not explain the reasoning behind the choices of the technology. Appendix C is a guide to 3GPP documents that disclose this reasoning.

4.1.2 Contents of the Physical Layer Technical Specifications

The physical layer specifications consist of a general document (TS 36.201) and four documents (TS 36.211 through 36.214) with contents summarized in TS 36.201 section 5 as follows:

- *TS 36.201: Physical layer – General description* [2].
  - The contents of the layer 1 documents (TS 36.2xx series).
  - A general description of LTE layer 1.
- *TS 36.211: Physical channels and modulation* [3].
  - Definition of the uplink and downlink physical channels.
  - The structure of the physical channels, frame format, physical resource elements, etc.
  - Modulation (BPSK, QPSK, etc.).
  - Physical shared channel in uplink and downlink.
  - Reference signals in uplink and downlink.
  - Random access channel.
  - Primary and secondary synchronization signals.
  - OFDM signal generation in downlink.

  - SC-FDMA signal generation in uplink.
  - Scrambling, modulation, and up conversion.
  - Uplink-downlink timing relation.
  - Layer mapping and precoding in downlink.
- *TS 36.212: Multiplexing and channel coding* [4].
  - Channel coding schemes.
  - Coding of layer 1/layer 2 control information.
  - Interleaving.
  - Rate matching.
- *TS 36.213: Physical layer procedures* [5].
  - Synchronization procedures including cell search procedure and timing synchronization.
  - Power control procedure.
  - Random access procedure.
  - Physical downlink shared channel related procedures including channel quality indicator (CQI) reporting and multiple-input-multiple-output (MIMO) feedback.
  - Physical uplink shared channel related procedures including user equipment (UE) sounding and hybrid automatic repeat request (HARQ) ACK/NACK detection.
  - Physical shared control channel procedures, including assignment of shared control channels.
- *TS 36.214: Physical layer – Measurements* [6].
  - Measurements to be performed by layer 1 in user equipment (UE) and in the network (E-UTRAN).
  - Reporting of measurement results to higher layers and the network.
  - Handover measurements, idle-mode measurements, etc.

4.2 Protocol Layers and Channels

Figure 4.1 shows the LTE radio interface protocol architecture. It indicates three categories of channels moving information between protocol layers and the radio transmitter and receiver: physical channels, transport channels, and logical channels. SC-FDMA and OFDM are the signal formats of the physical channels. Table 4.2 contains a list of the nine physical channels defined in the LTE specifications: six downlink physical channels and three uplink physical channels.

The physical layer uses transport channels to exchange user information and network control information with the medium access control (MAC) sublayer of layer 2. As indicated in Table 4.3, there are four downlink transport channels and two uplink transport channels. The physical layer

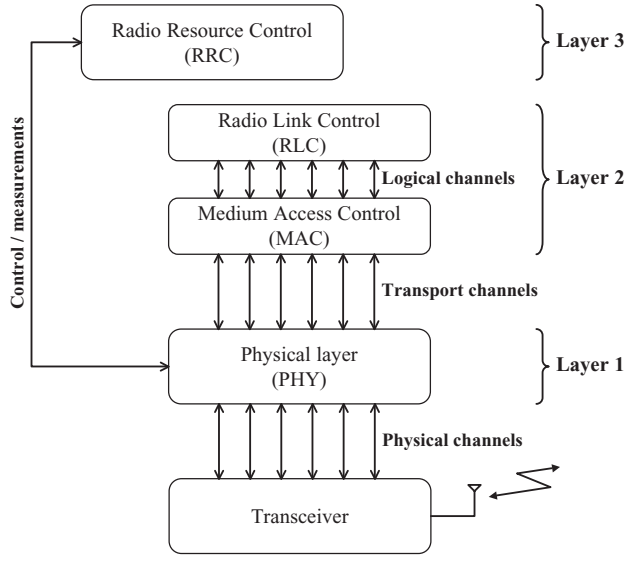

Figure 4.1 Protocol architecture of 3GPP LTE

Table 4.2 Physical channels

Physical channel name	Acronym	Downlink	Uplink
Physical broadcast channel	PBCH	x	
Physical control format indicator channel	PCFICH	x	
Physical downlink control channel	PDCCH	x	
Physical hybrid ARQ indicator channel	PHICH	x	
Physical downlink shared channel	PDSCH	x	
Physical multicast channel	PMCH	x	
Physical uplink control channel	PUCCH		x
Physical uplink shared channel	PUSCH		x
Physical random access channel	PRACH		x

Table 4.3 Transport channels

Transport channel name	Acronym	Downlink	Uplink
Broadcast channel	BCH	x	
Downlink shared channel	DL-SCH	x	
Paging channel	PCH	x	
Multicast channel	MCH	x	
Uplink shared channel	UL-SCH		x
Random access channel	RACH		x

Table 4.4 Logical channels

Logical channel name	Acronym	Control channel	Traffic channel
Broadcast control channel	BCCH	x	
Paging control channel	PCCH	x	
Common control channel	CCCH	x	
Multicast control channel	MCCH	x	
Dedicated control channel	DCCH	x	
Dedicated traffic channel	DTCH		x
Multicast traffic channel	MTCH		x

also communicates with the radio resources controller to exchange channel state information in the form of measurements and control commands that adapt the radio transmission to the state of the channel.

The LTE specifications use the term "logical channels" to refer to service access points for information transfer between the radio link control (RLC) sublayer of layer 2 and the MAC sublayer. The MAC sublayer assigns logical channels used by the radio link control sublayer of layer 2 to one of the transport channels in Table 4.3. Table 4.4 is a list of the seven LTE logical channels.

Figures 4.2 and 4.3 show the relationships among the physical channels, transport channels, and logical channels in Tables 4.2, 4.3, and 4.4. Figure 4.2 shows how the transport channels in Table 4.3 carry the downlink information to and from the logical channels of Table 4.4. The shared channel DL-SCH is capable of carrying information from all the logical channels except the paging control channel, which has its own transport channel,

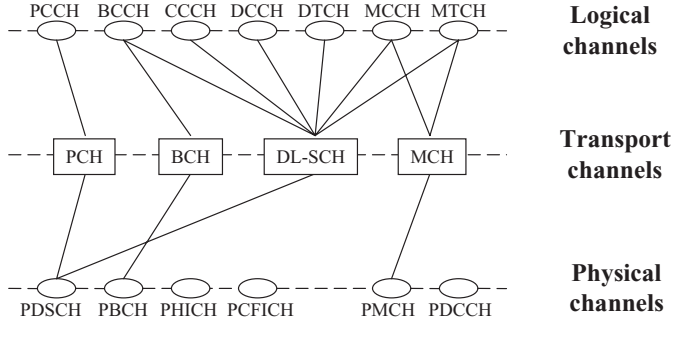

Figure 4.2 Downlink channels [7]. *Source:* ETSI (European Telecommunications Standards Institute) © 2008. 3GPP™ TSs and TRs are the property of ARIB, ATIS, CCSA, ETSI, TTA and TTC who jointly own the copyright in them. They are subject to further modifications and are therefore provided to you "as is" for information purposes only. Further use is strictly prohibited.

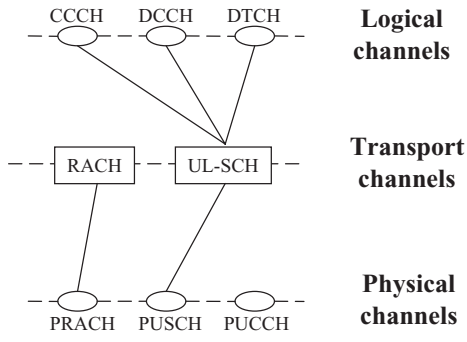

Figure 4.3 Uplink channels [7]. *Source:* ETSI (European Telecommunications Standards Institute) © 2008. 3GPP™ TSs and TRs are the property of ARIB, ATIS, CCSA, ETSI, TTA and TTC who jointly own the copyright in them. They are subject to further modifications and are therefore provided to you "as is" for information purposes only. Further use is strictly prohibited.

the PCH. Multicast traffic from the MTCH can be carried on the downlink shared channel or on a multicast physical channel, MCH.

As illustrated in Figure 4.3, all the uplink user information and network control information is carried in the uplink shared transport channel UL-SCH. The purpose of the random access channel is to send to the base station requests for transmission resources on the shared channel. Figure 4.3 also shows the three uplink physical channels. The Physical Uplink Shared Channel (PUSCH) carries user information and control information received on the uplink shared transport channel (UL-SCH). The Physical Uplink Control Channel (PUCCH) carries uplink control information received on the UL-SCH when there is no transmission on a PUSCH. The Physical Random Access Channel (PRACH) transmits a cyclic prefix (CP) and a signature sequence received from the random access transport channel. Its purpose is to transmit a request for transmission resources on one of the other types of physical channel.

In addition to user information and control information carried on physical channels, the physical layer transmits two types of reference signal in the uplink: Demodulation reference signals are used by the base station for uplink coherent demodulation and optional sounding reference signals are used for possible uplink channel quality estimation in uplink channel dependent scheduling. Demodulation reference signals appear in every PUSCH and every PUCCH transmission. Sounding reference signals require separate transmission resources.

3GPP publishes specifications for both time division duplex and frequency division duplex to carry information in both directions between user equipment and base stations.

4.3 Uplink Time and Frequency Structure

LTE specifies signal transmissions in six possible channel bandwidths ranging from 1.4 to 20 MHz. Each channel is divided into frequency bands of 15 kHz, each specified by a subcarrier frequency. For example, there are 72 subcarriers available in a 1.4 MHz channel and 1200 subcarriers available in a 20 MHz channel (as shown in Table 4.7 on page 70 [8]). All the LTE signals derive their timing from a clock operating at 30.72 MHz = 15 kHz $\times$ 2048. This is the timing required for the 2048 point discrete Fourier transform (DFT) specified for 20 MHz channels. Therefore, the basic time interval in an LTE physical channel is one clock period of duration:

$$T_S = 1/(30.72 \times 10^6) \approx 32.255 \text{ ns per clock period} \tag{4.1}$$

Table 4.5 summarizes the symbols used in the specifications and the remainder of this chapter to describe the uplink physical layer.

4.3.1 Frames and Slots

Downlink and uplink transmissions are organized into *radio frames* with

$$T_f = 307200 \times T_s = 10 \text{ msec per frame.} \tag{4.2}$$

As indicated in Figure 4.4, each frame consists of 20 slots, numbered from 0 to 19, each of duration 0.5 msec for frequency division duplex (FDD) transmissions. A consecutive pair of slots starting with an even-numbered slot is referred to as a *subframe*. The 1 msec duration of a subframe is an LTE *transmission time interval* (TTI). With FDD transmissions, all the slots can carry uplink physical channels or reference signals. The FDD frame structure is referred to as frame structure type 1.

Table 4.5 Summary of symbols for uplink physical layer description

Symbol	Description
T_s	Duration of basic LTE clock period; $1/(30.72 \times 10^6)$ seconds.
T_f	Duration of one radio frame: 0.5 msec.
N_{symb}^{UL}	Number of SC-FDMA symbols per resource block.
N_{sc}^{RB}	Number of subcarriers per resource block: 12.
N_{RB}^{UL}	Number of resource blocks in the uplink.
M_{SC}^{PUSCH}	Number of subcarriers allocated to the mobile terminal: $M_{sc}^{PUSCH} = N_{sc}^{RB} \times 2^{\alpha_2} \times 3^{\alpha_3} \times 5^{\alpha_5} \leq N_{sc}^{RB} \times N_{RB}^{UL}$, where α_2, α_3, and α_5 are nonnegative integers.
M	Total number of subcarriers including the guard band area. Also, the size of IDFT in the transmitter and DFT in the receiver.

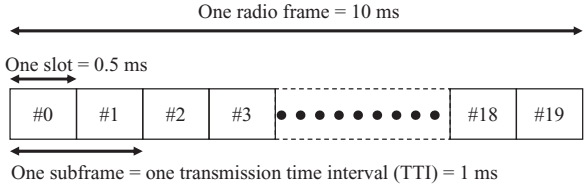

Figure 4.4 Frame structure for frequeny division duplex transmissions (frame structure type 1) [3]. *Source:* ETSI (European Telecommunications Standards Institute) © 2007. 3GPP™ TSs and TRs are the property of ARIB, ATIS, CCSA, ETSI, TTA and TTC who jointly own the copyright in them. They are subject to further modifications and are therefore provided to you "as is" for information purposes only. Further use is strictly prohibited.

The situation is more complicated for time division duplex (TDD) transmissions because the uplink and downlink transmissions share the same frequency band. Figure 4.5 shows the TDD frame structure, referred to as frame structure type 2. In each 10 msec frame, eight of the ten subframes carry physical channels. Subframes 0 and 5 always carry downlink physical channels. The other frames can carry either uplink or downlink physical channels. Subframes 1 and 6 carry synchronization signals. GP is a guard period, and UpPTS and DwPTS refer to uplink and downlink pilot time slots, respectively. Subframes 1 and 6 always contain GP and either DwPTS or UpPTS depending on the direction of transmission of the physical channels in the other subframes.

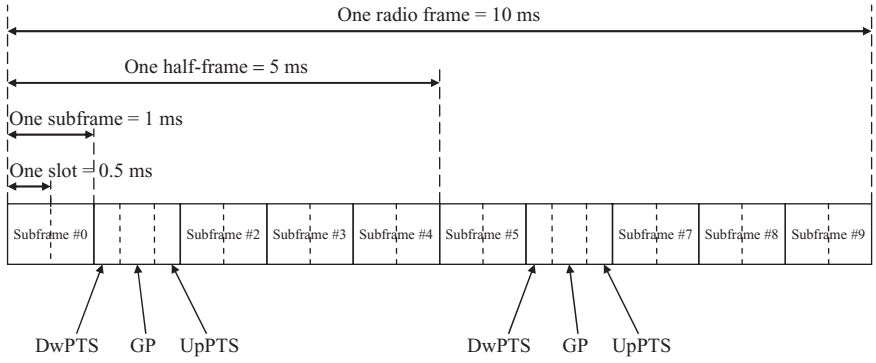

Figure 4.5 Frame structure for time division duplex transmissions (frame structure type 2) [3]. *Source:* ETSI (European Telecommunications Standards Institute) © 2007. 3GPP™ TSs and TRs are the property of ARIB, ATIS, CCSA, ETSI, TTA and TTC who jointly own the copyright in them. They are subject to further modifications and are therefore provided to you "as is" for information purposes only. Further use is strictly prohibited.

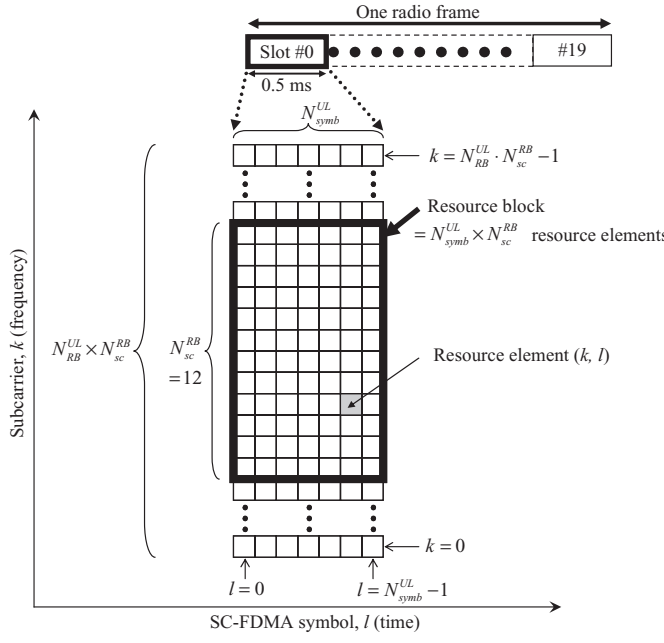

Figure 4.6 Uplink resource grid [3]. *Source:* ETSI (European Telecommunications Standards Institute) © 2007. 3GPP™ TSs and TRs are the property of ARIB, ATIS, CCSA, ETSI, TTA and TTC who jointly own the copyright in them. They are subject to further modifications and are therefore provided to you "as is" for information purposes only. Further use is strictly prohibited.

4.3.2 Resource Blocks

LTE assigns transmission resources to physical channels in time-frequency units referred to as *resource blocks*. A resource block has a duration of 0.5 msec (one slot) and a bandwidth of 180 kHz (12 subcarriers). A physical channel occupies a frequency band containing one or more contiguous resource blocks. The bandwidth of a physical channel is a multiple of 180 kHz and the LTE physical layer performs localized FDMA (LFDMA) scheduling, defined in Section 3.3. Figure 4.6 illustrates the uplink resource block structure; all the resource blocks in the available system bandwidth constitute a *resource grid*. The number of blocks in the resource grid ranges from six, for 1.4 MHz channels, to 100, for 20 MHz channels. In the time domain, each uplink slot carries six or seven *SC-FMDA symbols*. One *SC-FDMA* symbol contains the complex output samples of one inverse discrete Fourier transform (IDFT) in Figure 3.1 and a cyclic prefix. In a physical uplink shared channel (PUSCH), the demodulation reference signal appears in the fourth resource element of every subcarrier transmitted in a resource

Table 4.6 Normal cyclic prefix and extended cyclic prefix

	Normal cyclic prefix	Extended cyclic prefix
SC-FDMA symbols per resource block (N_{symb}^{UC})	7	6
Clock periods in the cyclic prefix	160 (symbol 0) 144 (symbols 1∼6)	512 (all six symbols)
Duration of the cyclic prefix	≈ 5.21 μsec (symbol 0) ≈ 4.69 μsec (symbols 1∼6)	≈ 16.67 μsec (all six symbols)

block. In a physical uplink control channel (PUCCH), the demodulation reference signal can appear in different resource elements depending on which of four PUCCH formats is employed.

LTE uses slots with six symbols in large cells subject to severe inter-symbol interference due to a long mulitpath delay spread. These cells require a relatively long cyclic prefix, referred to as an *extended cyclic prefix*. LTE uses slots with seven symbols in smaller cells requiring a *normal cyclic prefix*. Table 4.6 indicates that the duration of an extended cyclic prefix is 512 clock periods, $512 \times T_S = 16.67$ μsec. In slots with seven symbols, the duration of a normal cyclic prefix is 160 clock periods, $160 \times T_S = 5.21$ μsec, for the first symbol and 144 clock periods, $144 \times T_S = 4.69$ μsec, for the other six symbols.

LTE refers to the complex numbers produced by the IDFT and the complex numbers in the cyclic prefix as *samples*. Table 4.7 indicates the size of the IDFT ranges from 128 samples for 1.4 MHz channels to 2048 samples for 20 MHz channels.

As indicated in Figure 4.6, each entry in the resource grid is referred to as a "resource element" denoted by the index pair (k, l) where k and l are the indices in the frequency and time domain, respectively.

Note in Table 4.7 that the size of the IDFT for each channel bandwidth is larger than the number of modulated subcarriers. The remaining

Table 4.7 Resource block characteristics

Channel bandwidth [MHz]	1.4	3	5	10	15	20
Number of resource blocks (N_{RB}^{UL})	6	15	25	50	75	100
Number of occupied subcarriers	72	180	300	600	900	1200
IDFT(Tx)/DFT(Rx) size (M)	128	256	512	1024	1536	2048
Sample rate [MHz]	1.92	3.84	7.68	15.36	23.04	30.72
Samples per slot	960	1920	3840	7680	11520	15360

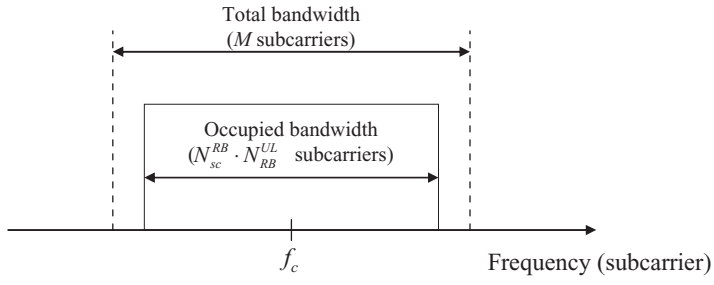

Figure 4.7 Physical mapping of a block in RF frequency domain (*fc*: carrier center frequency)

subcarriers in the IDFT have zero magnitude and constitute a guard band in the frequency domain to prevent out-of-band radiation. Figure 4.7 shows the spectrum occupancy of the signal transmitted by one terminal.

4.4 Basic Uplink Physical Channel Processing

The baseband signal representing the physical uplink shared channel is defined in terms of the operations shown in Figure 4.8. For comparison,

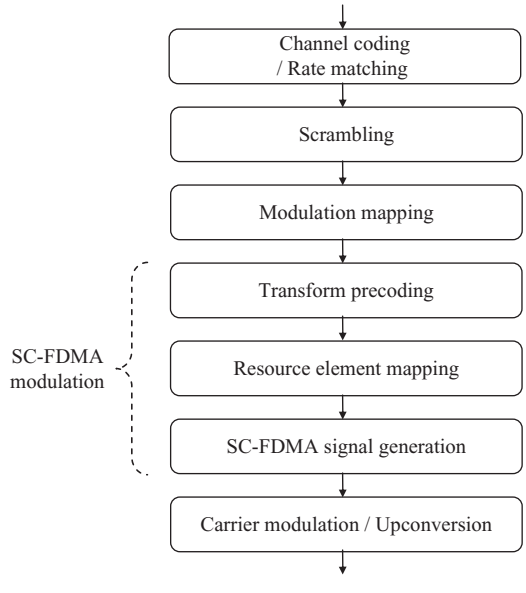

Figure 4.8 Basic uplink physical channel processing

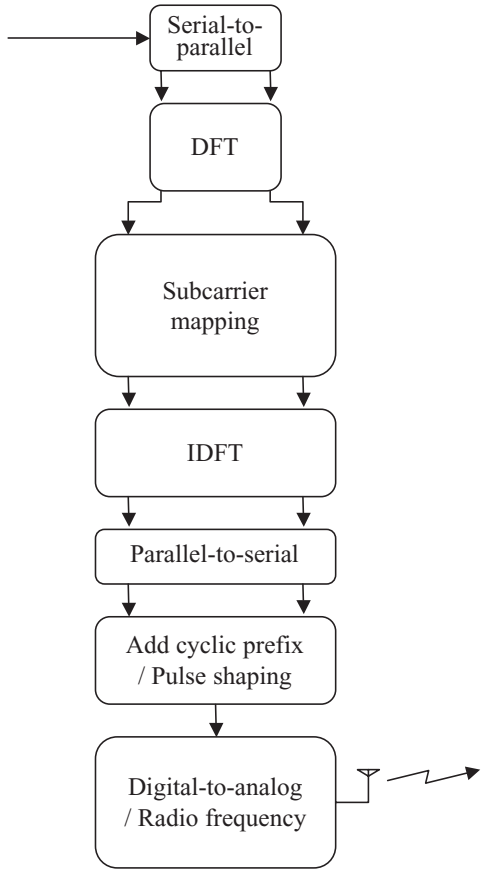

Figure 4.9 Generic SC-FDMA transmitter

Figure 4.9 duplicates the transmitter portion of a generic SC-FDMA system (see Figure 3.1).

LTE specifies two rate 1/3 *channel coding* techniques: tail-biting convolution coding and turbo coding [4]. Each coder produces three separate bit streams, corresponding to code rate 1/3. The bit streams are interleaved separately and the interleaved streams are fed to a circular *rate-matching* buffer. The output bits of the circular buffer are *scrambled* with a length-33 Gold sequence [3]. Depending on channel quality, the physical uplink shared channel (PUSCH) can use QPSK, 16-QAM, and 64-QAM *modulations*. The physical uplink control channel (PUCCH) can use BPSK and QPSK *modulations*. The output symbols of the modulation mapping operation correspond to the input signal of Figure 4.9.

Transform precoding corresponds to the DFT operation in Figure 4.9. In a physical uplink shared channel (PUSCH), the size of the DFT-precoding corresponds to the number of scheduled subcarriers used for PUSCH transmission in an SC-FDMA symbol, M_{sc}^{PUSCH}. M_{sc}^{PUSCH} adheres to the following constraint to facilitate efficient DFT implementation:

$$\begin{aligned} M_{sc}^{PUSCH} &= N_{sc}^{RB} \times 2^{\alpha_2} \times 3^{\alpha_3} \times 5^{\alpha_5} \leq N_{sc}^{RB} \times N_{RB}^{UL} \\ &= 12 \times 2^{\alpha_2} \times 3^{\alpha_3} \times 5^{\alpha_5} \leq 12 \times N_{RB}^{UL} \end{aligned} \tag{4.3}$$

where α_2, α_3, and α_5 are non-negative integers. Because of this constraint, the number of resource blocks that can be assigned to a mobile terminal is in the set of integers up to 100 that are multiples of 2, 3, and 5: $\{1, 2, 3, 4, 5, 6, 8, 9, 10, 12, 15, \ldots, 100\}$. For example, if the mobile terminal is allocated ten resource blocks, then, $M_{sc}^{PUSCH} = N_{RB}^{sc} \times 2 \times 5 = 12 \times 2 \times 5 = 120$.

The operation of *resource element mapping* corresponding to subcarrier mapping in Figure 4.9 assigns DFT outputs to subcarriers in the resource block used by the physical channel.

The operation of *SC-FDMA signal generation* corresponds to the sequence of four operations shown in Figure 4.9: IDFT, parallel-to-serial conversion, addition of cyclic prefix symbols, and digital-to-analog conversion. The result is a continuous signal, $s_l(t)$. The duration of $s_l(t)$ is the duration of one resource element: either 0.5/6 msec or 0.5/7 msec, depending on whether the transmission uses an extended cyclic prefix (six resource elements per time slot) or a normal cyclic prefix (seven resource elements per time slot). The subscript l in $s_l(t)$ is the time index of the resource element: With a normal cyclic prefix $0 \leq l \leq 6$ and with an extended cyclic prefix $0 \leq l \leq 5$. In the resource elements assigned to a PUSCH (physical uplink shared channel) or a PUCCH (physical uplink control channel), $s_l(t)$ is the sum of the $12 \cdot N_{RB}^{UL}$ subcarriers in the physical channel, each modulated by an output of the transform precoding (DFT) operation. In resource elements occupied by demodulation reference signals ($l = 3$ for PUSCH), sounding reference signals, or a PRACH (physical random access channel), the subcarriers are modulated by a sequence of symbols (described in Section 4.5) with favorable autocorrelation properties.

Finally, $s_l(t)$ modulates the radio frequency carrier (f_c Hz) assigned to the mobile terminal. Figure 4.10 shows a balanced mixer performing this upconversion. The RF filtering following the upconversion corresponds to the pulse shaping in Figure 4.9.

Figure 4.11 illustrates the use of a discrete Fourier transform (DFT) and an inverse transform (IDFT) to implement the three SC-FDMA

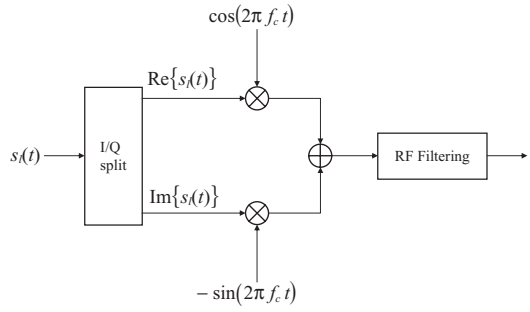

Figure 4.10 Carrier modulation and upconversion [3]. *Source:* ETSI (European Telecommunications Standards Institute) © 2007. 3GPP™ TSs and TRs are the property of ARIB, ATIS, CCSA, ETSI, TTA and TTC who jointly own the copyright in them. They are subject to further modifications and are therefore provided to you "as is" for information purposes only. Further use is strictly prohibited.

modulation operations (transform precoding, resource element mapping, and SC-FDMA signal generation) in Figure 4.8.

In the case of a 5 MHz transmission channel, the result of this sequence of operations is the resource block shown in Figure 4.12 with time slots occupied according to Figure 4.13.

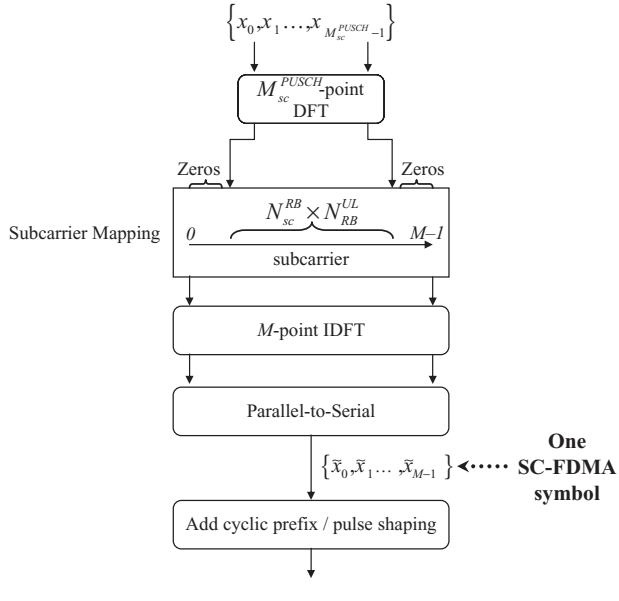

Figure 4.11 SC-FDMA modulation using DFT and IDFT

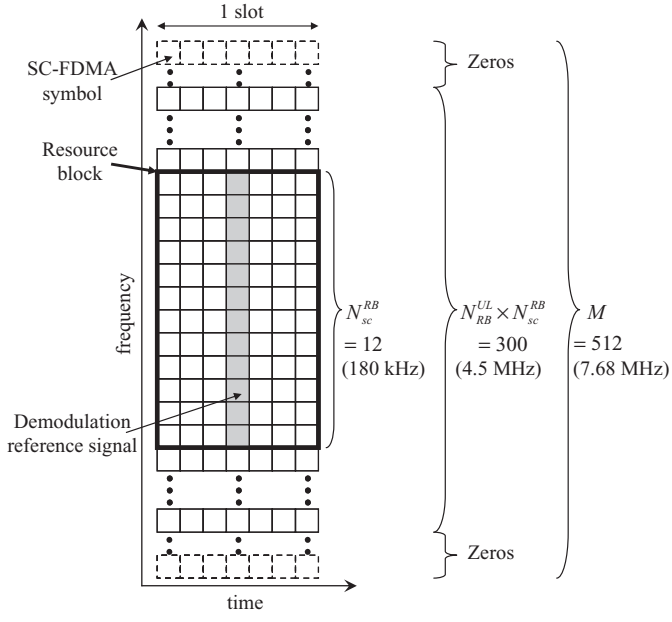

Figure 4.12 Uplink slot structure of PUSCH in the frequency domain for 5 MHz bandwidth configuration (normal cyclic prefix)

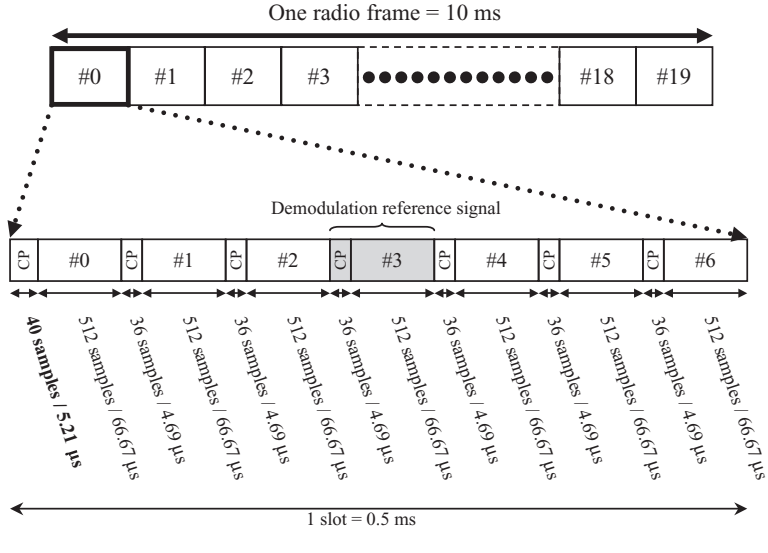

*Sample period = $4 \times T_s \oplus 0.13$ µs

Figure 4.13 Uplink slot structure of PUSCH in the time domain for 5 MHz bandwidth configuration (normal cyclic prefix)

4.5 Reference (Pilot) Signal Structure

In addition to user information and network control information, the LTE uplink transmits known demodulation reference signals to facilitate coherent demodulation at the base station and known sounding reference signals to facilitate channel dependent scheduling. In a physical uplink shared channel (PUSCH), the demodulation reference signal appears in the fourth resource element of every subcarrier transmitted in a resource block. In a PUCCH, the demodulation reference signal can appear in resource elements 1, 2, 3, 4, or 5 depending on which of four PUCCH formats is employed. The symbols of the reference signal are Zadoff-Chu sequences with low autocorrelation sidelobes [9].

As described earlier in this chapter, the LTE uplink transmits demodulation reference signals with every resource block in a PUSCH and a PUCCH. It is also capable of transmitting sounding reference signals in separate resource blocks. Demodulation reference signals are used at the base station for channel estimation in the frequency domain equalizer and for coherent demodulation. Sounding reference signals assist uplink channel quality estimation for uplink channel dependent scheduling. The same set of base sequences is used for demodulation and sounding reference signals.

In PUSCH, the demodulation reference signal resides in the fourth SC-FDMA symbol ($l = 3$) of the slot. In PUCCH, the location of the demodulation reference signal varies depending on the PUCCH format and the length of the CP [3].

If the number of resource blocks assigned to a physical channel is one or two, the reference signal is generated according to a table in Section 5.5.1.2 of Reference 3. When the number of assigned resource blocks is three or more, the reference signal is generated using CAZAC (Constant Amplitude Zero Auto-Correlation) sequences such as Zadoff-Chu polyphase sequences [9]. Zadoff-Chu CAZAC sequences are defined as

$$a_k = \begin{cases} e^{-j2\pi \frac{r}{L}\left(\frac{k^2}{2}+qk\right)}, & k=0,\ 1,\ 2,\ldots,\ L-1;\ \text{for } L \text{ even} \\ e^{-j2\pi \frac{r}{L}\left(\frac{k(k+1)}{2}+qk\right)}, & k=0,\ 1,\ 2,\ldots,\ L-1;\ \text{for } L \text{ odd} \end{cases} \tag{4.4}$$

where r is any integer relatively prime to L and q is any integer.

The set of Zadoff-Chu CAZAC sequences has the following properties [9]:

- constant amplitude;
- zero circular autocorrelation;

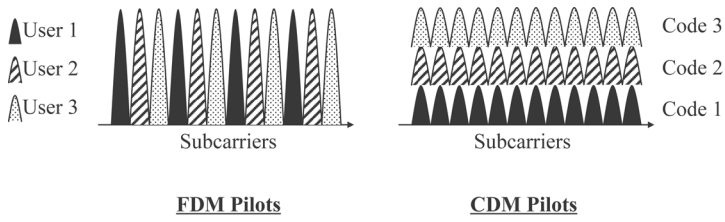

Figure 4.14 FDM and CDM reference for three simultaneous users with 12 subcarriers

- flat frequency domain response;
- circular cross-correlation between two sequences is low and with constant magnitude, provided that L is a prime number.

Section 5.5.1 of Reference 3 contains the details of the reference signal sequence generation in the LTE uplink.

Orthogonality among uplink reference signals from different terminals can be achieved by means of frequency division multiplexing, code division multiplexing, or time division multiplexing. With frequency division multiplexing, each uplink reference signal is transmitted across a distinct set of subcarriers. This solution achieves signal orthogonality in the frequency domain. With code division multiplexing, reference signals are constructed that are orthogonal in the code domain with the signals transmitted across a common set of subcarriers. As an example, individual reference signals may be distinguished by a specific cyclic shift of a single CAZAC sequence. With time division multiplexing, terminals transmit reference signals in different time blocks.

Figure 4.14 illustrates an example of FDM and CDM reference signals.

The LTE uplink uses frequency division multiplexing for single antenna transmission of demodulation reference signals and code division multiplexing for multi-user MIMO transmission. It uses code division multiplexing of sounding reference signals when terminals share the same bandwidth and a combination of code division and frequency division when there are multiple sounding bandwidths.

4.6 Summary

In this chapter, we described the uplink of the 3GPP specifications of technology for the long term evolution (LTE) of cellular systems. In particular, the chapter presents the design parameters of SC-FDMA

modulation. All the 3GPP LTE standard specifications can be downloaded from 3GPP's website at http://www.3gpp.org/ftp/Specs/html-info/36-series.htm. A list of the 44 Technical Specifications and eight Technical References in effect as of April 2008 is provided in the Appendix at the end of this chapter.

References

[1] 3rd Generation Partnership Project, http://www.3gpp.org.

[2] 3rd Generation Partnership Project, *3GPP TS 36.201 – Technical Specification Group Radio Access Network; Evolved Universal Terrestrial Radio Access (E-UTRA); LTE Physical Layer – General Description (Release 8)*, Nov. 2007.

[3] 3rd Generation Partnership Project, *3GPP TS 36.211 – Technical Specification Group Radio Access Network; Evolved Universal Terrestrial Radio Access (E-UTRA); Physical Channels and Modulation (Release 8)*, Nov. 2007.

[4] 3rd Generation Partnership Project, *3GPP TS 36.212 – Technical Specification Group Radio Access Network; Evolved Universal Terrestrial Radio Access (E-UTRA); Multiplexing and Channel Coding (Release 8)*, Nov. 2007.

[5] 3rd Generation Partnership Project, *3GPP TS 36.213 – Technical Specification Group Radio Access Network; Evolved Universal Terrestrial Radio Access (E-UTRA); Physical Layer Procedures (Release 8)*, Nov. 2007.

[6] 3rd Generation Partnership Project, *3GPP TS 36.214 – Technical Specification Group Radio Access Network; Evolved Universal Terrestrial Radio Access (E-UTRA); Physical Layer - Measurements (Release 8)*, Nov. 2007.

[7] 3rd Generation Partnership Project, *3GPP TS 36.321 – Technical Specification Group Radio Access Network; Evolved Universal Terrestrial Radio Access (E-UTRA); Medium Access Control (MAC) Protocol Specification (Release 8)*, Dec. 2007.

[8] 3rd Generation Partnership Project, *3GPP TS 36.104 – Technical Specification Group Radio Access Network; Evolved Universal Terrestrial Radio Access (E-UTRA); Base Station Radio Transmission and Reception (Release 8)*, Dec. 2007.

[9] Popovic, B.M., "Generalized Chirp-like Polyphase Sequences with Optimal Correlation Properties," *IEEE Trans. Info. Theory*, vol. **38**, July 1992, pp. 1406–1409.

4.7 Appendix – List of 3GPP LTE Standards

Document number	Title
TS 36.101	Evolved Universal Terrestrial Radio Access (E-UTRA); User Equipment (UE) radio transmission and reception
TS 36.104	Evolved Universal Terrestrial Radio Access (E-UTRA); Base Station (BS) radio transmission and reception

TS 36.106	Evolved Universal Terrestrial Radio Access (E-UTRA); Repeater radio transmission and reception
TS 36.113	Evolved Universal Terrestrial Radio Access (E-UTRA); Base Station (BS) and repeater Electro-Magnetic Compatibility (EMC)
TS 36.133	Evolved Universal Terrestrial Radio Access (E-UTRA); Requirements for support of radio resource management
TS 36.141	Evolved Universal Terrestrial Radio Access (E-UTRA); Base Station (BS) conformance testing
TS 36.143	Evolved Universal Terrestrial Radio Access (E-UTRA); Repeater conformance testing
TS 36.201	Evolved Universal Terrestrial Radio Access (E-UTRA); Long Term Evolution (LTE) physical layer; General description
TS 36.211	Evolved Universal Terrestrial Radio Access (E-UTRA); Physical channels and modulation
TS 36.212	Evolved Universal Terrestrial Radio Access (E-UTRA); Multiplexing and channel coding
TS 36.213	Evolved Universal Terrestrial Radio Access (E-UTRA); Physical layer procedures
TS 36.214	Evolved Universal Terrestrial Radio Access (E-UTRA); Physical layer; Measurements
TS 36.300	Evolved Universal Terrestrial Radio Access (E-UTRA) and Evolved Universal Terrestrial Radio Access (E-UTRAN); Overall description; Stage 2
TS 36.302	Evolved Universal Terrestrial Radio Access (E-UTRA); Services provided by the physical layer
TS 36.304	Evolved Universal Terrestrial Radio Access (E-UTRA); User Equipment (UE) procedures in idle mode
TS 36.306	Evolved Universal Terrestrial Radio Access (E-UTRA); User Equipment (UE) radio access capabilities
TS 36.321	Evolved Universal Terrestrial Radio Access (E-UTRA); Medium Access Control (MAC) protocol specification
TS 36.322	Evolved Universal Terrestrial Radio Access (E-UTRA); Radio Link Control (RLC) protocol specification
TS 36.323	Evolved Universal Terrestrial Radio Access (E-UTRA); Packet Data Convergence Protocol (PDCP) specification
TS 36.331	Evolved Universal Terrestrial Radio Access (E-UTRA); Radio Resource Control (RRC); Protocol specification
TS 36.401	Evolved Universal Terrestrial Radio Access Network (E-UTRAN); Architecture description
TS 36.411	Evolved Universal Terrestrial Radio Access Network (E-UTRAN); S1 layer 1

TS 36.412	Evolved Universal Terrestrial Radio Access Network (E-UTRAN); S1 signaling transport
TS 36.413	Evolved Universal Terrestrial Access (E-UTRA); S1 Application Protocol (S1AP)
TS 36.414	Evolved Universal Terrestrial Radio Access Network (E-UTRAN); S1 data transport
TS 36.420	Evolved Universal Terrestrial Radio Access Network (E-UTRAN); X2 general aspects and principles
TS 36.421	Evolved Universal Terrestrial Radio Access Network (E-UTRAN); X2 layer 1
TS 36.422	Evolved Universal Terrestrial Radio Access Network (E-UTRAN); X2 signaling transport
TS 36.423	Evolved Universal Terrestrial Radio Access Network (E-UTRAN); X2 Application Protocol (X2AP)
TS 36.424	Evolved Universal Terrestrial Radio Access Network (E-UTRAN); X2 data transport
TS 36.440	Evolved Universal Terrestrial Radio Access Network (E-UTRAN); General aspects and principles for interfaces supporting Multimedia Broadcast Multicast Service (MBMS) within E-UTRAN
TS 36.441	Evolved Universal Terrestrial Radio Access Network (E-UTRAN); Layer 1 for interfaces supporting Multimedia Broadcast Multicast Service (MBMS) within E-UTRAN
TS 36.442	Evolved Universal Terrestrial Radio Access Network (E-UTRAN); Signaling Transport for interfaces supporting Multimedia Broadcast Multicast Service (MBMS) within E-UTRAN
TS 36.443	Evolved Universal Terrestrial Radio Access Network (E-UTRAN); M2 Application Protocol (M2AP)
TS 36.444	Evolved Universal Terrestrial Radio Access Network (E-UTRAN); M3 Application Protocol (M3AP)
TS 36.445	Evolved Universal Terrestrial Radio Access Network (E-UTRAN); M1 Data Transport
TS 36.446	Evolved Universal Terrestrial Radio Access Network (E-UTRAN); M1 User Plane protocol
TS 36.508	Evolved Universal Terrestrial Radio Access (E-UTRA) and Evolved Universal Terrestrial Radio Access Network (E-UTRAN); Common test environments for User Equipment (UE) conformance testing
TS 36.521-1	Evolved Universal Terrestrial Radio Access (E-UTRA) and Evolved Universal Terrestrial Radio Access Network (E-UTRAN); User Equipment (UE) conformance specification; Radio transmission and reception Part 1: conformance testing

TS 36.521-2	Evolved Universal Terrestrial Radio Access (E-UTRA) and Evolved Universal Terrestrial Radio Access Network (E-UTRAN); User Equipment (UE) conformance specification; Radio transmission and reception Part 2: ICS
TS 36.523-1	Evolved Universal Terrestrial Radio Access (E-UTRA) and Evolved Universal Terrestrial Radio Access Network (E-UTRAN); User Equipment (UE) conformance specification; Part 1: Protocol conformance specification
TS 36.523-2	Evolved Universal Terrestrial Radio Access (E-UTRA) and Evolved Universal Terrestrial Radio Access Network (E-UTRAN); User Equipment (UE) conformance specification; Part 2: ICS
TS 36.523-3	Evolved Universal Terrestrial Radio Access (E-UTRA) and Evolved Universal Terrestrial Radio Access Network (E-UTRAN); User Equipment (UE) conformance specification; Part 3: Abstract Test Suites (ATS)
TR 36.801	Evolved Universal Terrestrial Radio Access (E-UTRA); Measurement Requirements
TR 36.803	Evolved Universal Terrestrial Radio Access (E-UTRA); User Equipment (UE) radio transmission and reception
TR 36.804	Evolved Universal Terrestrial Radio Access (E-UTRA); Base Station (BS) radio transmission and reception
TR 36.902	Evolved Universal Terrestrial Radio Access Network (E-UTRAN); Self-configuring and self-optimizing network use cases and solutions
TR 36.913	Requirements for LTE-Advanced
TR 36.938	Improved network controlled mobility between LTE and 3GPP2/mobile WiMAX radio technologies
TR 36.942	Evolved Universal Terrestrial Radio Access (E-UTRA); Radio Frequency (RF) system scenarios
TR 36.956	Evolved Universal Terrestrial Radio Access (E-UTRA); Repeater planning guidelines and system analysis

5

Channel Dependent Scheduling

5.1 Introduction

Frequency division techniques were originally proposed for broadband wireless transmission systems to avoid the severe inter-symbol interference that would be present in time division or code division transmissions. This chapter presents another advantage of frequency division transmissions – the opportunity to apply channel dependent scheduling in the process of subcarrier mapping and thereby obtain performance improvements due to multi-user diversity. The benefits of channel dependent scheduling are consequences of the frequency selective nature of broadband channel transfer functions. When terminals are dispersed spatially, each one has a different channel transfer function.

Figure 5.1 shows the frequency responses of channels assigned to two terminals, represented as the square of the channel gain at each of 256 subcarriers. The two curves conform to the TU6 propagation model [1]. For the most part the two terminals (labeled User 1 and User 2) have distinctly different channel gains in most regions of the frequency band spanned by the 256 subcarriers. As the terminals move, the frequency responses change. As a consequence, a practical system would have to monitor periodically the frequency response of each terminal and devise a new schedule matched to the current frequency responses of all the terminals sharing the frequency band.

Channel dependent scheduling is a form of subcarrier mapping that can be employed in SC-FDMA and OFDMA applications. The idea of channel

Single Carrier FDMA: A New Air Interface for Long Term Evolution Hyung G. Myung and David J. Goodman
 ISBN: 978-0-470-72449-1

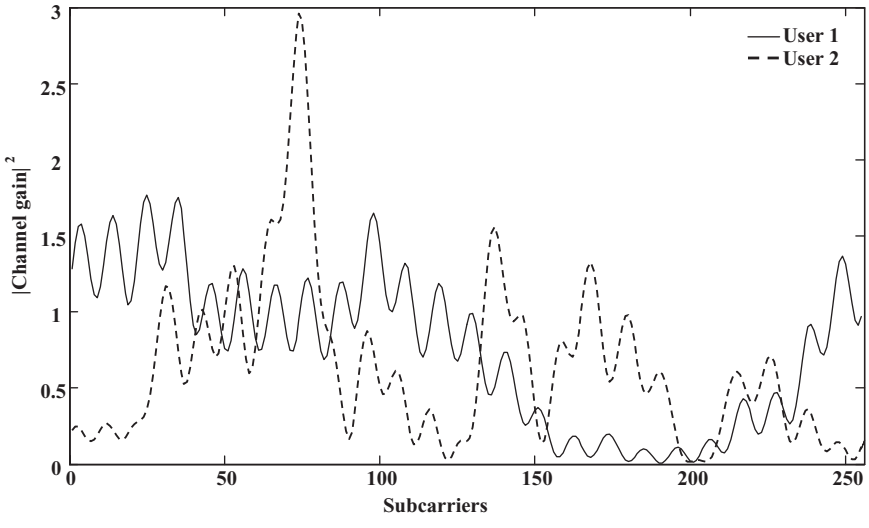

Figure 5.1 Channel impulse response of two different terminals

dependent scheduling is to map the transmissions of each terminal to a set of subcarriers with favorable transmission characteristics. In practice, this requires a scheduler at the base station to measure the channel characteristics and learn the transmission requirements of each terminal. The scheduler then performs an optimization algorithm to derive subcarrier assignments for each terminal. Finally, the base station transmits the assignments to the terminals. Figure 5.2 is a block diagram of an SC-FDMA system emphasizing the scheduling operations at the base station.

Figure 5.3 shows the results of one scheduling algorithm applied to the two channel responses of Figure 5.1. In this algorithm, the only scheduling constraint is that subcarriers have to be assigned in "chunks" rather than individually. Each chunk is a set of 16 contiguous subcarriers. The algorithm assigns each chunk to the terminal with the higher average channel gain over the 16 subcarriers in the chunk. The average is represented by the height of the horizontal bars in Figure 5.3. For this pair of frequency responses, the algorithm has allocated nine chunks to User 1 and the other seven chunks to User 2.

In practice, scheduling algorithms conform to constraints in addition to the requirement that subcarriers be assigned in chunks. For example, algorithms are constrained to conform to one of the approaches described in Section 3.3: either localized FDMA, in which all subcarriers in a schedule are contiguous; or distributed FDMA with subcarriers assigned in equal

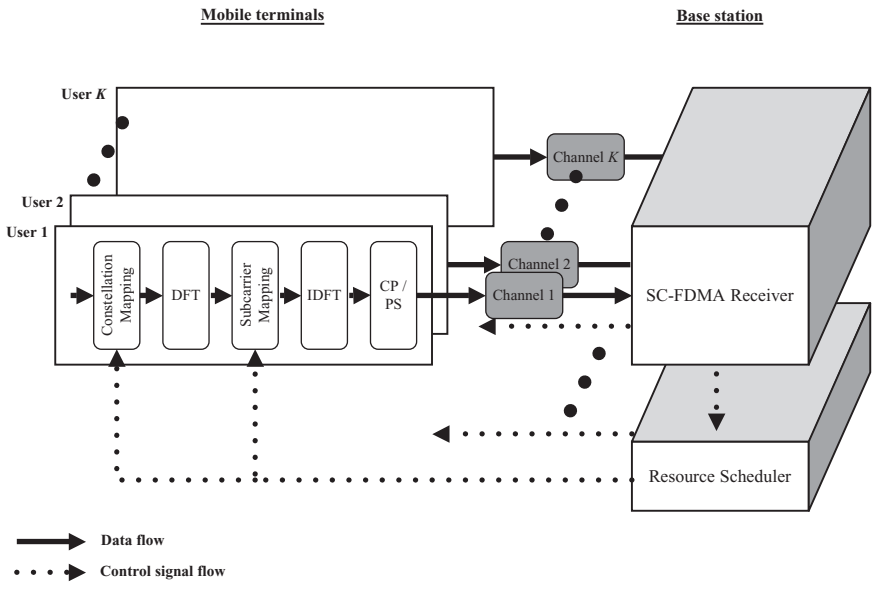

Figure 5.2 SC-FDMA with channel dependent scheduling

intervals across the channel bandwidth. The LTE system standardized by 3GPP, the subject of Chapter 4, requires the application of localized FDMA scheduling algorithms. This constraint and the fact that more than two terminals share the frequency band make optimum schedules more difficult to derive than the one shown in Figure 5.3.

To assess the benefits of channel dependent scheduling, researchers derive the properties of channel transfer functions from propagation models. They use mathematical analysis and computer simulation to examine the benefits of optimum or heuristic scheduling algorithms on the quality of a transmission system. Initial studies assume that the base station has perfect knowledge of all channel transfer functions at all times and instantaneously communicates schedules to all terminals. For the most promising algorithms, subsequent studies investigate the effects of inevitable deviations in practice from this ideal situation. The differences are due to inaccuracies in measuring channel characteristics and to time delays between measurement of channel properties and application at a terminal of a schedule calculated at a base station.

A paper published by Wang *et al.* in December 2007 [2] provides a comprehensive mathematical framework for the design and analysis of scheduling algorithms in a variety of communication systems. It contains 93 references to prior work, mainly mathematical in nature, with some

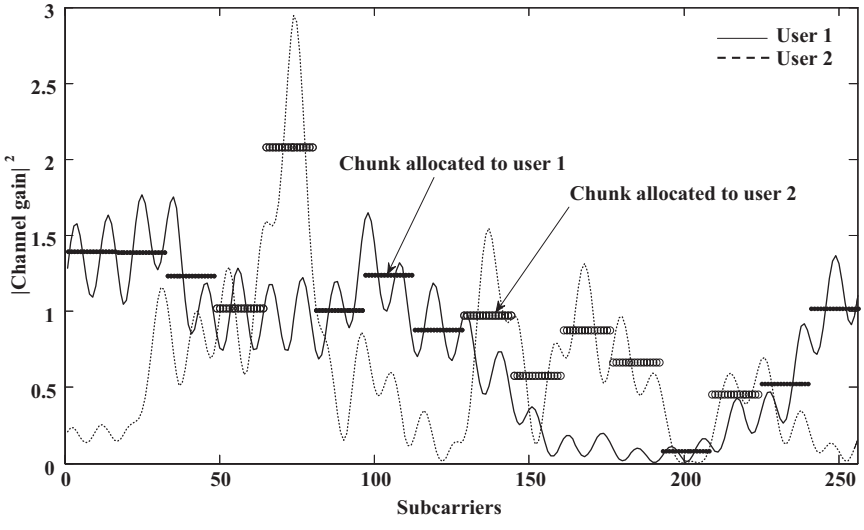

Figure 5.3 Chunk allocations for the two terminals with channel impulse response in Figure 5.1

relating to practical protocols. The paper adopts a broad definition of scheduling as "allocating optimally channel, rate, and power resources to multiple connections with diverse quality-of-service requirements". Within this definition, SC-FDMA systems first allocate channel resources to terminals in the context of subcarrier mapping. They then apply adaptive modulation and coding (AMC) [3] to the transmissions on the assigned subcarriers, within the power limits of the terminals sharing the transmission band. In the LTE system described in Chapter 4, the scheduling operations take place in the medium access control (MAC) sublayer at layer 2 of Figure 4.1.

AMC matches the modulation technique and error correcting code to the quality of transmission on the assigned subcarriers. The motivation for AMC is that modulation and coding techniques can be adapted to tradeoff bandwidth efficiency for received signal quality. The signal quality can be expressed as the binary error rate or as the frame error rate, which directly influences the throughput of a communication link. Figure 5.4 shows graphs of throughput as a function of channel signal-to-noise ratio for eight different modulation techniques: binary phase shift keying (BPSK) with $B = 1$ bit per symbol, quaternary phase shift keying (QPSK) with $B = 2$ bits per symbol, and quadrature amplitude modulation (QAM) with $B = 3$, $4, \ldots, 8$ bits per symbol [4]. In this example, the transmitter uses one resource block consisting of seven SC-FDMA symbols on each of

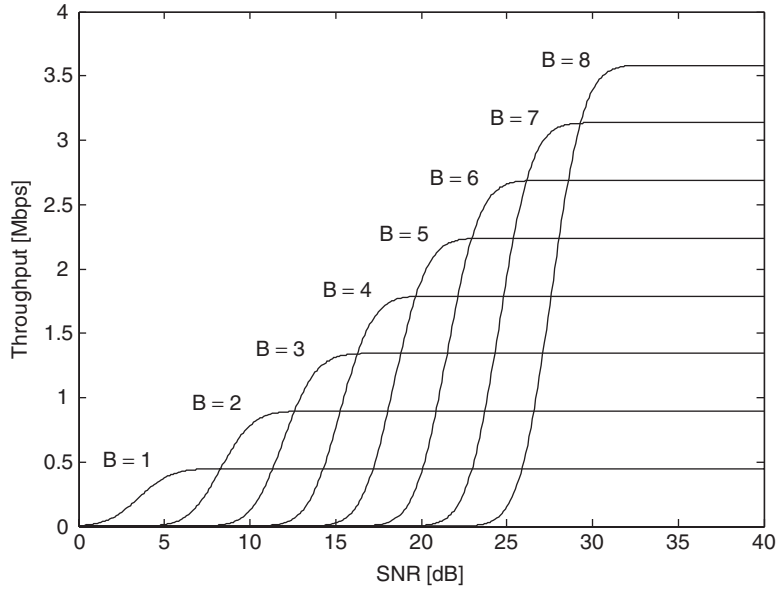

Figure 5.4 Throughput of a modulation technique transmitting 448,000 symbols per second with B bits per symbol

32 subcarriers every 0.5 msec. Therefore the symbol transmission rate is 448,000 symbols per second.

In Figure 5.4 each throughput curve increases with signal-to-noise ratio reaching a maximum corresponding to error-free transmission. The maximum value is $448{,}000 \times B$ bits per second (b/s). However, at low signal-to-noise ratios, throughput varies inversely with B because a modulation technique with a large number of bits per symbol has a higher frame error rate than a technique with fewer bits per symbol. As a consequence, at each signal-to-noise ratio, there is one modulation technique that has higher throughput than the others. Table 5.1 shows the optimum modulation technique (among the eight considered) as a function of signal-to-noise ratio. A system employing adaptive modulation would measure periodically the signal-to-noise ratio of the subcarriers assigned to a terminal and use Table 5.1 to determine the modulation technique to be employed for each transmission. In the LTE standard described in Chapter 4, a Physical Uplink Shared Channel (PUSCH) and a Physical Uplink Control Channel (PUCCH) both use rate 1/3 error-correcting codes. The modulation schemes available for the PUSCH are QPSK, 16-QAM, and 64-QAM. The PUCCH can use BPSK and QPSK.

Table 5.1 Signal-to-noise ratio ranges where each modulation technique in Figure 5.4 provides maximum throughput

SNR (dB)	Bits per symbol (B)	Modulation
<8.7	1	BPSK
$8.7 \sim 13.0$	2	QPSK
$13.0 \sim 16.7$	3	8-QAM
$16.7 \sim 20.0$	4	16-QAM
$20.0 \sim 23.3$	5	32-QAM
$23.3 \sim 26.6$	6	64-QAM
$26.6 \sim 29.6$	7	128-QAM
>29.6	8	256-QAM

The material in this chapter is mainly an account of channel dependent scheduling studies, related specifically to SC-FDMA, performed by the authors and our colleagues at Polytechnic University. Following this introduction, we first discuss the objectives of channel dependent scheduling in terms of performance measures. We then describe the scheduling techniques we have studied, primarily by means of computer simulation. The simulations adopt channel models published by 3GPP and examine the performance of systems with channel dependent scheduling and systems that use static scheduling that is independent of channel characteristics. Section 5.4 presents performance estimates obtained from the simulations, first for an idealized situation in which the base station has perfect knowledge of channel conditions. We then examine the effects of imperfect channel estimates due to the inevitable delay between the time of measuring the channel and the time of applying a transmission schedule.

5.2 SC-FDMA Performance Measures

The purpose of a communication link is to transmit user information to a receiver. The two precious resources of a mobile wireless system are channel bandwidth and the energy in the batteries of portable terminals. Therefore, the quality of a scheduling scheme for uplink transmissions can be described in terms of the amount of information transferred from terminals to a base station, the power consumed by the terminals, and the time-bandwidth occupancy of the channel. Channel dependent subcarrier mapping uses system bandwidth and terminal energy in two ways. The obvious one is the bandwidth and power devoted to transmitting user information. In addition, terminals use battery energy and system bandwidth to transmit channel sounding reference signals that enable the base station

to make channel quality measurements such as those shown in Figure 5.1. These measurements show an idealized situation in which the base station learns the channel gain of all terminals at all available subcarriers. In practice, this level of resolution would be too costly in terms of system bandwidth and terminal energy. A practical implementation has to determine how many subcarriers to use for channel sounding and how frequently to perform channel sounding transmissions. In doing so, the system adopts a tradeoff between the positive impact of the schedule on throughput and the resources used to obtain channel quality measurements at the base station.

As described in Chapter 4, the LTE system specifies two types of reference signals used by a base station for learning channel characteristics: demodulation reference signals and sounding reference signals. Demodulation reference signals are integrated with every shared channel and control channel transmission. However, they provide information about the channel quality only within the band occupied by that transmission. The terminal has to transmit sounding reference signals spanning the entire system bandwidth in order for the base station to acquire the channel state information necessary for channel dependent scheduling. The accuracy of the channel state information depends on how frequently sounding signals are transmitted and on the number of subcarriers occupied by a sounding reference signal. The transmission resources consumed by the sounding reference signals offset efficiency improvements provided by channel dependent scheduling.

In addition to the power and bandwidth used by terminals to transmit user information, control information, and channel sounding reference signals, other figures of merit for a channel dependent scheduling scheme are the complexity of the scheduling algorithm employed at base stations and the downlink bandwidth employed in transmitting transmission schedules to terminals.

Throughput and power dissipation in portable terminals are two quality of service metrics for a transmission link. We have examined two different throughput measures for individual terminals: Shannon capacity and the number of bits per second received accurately. The Shannon capacity is an upper bound on the number of bits per second (b/s) that can be received without error at a base station:

$$C = W \cdot \log_2 (1 + SNR) \text{ b/s} \tag{5.1}$$

where W Hz is the bandwidth occupied by the transmitted signal and SNR is the signal-to-noise ratio of a white Gaussian noise channel. Because C is independent of the modulation and coding techniques used in the transmission, it can be used to assess the potential impact of scheduling schemes

on throughput across all possible modulation and coding schemes. In our studies, we have used this formula as one quality measure even though it does not strictly apply to SC-FDMA because the white Gaussian noise model does not apply to the fading channels. To compute C_i (the capacity of terminal i), we determine the signal-to-noise ratio, $\gamma_{i,k}$ ($k = 1, 2, \ldots, N_i$) for each of the N_i subcarriers assigned to terminal i. We then use the following formula to obtain γ_i, the signal-to-noise ratio of the SC-FDMA signal after frequency domain equalization at the receiver [5]:

$$\gamma_i = \left(\frac{1}{\frac{1}{N_i} \sum_{k=1}^{N_i} \frac{\gamma_{i,k}}{\gamma_{i,k}+1}} - 1 \right)^{-1} \tag{5.2}$$

The capacity of terminal i is

$$C_i = B_{sc} \cdot N_i \cdot \log_2 (1 + \gamma_i) \text{ b/s} \tag{5.3}$$

where B_{sc} Hz is the bandwidth occupied by each subcarrier.

To take account of specific modulation, coding, and retransmission schemes, it is necessary to determine FER_i, the frame error rate of terminal i, observed at the medium access control (MAC) sublayer in Figure 4.1. The throughput of an individual terminal is

$$T_i = R_i \cdot PSR_i \text{ b/s} \tag{5.4}$$

where R_i b/s is the information transmission rate (exclusive of overhead and channel coding bits) of terminal i and $PSR_i = 1 - FER_i$ is the packet success rate for terminal i. PSR_i is the probability that a MAC-layer data unit is correctly decoded by the forward error correcting channel coder.

The figure of merit for a scheduling scheme is the average aggregate capacity or aggregate throughput of all the terminals transmitting simultaneously where the average is taken across the statistical distribution of fading channel characteristics. An obvious way to aggregate the capacity or throughput measures of separate terminals is simply to add them. With K terminals transmitting simultaneously, the aggregate capacity and throughput are

$$C_{sum} = \sum_{i=1}^{K} C_i \quad \text{or} \quad T_{sum} = \sum_{i=1}^{K} T_i \text{ b/s} \tag{5.5}$$

However, a problem with this approach is that scheduling techniques that maximize C_{sum} or T_{sum} assign a high proportion of system bandwidth to terminals with high signal-to-noise ratio, typically terminals near the base station, at the expense of terminals further from the base station. To promote fairness, it is customary to use the product of individual capacity or throughput measures as an aggregate. Maximizing the product corresponds to maximizing the sum of logarithms:

$$C_{fair} = \sum_{i=1}^{K} \log C_i \quad \text{or} \quad T_{fair} = \sum_{i=1}^{K} \log T_i \text{ b/s} \tag{5.6}$$

Outage is a figure of merit related to capacity and throughput. Outage is measured by reference to a target capacity or target throughput. The outage of an individual terminal is the probability that the capacity or actual number of bits per second received at the base station falls below a target, C_{target} or T_{target}:

$$P\left\{C_i < C_{target}\right\} \quad \text{or} \quad P\left\{T_i < T_{target}\right\} \tag{5.7}$$

Although figures of merit that are functions of terminal capacity or terminal throughput measure the efficiency of bandwidth utilization, they do not explicitly take into account the battery power dissipated by terminals. Engineers refer to the concept of *utility*, borrowed from microeconomics, to account for both bandwidth efficiency and power dissipation. The most customary measures of utility are the ratio of capacity to power and the ratio of throughput to power. For an individual terminal the utility is

$$U_i = \frac{C_i}{P_i} \quad \text{or} \quad U_i = \frac{T_i}{P_i} \text{ b/J} \tag{5.8}$$

The measurement unit, bits per Joule, is the amount of information transferred per unit of energy used to transmit the information.

5.3 Scheduling Algorithms

To derive a schedule that optimizes one of the figures of merit in Section 5.2, it is theoretically possible to assume that the scheduler can assign subcarriers individually. Allocating individual subcarriers is, however, a prohibitively complex combinatorial optimization problem in systems with a large number of subcarriers and user terminals. Moreover, assigning subcarriers individually would introduce unacceptable control signaling overhead. Practical systems allocate subcarriers in chunks, which are disjoint sets of subcarriers. In addition to simplifying the scheduling task, chunk-based transmission improves the efficiency of the DFT in the transmitter

and the IDFT in the receiver of Figure 3.1. With respect to the two scheduling families of greatest interest in SC-FDMA, a chunk consists of consecutive subcarriers in localized FDMA (LFDMA) and in interleaved FDMA (IFDMA) a chunk consists of subcarriers equally spaced across the signal band.

Even with subcarriers assigned in chunks, optimum scheduling is extremely complex for two reasons: i) The objective function is complicated, consisting of nonlinear and discrete constraints dependent on the channel gains of the assigned subcarriers; and ii) there is a total transmit power constraint for each user. Furthermore, the optimum solution entails combinatorial comparisons with high complexity. Instead of directly solving the optimization problem, we can use "greedy" sub-optimal chunk allocation schemes for both IFDMA and LFDMA to obtain most of the benefits of channel dependent scheduling [6].

For LFDMA, we can apply a greedy chunk selection method where each chunk is assigned to the terminal that would maximize the figure of merit by transmitting symbols on the subcarriers in that chunk. For IFDMA, we can achieve the benefit of multi-user diversity by selecting users in order of the estimated figure of merit based on the average channel quality over the entire set of subcarriers. In general, more chunks are assigned to terminals with high channel gains than users with lower channel gains.

The LTE system, described in Chapter 4, uses localized FDMA with 12 subcarriers per chunk. It allocates chunks in resource blocks of duration 0.5 msec. With subcarriers at 15 kHz intervals in the LTE system, the frequency-time resolution of the scheduling process is 180 kHz $\times$ 0.5 msec.

In our work we have simulated the effects of greedy channel dependent scheduling algorithms by calculating figures of merit in Section 5.2 and comparing them with the same figures of merit obtained with static scheduling algorithms that make no reference to channel state information.

In addition to allocation of subcarriers to terminals, the other aspects of scheduling are rate allocation and power control. To limit algorithmic complexity and the burden on signaling resources, it makes sense to assign equal rate and equal power to all subcarriers within a chunk. However, with different chunks assigned to different terminals there are the four following approaches, in order of increasing algorithmic complexity and increasing demand on signaling:

- equal rate and equal power for all chunks;
- channel-dependent rate, equal power;
- equal rate, channel-dependent power;
- channel-dependent rate and channel-dependent power.

Our colleague, Dr. Junsung Lim, has compared the performance achieved with three approaches to rate and power scheduling [5]. He found that channel dependent scheduling of subcarriers produces significant performance advantages over channel independent (static) scheduling. However, with channel dependent scheduling, there is no appreciable advantage to applying different rate and different power allocations to the subcarriers in a chunk. The reason is that with channel dependent scheduling, the chunks assigned to a terminal are similar in channel quality, and there are only minor differences in power and rate allocations across chunks. On the other hand, with channel independent assignment of chunks to terminals, rate adaptation and power control across chunks can provide appreciable performance improvements.

5.4 Channel Models used in Scheduling Studies

The remainder of this chapter presents the data derived from some of our simulation studies. Our purpose is to compare channel dependent scheduling algorithms with subcarrier mapping schemes that make no reference to channel state information and to compare the performance of LFDMA with IFDMA.

The channel model used in the simulations takes into account multipath propagation, Doppler effects due to terminal mobility, and distance between the terminal and the base station. We assume that terminals are independently and uniformly distributed in a circular cell with a radius of 1 km. The probability density function of the distance d km of each terminal from the base station is $f_D(d) = 2d$ $(0 \le d \le 1\,\text{km})$. The average signal power is proportional to $d^{-3.76}$ and there is shadow fading with standard deviation 8 dB. The attenuation at the edge of the cell is 128.1 dB. Therefore, attenuation of a signal arriving at terminal k, located d_k km from the base station, is $128.1 + 37.6\log_{10} d_k + \xi_k$ dB, where ξ_k is a sample of a zero-mean Gaussian random variable with standard deviation 8 dB. With a transmitter power of 0.25 W (24 dBm), the average received signal power at the edge of the cell is -104.1 dBm.

A channel with R propagation paths has the following discrete time impulse response at time t_1 seconds:

$$h^{(t_1)}(n) = \sum_{r=0}^{R-1} A \cdot \sqrt{P_{rel}(\tau_r)} \cdot w_r^{(t_1)} \cdot \delta\left(n - \frac{\tau_r}{T_s}\right);\ n = 0,\ 1, \ldots,\ 255 \tag{5.9}$$

Table 5.2 Relative delay and relative power of the six propagation paths in the TU6 multipath propagation model

Delay (μsec)	0.0	0.2	0.6	1.6	2.4	5.0
Relative power $P_{rel}(\tau_r)$ (dB)	−3.0	0.0	−2.0	−6.0	−8.0	−10.0

where $w_r^{(t_1)}$ are zero mean, mutually independent complex Gaussian random variables and τ_r seconds is the propagation delay of path r. $P_{rel}(\tau_r)$ watts is the relative power of the delay profile model for path r, T_s seconds is the symbol duration, A is a normalization parameter such that the average channel gain is unity, and $\delta(n)$ is the discrete time Dirac-delta function. For a given channel model, we round τ_r such that each τ_r/T_s is an integer for $r = 0, 1, \ldots, R-1$. The simulation studies described in this section use the TU6 channel model (typical urban model with six propagation paths) published by 3GPP [1]. Table 5.2 displays the six path delays, τ_r μsec, and relative power levels, $10\log_{10}P_{rel}(\tau_r)$ of the TU6 model.

Figure 5.5 shows the impulse response of the multipath channel in Table 5.2 with all amplitude levels at the average values ($w_r = 1$ in Equation (5.9)).

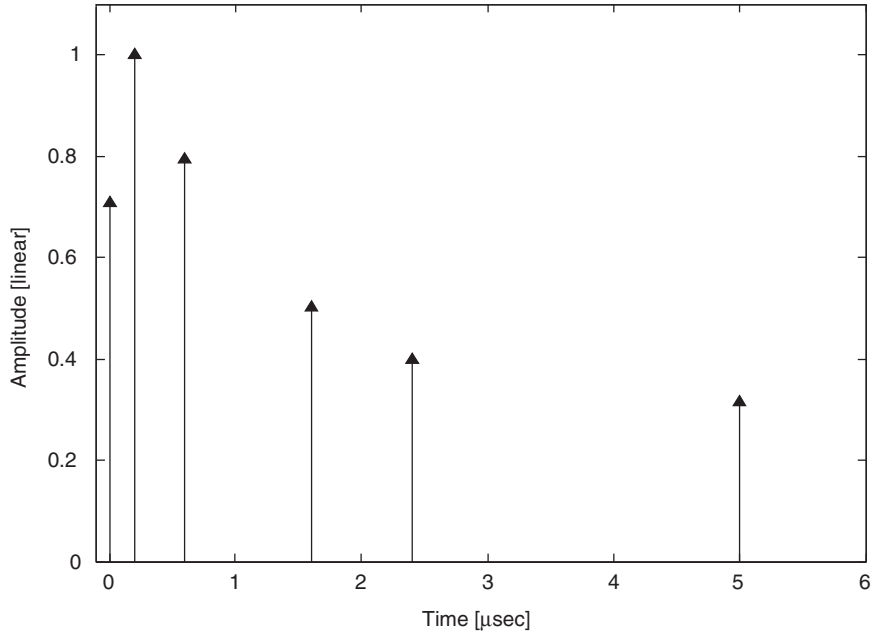

Figure 5.5 Average impulse response of the TU6 channel model

Because a terminal is moving, the impulse response changes with time. The impulse response at time t_2 takes the same form as Equation (5.9), but with a different value of the gains of the R propagation paths. The changing path gains are reflected in the time series $\{w_r^{(t)}\}$. If $\rho(\Delta t)$ is the correlation coefficient of the path gain at t_1 and the path gain at $t_2 = t_1 + \Delta t$, the gain coefficient $w_r^{(t_2)}$can be generated as a Gauss-Markov time series that evolves according to

$$w_r^{(t_2)} = \rho(\Delta t) w_r^{(t_1)} + \sqrt{1 - \rho^2(\Delta T)} n_r^{(t_2)} \tag{5.10}$$

where each sample of $n_r^{(t)}$is a zero mean Gaussian random variable independent of all other values. The simulation program generates a new impulse response function $h^{(t)}(n)$ for each transmission block and each terminal. The correlation coefficient $\rho(\Delta t)$ depends on the velocity of the terminal. In our studies we have used the formula derived for a Rayleigh fading signal envelope:

$$\rho(\Delta t) = J_0(2\pi v \Delta t/\lambda) = J_0(2\pi f_D \Delta t) \tag{5.11}$$

where $J_0(\ )$ is the zero-order Bessel function, $f_D = v/\lambda$ Hz is the maximum Doppler frequency, v m/s is the velocity of the mobile terminal, and λ m is the wavelength of the carrier signal [7]. In our study of channel dependent scheduling, Δt seconds is the difference between the time of measurement of channel state information and the time that a signal is transmitted with a subcarrier assignment based on the measurement.

For each channel impulse response, the simulation uses a 256-point DFT to produce the frequency domain channel transfer function for user i: $H_{i,k}$; $k = 0, 1, \ldots, 255$. Here $H_{i,k}$ is the path gain of subcarrier k in the propagation channel of terminal i. It is proportional to the signal-to-noise ratio $\gamma_{i,k}$ of subcarrier k received by terminal i. Equation (5.2) is the signal-to-noise ratio of terminal i after frequency domain equalization. It is a function of the signal-to-noise ratios of the individual carrier signals:

$$\gamma_{i,k} = \frac{(P_i/N) \cdot H_{i,k}}{\sigma_k^2} \tag{5.12}$$

where P_i watts is the total transmit power of user i, P_i/N, is the power in each of the N subcarriers in the chunk assigned to terminal i, and σ_k^2 is the noise power of subcarrier k.

5.5 Channel-Dependent Scheduling Simulation Studies

The channel model described in Section 5.4 is the basis of an extensive set of computer simulations that refer to the figures of merit in Section 5.2

in order to assess the effectiveness of various scheduling strategies. This section presents a few examples of the results of these studies. These examples compare the performance of localized FDMA with interleaved FDMA with both channel dependent scheduling and channel independent scheduling.

We first find upper limits on performance by assuming that the channel dependent schedules are obtained from perfect channel state information and that transmissions using the schedules take place immediately after the channel state measurements are performed. Our main conclusion is that with channel dependent scheduling, localized FDMA can offer substantial advantages over SC-FDMA systems with channel independent (static) schedules. With interleaved FDMA, channel dependent scheduling produces more modest improvements relative to static scheduling. We then consider the effects of the time delay between the time channel state information is measured and the time of transmission of signals using the schedule based on the channel state measurements. These effects depend on the velocity of the transmitting terminal. If the product of Doppler frequency and time delay exceeds 0.25, the value of channel dependent localized FDMA disappears.

The simulations assume that the carrier frequency is 2 GHz. The total transmission bandwidth is 5 MHz containing 256 subcarriers. As in the LTE system, we transmit data in time slots of duration 0.5 msec, with each slot divided into seven blocks of modulation symbols. The simulations also assume that all the terminals sharing the channel have a large amount of data to send, so that the entire transmission band is occupied in every time slot. In the results reported in this chapter, there are eight subcarriers per chunk and the system assigns one and only one chunk per terminal. Therefore up to 32 terminals can transmit simultaneously. We have also simplified the radio resources management algorithm by assuming that terminals always transmit at a power level of 0.25 W. There is white Gaussian noise in the receiver with power spectral density -160 dBm/Hz. The modulation technique is one of the eight techniques in Table 5.1 (see page 88) depending on the signal-to-noise ratio, γ_i in Equation (5.1). Table 5.1 and Figure 5.4 show the range of signal-to-noise ratios for each of the modulation techniques.

5.5.1 Schedules Based on Perfect Channel State Information

Figures 5.6 and 5.7 show the aggregate Shannon capacity, C_{sum} in Equation (5.5) as a function of the number of terminals in the cell. In Figure 5.6, the scheduling algorithm aims to maximize C_{sum} itself. There are four curves.

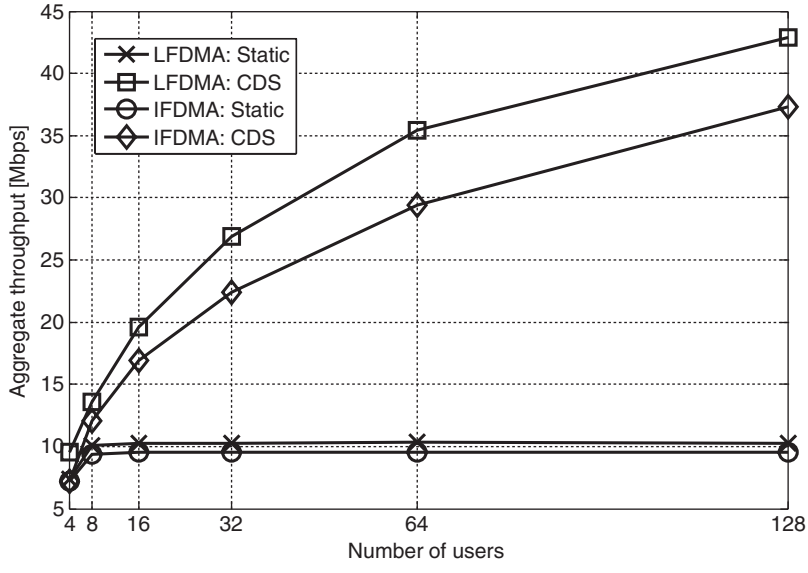

Figure 5.6 Rate sum capacity as a function of number of terminals sharing a channel. LFDMA is localized FDMA and IFDMA is interleaved FDMA. The figure of merit is aggregate capacity. The channel dependent schedules maximize sum of capacity

The curves labeled "LFDMA: Static" and "IFDMA: Static" apply to localized FDMA and interleaved FDMA, respectively with static (round robin) scheduling. The curves labeled "LFDMA: CDS" and "IFDMA: CDS" apply to localized FDMA and interleaved FDMA, respectively with channel dependent scheduling. In Figure 5.7, the capacity values are lower because the scheduling algorithm aims to maximize the sum of logarithms of capacity, C_{fair}, in Equation (5.6).

Figure 5.6 shows that when the figure of merit is C_{sum} the advantage of channel dependent scheduling over static scheduling increases as the number of terminals increases. This is because the scheduler favors terminals near the base station. These terminals have high signal-to-noise ratio and therefore they can transmit at high data rates. As the number of terminals increases, the probability of locating terminals nearer and nearer the base station increases. As a result, channel dependent scheduling achieves significant improvements for both IFDMA and LFDMA as the number of terminals increases.

Figure 5.7 shows that when the figure of merit is C_{fair}, the sum of the logarithm of capacity, the benefit of channel dependent scheduling does not increase with number of terminals beyond approximately 32 terminals. The

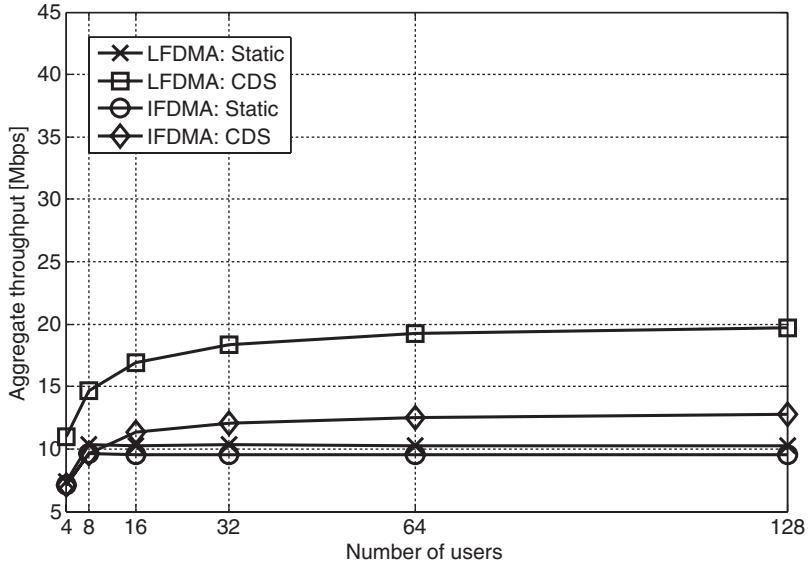

Figure 5.7 Rate sum capacity as a function of number of terminals sharing a channel. LFDMA is localized FDMA and IFDMA is interleaved FDMA. The channel dependent schedules maximize sum of logarithm of capacity

reason is that with eight subcarriers per chunk, 32 terminals occupy all the 256 subcarriers in the system. The fair scheduling criterion provides transmission resources to all terminals regardless of location. With 32 terminals, maximizing the logarithm of capacity can increase system capacity relative to static scheduling by a factor of 1.8 (from $C_{fair} = 10$ Mb/s to 18 Mb/s) for LFDMA. The improvement ratio is 1.26 for IFDMA ($C_{fair} = 12.6$ Mb/s).

Figures 5.8 and 5.9 display the throughput, C_i in Equation (5.3) of individual terminals as a function of the distance from the base station. Throughput decreases with distance for all four scheduling schemes. However, Figure 5.8 shows that when the figure of merit is C_{sum}, the terminals more than 500 meters from the base station are effectively excluded from the system ($C_i \approx 0$) with localized FDMA and channel dependent scheduling. With interleaved FDMA and channel dependent scheduling, terminals more than 800 meters from the base station have $C_i \approx 0$. By contrast, Figure 5.9 shows that the scheduling scheme that maximizes C_{fair} provides proportional fairness with the relative throughput of the four scheduling schemes effectively constant as a function of distance from the base station.

Figure 5.10 shows the outage probability $P\{C_i < 144\,\text{kb/s}\}$ as a function of number of terminals. Clearly the outage probability of scheduled

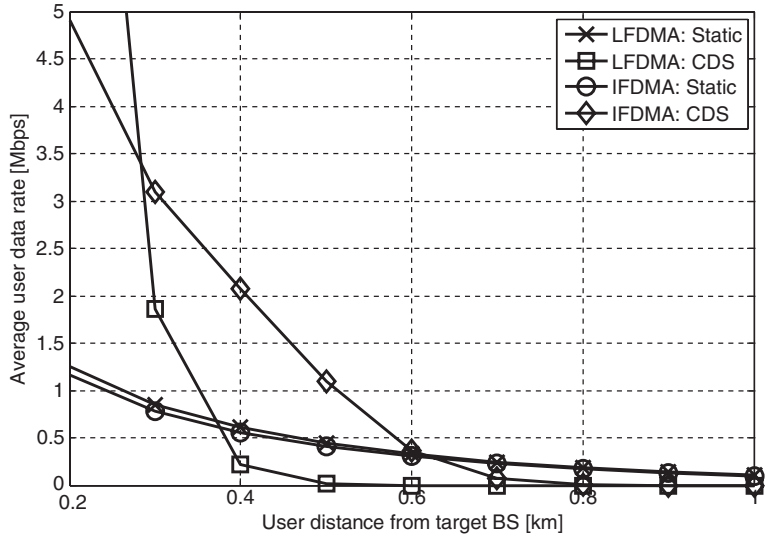

Figure 5.8 Average user data rate as a function distance between a terminal and the base station. LFDMA is localized FDMA and IFDMA is interleaved FDMA. The figure of merit is aggregate throughput. The channel dependent schedules maximize sum of throughput

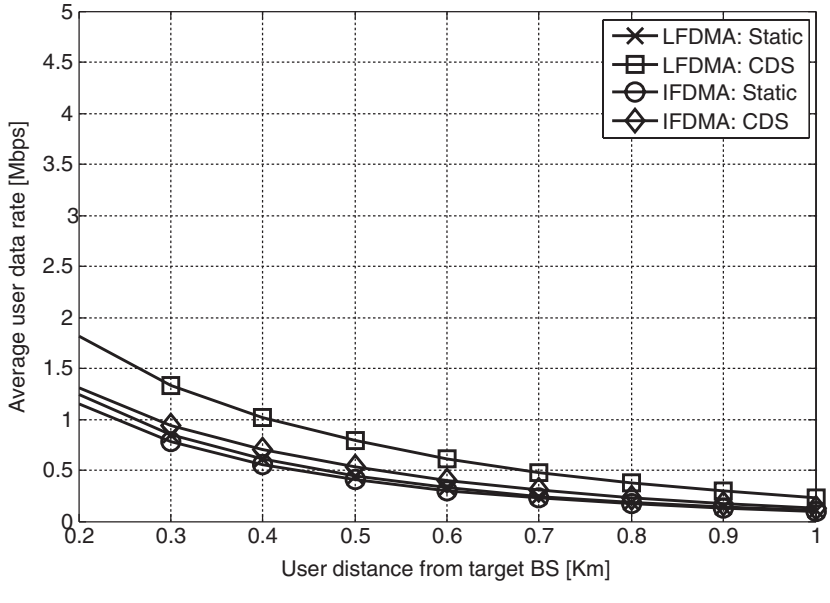

Figure 5.9 Fair scheduling. The channel dependent schedules maximize the sum of logarithm of throughput. Average user data rate is a function of distance between a terminal and the base station. LFDMA is localized FDMA and IFDMA is interleaved FDMA

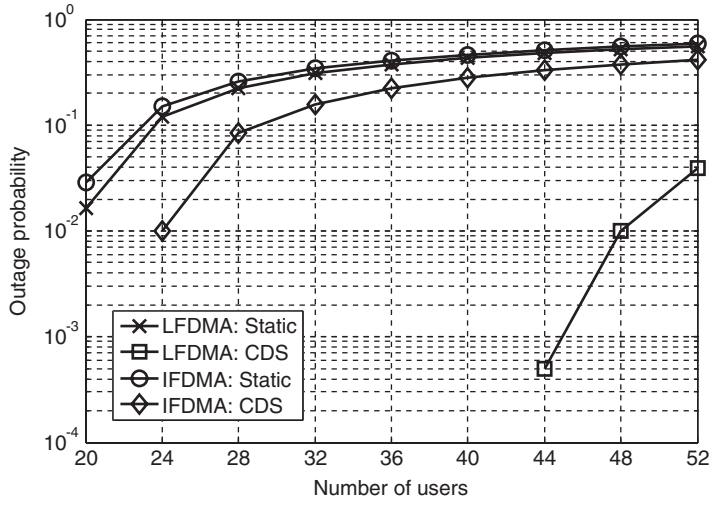

Figure 5.10 Outage probability when the optimization criterion is maximizing the sum of logarithms of throughput

localized FDMA is considerably lower than the outage probability of the other schemes. If a system has to operate with less than 1 % outage at a bit rate of 144 kb/s, scheduled localized FDMA can allow up to 48 terminals to transmit to the base station. By contrast, the maximum number of terminals is only 24 for interleaved FDMA with channel dependent scheduling and is less than 20 for interleaved FDMA with static scheduling. Table 5.3 shows

Table 5.3 Comparisons between channel dependent scheduling ("LFDMA: CDS" and "IFDMA: CDS") and static scheduling ("LFDMA: Static" and "IFDMA: Static") when the optimization criterion is the sum of the logarithms of throughput

Type	LFDMA: CDS	LFDMA: Static	IFDMA: CDS	IFDMA: Static
Rate-sum capacity (32 users)	18 Mb/s	10 Mb/s	12 Mb/s	9.55 Mb/s
Fairness (32 users)	0.417	0.334	0.352	0.334
User capacity	48 users	less than 20	24 users	less than 20

Fairness = average user data rate of users at the cell boundary (900 m–1 km)/ average user data rate.

User capacity: number of users achieving 1 % outage probability when the minimum rate equals to 144 Kb/s.

various properties of the four scheduling schemes when the figure of merit is C_{fair} and 32 terminals share the channel. In the table, fairness is defined as the ratio of capacity at the edge of the cell to the average capacity of all 32 terminals.

5.5.2 Schedules Based on Delayed Channel State Information

In practical systems there is an inevitable delay between the time the base station measures the signal-to-noise ratio of all the subcarriers and the time that the terminal applies a schedule based on these channel state measurements. When the transmitting terminal is moving, the channel state changes with time and therefore the subcarrier mapping used in the transmission will not be perfectly matched to the current channel state. As a consequence performance will be degraded relative to the case with perfect, instantaneous channel state information. To describe the effects of this time delay on performance we begin with Figure 5.11, which applies to scheduling with perfect channel state information. The curves show throughput in Mb/s as a function of the number of terminals using a base station. The terminals apply adaptive modulation, using the eight techniques in Figure 5.4 according to the signal-to-noise ratio thresholds in Table 5.1. The schedule aims to maximize the sum of the logarithms of user throughput. As in the case of Shannon capacity, we see that channel dependent

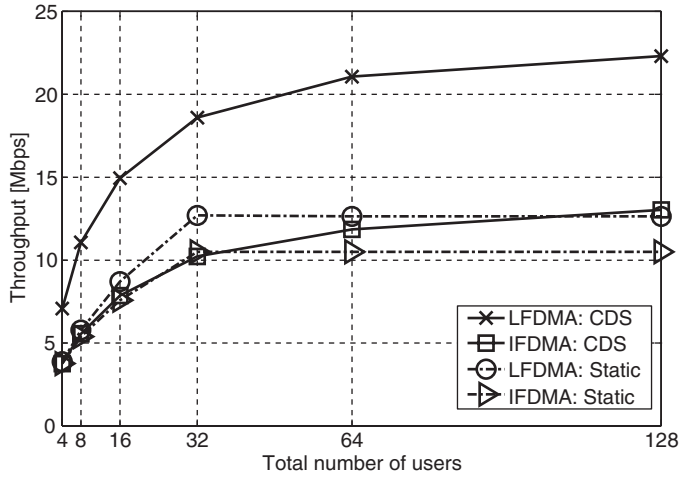

Figure 5.11 Aggregate throughput as a function of the number of terminals using a base station. LFDMA is localized FDMA and IFDMA is interleaved FDMA. The channel dependent schedules maximize sum of logarithm of throughput

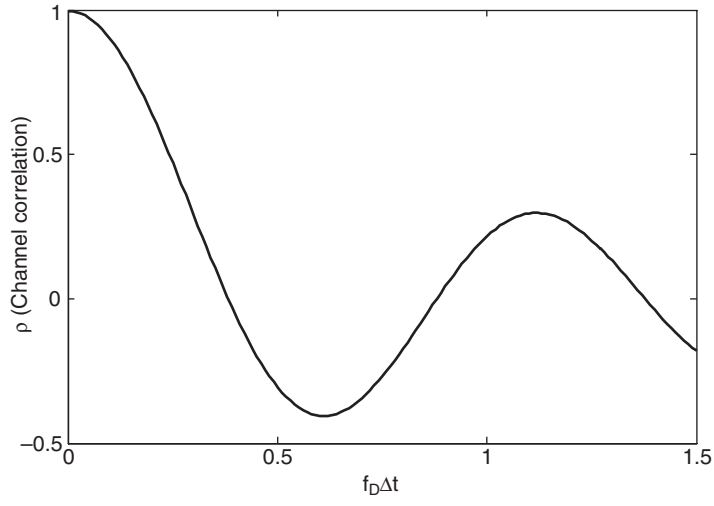

Figure 5.12 Rayleigh fading correlation coefficient as a function of the number of wavelengths of the Doppler frequency

scheduling (LFDMA: CDS) with localized FDMA provides a big performance gain relative to static scheduling (LFDMA: Static). However, channel dependent scheduling offers little or no advantage to interleaved FDMA; the throughput of "IFDMA: CDS" is very similar to the throughput of "IFDMA: Static".

The correlation coefficient $\rho(\Delta t)$ in Equation (5.10) is a measure of the relative change in channel state after a delay of Δt seconds. Figure 5.12 is a graph of the channel correlation ρ as a function of $f_D \Delta t$. The scale of the horizontal axis is normalized to the period of the maximum Doppler frequency f_D Hz. For a moving terminal, this quantity can be interpreted as distance traveled relative to the wavelength of the carrier frequency. It shows that the channel state information used to derive a schedule becomes less and less correlated with actual channel state information as the terminal moves. This situation is reflected in Figure 5.13, which shows that when 128 terminals share the channel and all of them are moving at the same velocity, the advantage of channel dependent scheduling in LFDMA disappears as $f_D \Delta t$ approaches 0.25. Moreover, channel dependent scheduling (LFDMA: CDS) results in lower aggregate throughput than static scheduling (LFDMA: Static) for $f_D \Delta t > 0.25$ because for certain delays there is negative correlation in Figure 5.12 between two sets of channel state measurements.

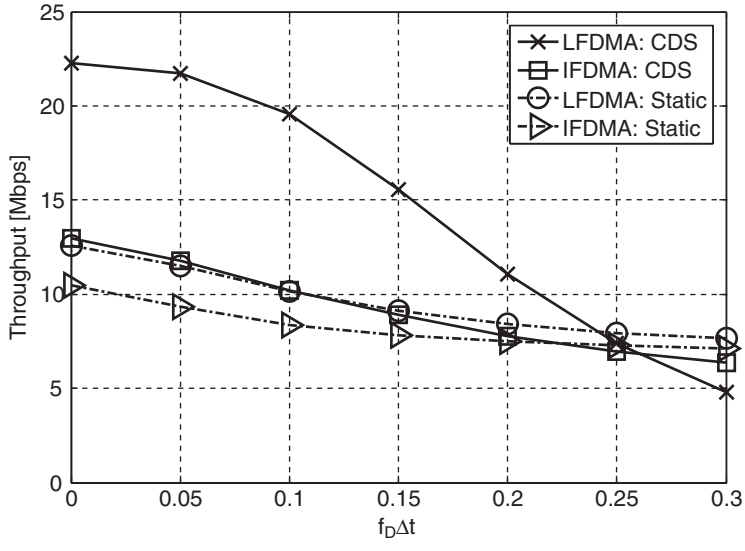

Figure 5.13 Aggregate throughput as a function of the number of wavelengths of the Doppler frequency of moving terminals with 128 terminals using the same base station. LFDMA is localized FDMA and IFDMA is interleaved FDMA. The channel dependent schedules maximize sum of logarithm of throughput

Figures 5.14 and 5.15 present different views of the information in Figure 5.13, by introducing practical values of the Doppler frequency f_D Hz and the feedback delay Δt seconds. In Figure 5.14, $f_D = 111$ Hz, corresponding to a speed of 60 km/h with a carrier frequency 2 GHz. The horizontal axis is feedback delay, Δt in milliseconds. This graphs shows that the advantage of channel dependent scheduling disappears when Δt exceeds approximately 2 msec. In Figure 5.15, $\Delta t = 3$ msec and the horizontal axis shows both speed of the terminal, v km/h, and Doppler frequency, f_D Hz. The carrier frequency is 2 GHz. In this case, channel dependent scheduling loses its benefit when v exceeds approximately 40 km/h corresponding to $f_D = 74$ Hz.

5.5.3 Discussion of Scheduling Studies

The simulation results presented in this chapter show numerically the potential advantages of channel dependent scheduling with localized FDMA transmissions. Channel dependent scheduling provides multi-user diversity because terminals in different locations have different channel selective fading frequency responses when transmitting to a base station. Channel

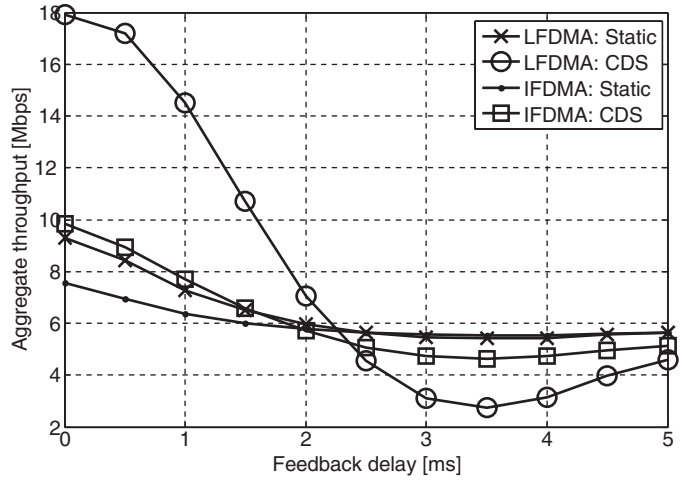

Figure 5.14 Aggregate throughput with CDS and adaptive modulation; mobile speed = 60 km/h (Doppler frequency = 111 Hz) [8]

dependent scheduling makes it possible for many terminals to use subcarriers with favorable transmission characteristics. However, the value of channel dependent scheduling depends on the quality of the channel state information used to derive a schedule. In the uplink of a cellular system,

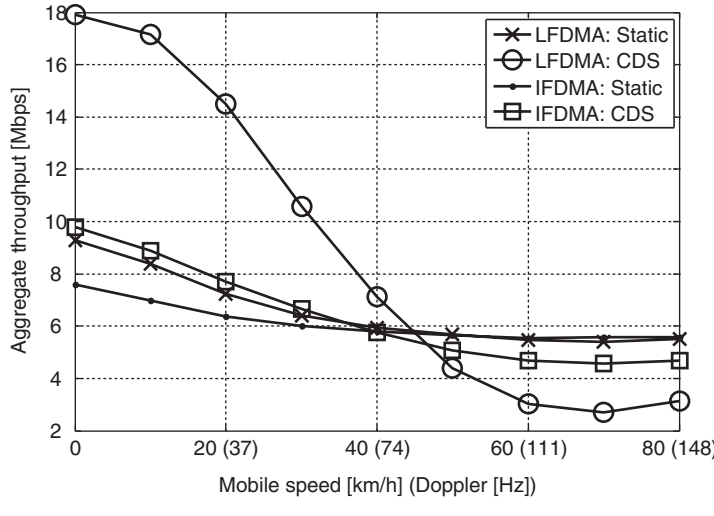

Figure 5.15 Aggregate throughput with CDS and adaptive modulation with feedback delay of 3 msec and different mobile speeds [8]

acquisition of channel state information uses system bandwidth because a terminal has to transmit channel sounding signals that span the entire frequency range of the channel, even though information signals occupy only a fraction of the band. Moreover, the channel sounding signals have to be transmitted frequently because the channel state information at two different times is uncorrelated or negatively correlated when the measurements times are separated by less than one period of the Doppler frequency. There are other sources of inaccuracy in channel state information that need to be investigated. Preliminary results of research into the effects of these inaccuracies suggest that they are less harmful than the effects of using schedules based on delayed channel state information.

5.6 Summary

In principle, channel dependent scheduling has the potential to improve the throughput of SC-FDMA transmissions by taking advantage of frequency selective fading in wireless channels. The value of channel dependent scheduling is considerably more pronounced in connection with localized FDMA than with interleaved FDMA. On the other hand, channel dependent scheduling consumes system bandwidth because it requires terminals to transmit channel sounding signals that span the entire frequency band of the system and requires the base station to transmit schedules to all the terminals sharing a channel. Moreover, when terminals are moving, the channel sounding and transmission of schedule information have to be performed frequently. Otherwise, the schedule used for transmission will not be matched to the channel conditions at the time of the transmission and the throughput of localized FDMA could be even lower than the throughput obtained with static scheduling.

References

[1] 3rd Generation Partnership Project, *3GPP TS 45.005 – Technical Specification Group GSM/EDGE Radio Access Network; Radio Transmission and Reception (Release 7)*, Sep. 2006.

[2] Wang, X., Giannakis, G.B., and Marques, A.G., "A Unified Approach to QoS-Guaranteed Scheduling or Channel-Adaptive Wireless Networks", *Proceeings of the IEEE*, vol. **95**, no. 12, Dec. 2007, pp. 2410–2431.

[3] Goldsmith, A., *Wireless Communications*, Cambridge University Press, 2005.

[4] Goldsmith, A.J. and Chua, S.-G., "Variable-Rate Variable-Power MQAM for Fading Channels," *IEEE Trans. Commun.*, vol. **45**, no. 10, Oct. 1997, pp. 1218–1230.

[5] Lim, J., "Adaptive Radio Resource Management for Uplink Wireless Networks," Ph.D. Dissertation, Polytechnic University, June 2006, Chapter 3.

[6] Lim, J., Myung, H.G., Goodman, D.J., *et al*., "Proportional Fair Scheduling of Uplink Single-Carrier FDMA Systems," *The 17th Annual IEEE International Symposium on Personal, Indoor and Mobile Radio Communications (PIMRC '06)*, Helsinki, Finland, Sep. 2006.

[7] Jakes, W.C., *Microwave Mobile Communications*, IEEE Communications Society, 1994.

[8] Myung, H.G., Oh, K., Lim, J., *et al*., "Channel-Dependent Scheduling of an Uplink SC-FDMA System with Imperfect Channel Information," *IEEE Wireless Communications and Networking Conference (WCNC) 2008*, Las Vegas, USA, Mar. 2008.

6

MIMO SC-FDMA

6.1 Introduction

Multiple input multiple output (MIMO) techniques have gathered much attention in recent years as a way to improve drastically the performance of wireless mobile communications. The MIMO technique utilizes multiple antenna elements at the transmitter and the receiver to improve communication link quality and/or communication capacity. A MIMO system can provide two types of gain: *spatial diversity* gain and *spatial multiplexing* gain. Spatial diversity improves the reliability of communication in fading channels and spatial multiplexing increases the capacity by sending multiple streams of data in parallel through multiple spatial channels. Transmit eigen-beamforming (TxBF) with unitary precoding is a spatial multiplexing technique that utilizes the eigen-structure of the channel to generate independent spatial channels. Practical considerations of TxBF that affect the performance and the overhead of the system are precoder quantization/averaging and feedback delay.

In this chapter, we first give a general overview of MIMO concepts. In Section 6.3, we describe the parallel decomposition of a MIMO channel for narrowband and wideband transmission. We also illustrate the realization of MIMO spatial multiplexing in SC-FDMA. In Section 6.4, we introduce the SC-FDMA TxBF with unitary precoding technique and numerically analyze the link level performance with practical considerations. In Section 6.5, we describe the SC-FDMA spatial diversity schemes.

Single Carrier FDMA: A New Air Interface for Long Term Evolution Hyung G. Myung and David J. Goodman
 ISBN: 978-0-470-72449-1

6.2 Spatial Diversity and Spatial Multiplexing in MIMO Systems

The basic idea behind spatial diversity techniques is to combat channel fading by having multiple copies of the transmitted signal go through independently fading propagation paths. At the receiver, multiple independently faded replicas of the transmitted data signal are coherently combined to achieve more reliable reception. Spatial diversity gain is the signal-to-noise ratio (SNR) exponent of the error probability and intuitively it corresponds to the number of independently faded paths. It is well known that in a system with N_t transmit antennas and N_r receive antennas, the maximal diversity gain is $N_t \cdot N_r$, assuming the path gains between the individual transmit and receive antenna pairs are independently and identically distributed (i.i.d.) Rayleigh-faded [1]: Smart antenna techniques [2], Alamouti transmit diversity scheme [3], and space-time coding [4] are some well known spatial diversity techniques.

If spatial diversity is a means to combat fading, spatial multiplexing is a way to exploit fading to increase the data throughput. In essence, if the path gains among individual transmit–receive antenna pairs fade independently such that the channel matrix is well-conditioned, multiple parallel spatial channels can be created and the data rate can be increased by transmitting multiple streams of data through the spatial channels. Spatial multiplexing is especially important in the high-SNR regime where the system is degree-of-freedom limited as opposed to power limited in the low-SNR regime. A scheme achieves a spatial multiplexing gain of r if the supported data rate approaches $r \cdot \log(SNR)$ (b/s/Hz) and we can think of the multiplexing gain as the total number of degrees of freedom to communicate. In a system with N_t transmit antennas and N_r receive antennas for high SNR, Foschini [5] and Telatar [6] showed that the capacity of the channel increases linearly with $m = \min(N_t, N_r)$ if the channel gains among the antenna pairs are i.i.d. Rayleigh-faded. Thus there is m number of parallel channels or m number of degrees of freedom. BLAST (Bell Labs Layered Space-Time) [5] is a typical spatial multiplexing technique.

For a given MIMO channel, both diversity and multiplexing gains can be achieved simultaneously but there is a fundamental tradeoff between the two gains. For example, Zheng and Tse [7] showed that the optimal diversity gain achievable by any coding scheme of block length larger than $N_t + N_r - 1$ with multiplexing gain m (integer) is precisely $(N_t - m) \cdot (N_r - m)$ for i.i.d. Rayleigh slowly-fading channels with N_t transmit and N_r receive antennas. This implies that out of the total resource of N_t transmit and N_r receive antennas, it is as though m transmit and m receive antennas were used

for multiplexing and the remaining $N_t - m$ transmit and $N_r - m$ receive antennas provided the diversity. In summary, higher spatial diversity gain comes at the price of lowering spatial multiplexing gain and vice versa.

6.3 MIMO Channel

First, we consider the narrowband MIMO channel. A point-to-point narrowband MIMO channel with N_t transmit antennas and N_r receive antennas is illustrated in Figure 6.1. We can represent such a MIMO system by the following discrete-time model:

$$\underbrace{\begin{pmatrix} y_1 \\ \vdots \\ y_{N_r} \end{pmatrix}}_{=\underline{y}} = \underbrace{\begin{pmatrix} h_{11} & \cdots & h_{1N_t} \\ \vdots & \ddots & \vdots \\ h_{N_r 1} & \cdots & h_{N_r N_t} \end{pmatrix}}_{=H} \cdot \underbrace{\begin{pmatrix} x_1 \\ \vdots \\ x_{N_t} \end{pmatrix}}_{=\underline{x}} + \underbrace{\begin{pmatrix} n_1 \\ \vdots \\ n_{N_r} \end{pmatrix}}_{=\underline{n}} \tag{6.1}$$
$$\Rightarrow \underline{y} = H \cdot \underline{x} + \underline{n}$$

where $\underline{x}$ is the $N_t \times 1$ transmitted signal vector, $\underline{y}$ is the $N_r \times 1$ received signal vector, $\underline{n}$ is the $N_r \times 1$ zero-mean complex Gaussian noise, and H is the $N_r \times N_t$ complex matrix of channel gains h_{ij} representing the gain from jth transmit antenna to ith receive antenna.

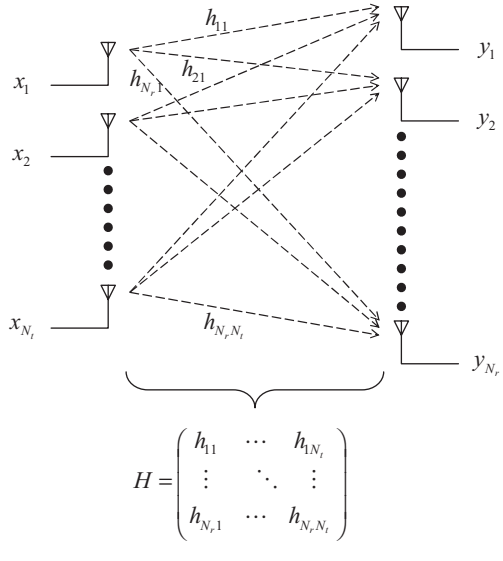

Figure 6.1 Description of a MIMO channel with N_t transmit antennas and N_r receive antennas

By the singular value decomposition (SVD) theorem, channel matrix H can be decomposed as follows:

$$H = UDV^H \tag{6.2}$$

where U is an $N_r \times N_r$ unitary matrix, V is an $N_t \times N_t$ unitary matrix, D is an $N_r \times N_t$ non-negative diagonal matrix, and $(\bullet)^H$ is a Hermitian (conjugate transpose) operation. The diagonal entries of D are the non-negative square roots of the eigenvalues of HH^H, the columns of U are the eigenvectors of HH^H, and the columns of V are the eigenvectors of $H^H H$.

We can rewrite Equation (6.1) using Equation (6.2) as

$$\underline{y} = UDV^H \underline{x} + \underline{n} \tag{6.3}$$

Multiplying U^H on both sides of Equation (6.3), it becomes

$$\begin{aligned} U^H \underline{y} &= \underbrace{U^H U}_{=I} DV^H \underline{x} + U^H \underline{n} \\ U^H \underline{y} &= DV^H \underline{x} + U^H \underline{n} \end{aligned} \tag{6.4}$$

Let $\widetilde{\underline{y}} = U^H \underline{y}$, $\widetilde{\underline{x}} = V^H \underline{x}$, and $\widetilde{\underline{n}} = U^H \underline{n}$, then,

$$\tilde{\underline{y}} = D\tilde{\underline{x}} + \widetilde{\underline{n}} \tag{6.5}$$

where $\widetilde{\underline{n}}$ has the same statistical properties as $\underline{n}$ since U is a unitary matrix. Thus $\widetilde{\underline{n}}$ is an $N_r \times 1$ zero-mean complex Gaussian noise.

We can see from Equation (6.5) that the MIMO transmission can be decomposed into up to $m = \min(N_t, N_r)$ parallel independent transmissions, which is the basis for the spatial multiplexing gain.

For a wideband MIMO channel, the entire band can be subdivided into sub-bands, or subcarriers. Then, the MIMO channel for each subcarrier becomes a narrowband MIMO channel. Let the entire band be subdivided into M subcarriers, then for k^{th} subcarrier $(0 \le k \le M-1)$

$$\begin{aligned} &\underbrace{\begin{pmatrix} Y_{1,k} \\ \vdots \\ Y_{N_r,k} \end{pmatrix}}_{=\underline{y}_k} = \underbrace{\begin{pmatrix} H_{11,k} & \cdots & H_{1N_t,k} \\ \vdots & \ddots & \vdots \\ H_{N_r1,k} & \cdots & H_{N_rN_t,k} \end{pmatrix}}_{=H_k} \cdot \underbrace{\begin{pmatrix} X_{1,k} \\ \vdots \\ X_{N_t,k} \end{pmatrix}}_{=\underline{x}_k} + \underbrace{\begin{pmatrix} N_{1,k} \\ \vdots \\ N_{N_r,k} \end{pmatrix}}_{=\underline{N}_k} \\ &\Rightarrow \underline{Y}_k = H_k \cdot \underline{X}_k + \underline{N}_k \end{aligned} \tag{6.6}$$

where $\underline{X}_k$ is the $N_t \times 1$ transmitted signal vector, $\underline{Y}_k$ is the $N_r \times 1$ received signal vector, $\underline{N}_k$ is the $N_r \times 1$ zero-mean complex Gaussian noise, and H_k is the $N_r \times N_t$ complex matrix of channel gains $H_{ij,k}$ representing the gain

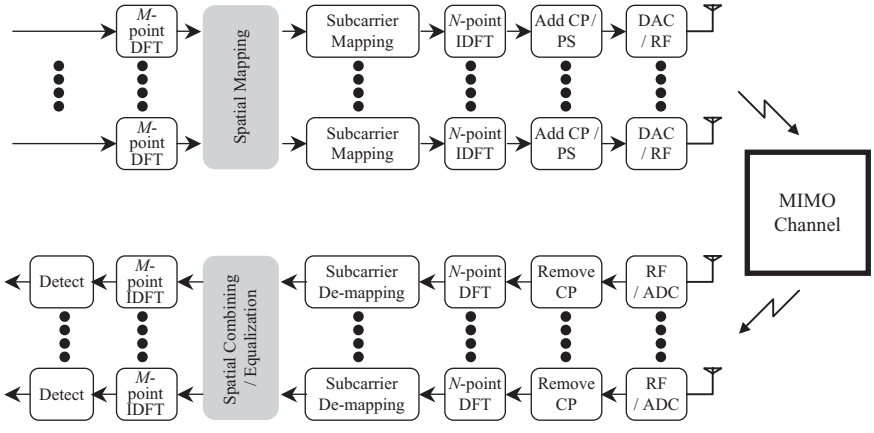

Figure 6.2 Block diagram of a spatial multiplexing MIMO SC-FDMA system

from *j*th transmit antenna to *i*th receive antenna. Similarly with a narrowband MIMO channel, H_k can be decomposed into $U_k D_k V_k^H$ and Equation (6.6) can be expressed as

$$\widetilde{\underline{Y}}_k = D_k \widetilde{\underline{X}}_k + \widetilde{\underline{N}}_k \tag{6.7}$$

where $\widetilde{\underline{Y}}_k = U_k^H \underline{Y}_k$, $\widetilde{\underline{X}}_k = V_k^H \underline{X}_k$, and $\widetilde{\underline{N}}_k = U_k^H \underline{N}_k$.

We can use spatial multiplexing MIMO techniques in SC-FDMA by applying the spatial processing on a subcarrier-by-subcarrier basis, somewhat similar to MIMO-OFDM [8], in the frequency domain after DFT. A block diagram of a spatial multiplexing MIMO SC-FDMA system is shown in Figure 6.2.

6.4 SC-FDMA Transmit Eigen-Beamforming with Unitary Precoding

Transmit eigen-beamforming (TxBF) with unitary precoding utilizes the eigen-structure of the channel to achieve spatial multiplexing [9], [10]. Figure 6.3 illustrates a simplified block diagram of a unitary precoded TxBF SC-FDMA MIMO system. We describe below the basic processes of unitary precoded TxBF system. We assume the channel is time-invariant and the channel estimation is perfect, and we follow the notations in Equation (6.6).

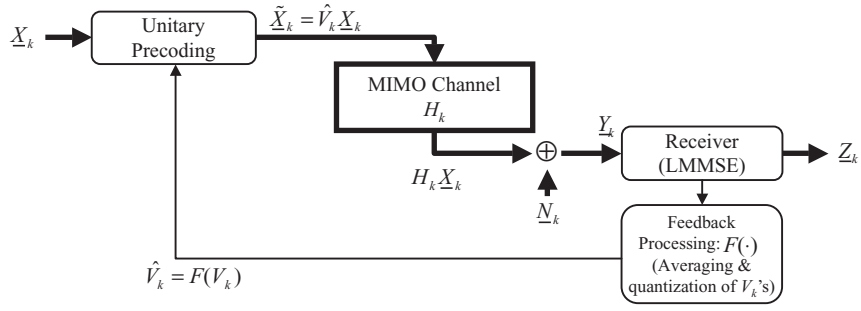

Figure 6.3 Simplified block diagram of a unitary precoded TxBF SC-FDMA MIMO system

First, the MIMO channel matrix H_k for subcarrier k is decomposed as follows using SVD for each subcarrier at the receiver:

$$H_k = U_k D_k V_k^H \tag{6.8}$$

We feedback V_k to the transmitter and use it as the precoding matrix for transmission. We may quantize and average the $\{V_k\}$s at the receiver to reduce feedback overhead. We denote the quantization and averaging processes as $F(\cdot)$ and $\hat{V}_k = F(V_k)$. The quantized and averaged $\{\hat{V}_k\}$s are then sent to the transmitter via the feedback channel. The transmitter precodes the data signal $\underline{X}_k$ with $\hat{V}_k$ as follows:

$$\tilde{\underline{X}}_k = \hat{V}_k \underline{X}_k \tag{6.9}$$

After the transmitted signal propagates through the MIMO channel H_k, the received signal $\underline{Y}_k$ is represented as follows:

$$\underline{Y}_k = H_k \tilde{\underline{X}}_k + \underline{N}_k \tag{6.10}$$

At the receiver, we perform linear minimum mean square error (LMMSE) estimation for joint equalization and MIMO detection. Let $\underline{Z}_k = A_k \underline{Y}_k$ where A_k is an $N_t \times N_r$ complex matrix. Then, our goal is to find A_k such that mean square error between $\underline{X}_k$ and $\underline{Z}_k$ ($E\{|\underline{X}_k - \underline{Z}_k|^2\}$) is minimum. By applying the orthogonality principle, we obtain the following solution for A_k:

$$A_k = R_{XX,k} \hat{H}_k^H \left(\hat{H}_k R_{XX,k} \hat{H}_k^H + R_{NN,k} \right)^{-1} \tag{6.11}$$

where $\hat{H}_k = H_k \hat{V}_k$, $R_{XX,k} = \underline{X}_k \underline{X}_k^H$, and $R_{NN,k} = \underline{N}_k \underline{N}_k^H$.

There are two practical factors that impact the performance of precoded TxBF: precoder quantization/averaging and feedback delay. Since the receiver feeds back the precoding matrix to the transmitter, the receiver often

quantizes and also averages across all subcarriers the precoding matrix to reduce feedback overhead. We could expect some degradation in performance because we lose some of the precoder information during quantization and averaging processes. Feedback delay becomes a major factor in the performance of precoded TxBF when the channel is changing very fast because the precoder is extracted directly from the current channel matrix.

In the following sections, we give numerical analysis for a 2×2 uplink MIMO system to quantify the impact of quantized and averaged feedback on the link level performance. We base the simulation setup on 3GPP LTE uplink and we use the following simulation parameters and assumptions:

- carrier frequency: 2.0 GHz;
- transmission bandwidth: 5 MHz;
- symbol rate: 7.68 million symbols/sec;
- TTI length: 0.5 msec;
- number of blocks per TTI: 6 long blocks (LB);
- number of occupied subcarriers per LB: 128;
- FFT block size: 512;
- Cyclic Prefix (CP) length: 32 symbols;
- subcarrier mapping: static distributed;
- pulse shaping: time domain squared-root raised-cosine filter (roll-off factor $= 0.22$) with $2\times$ oversampling;
- channel model: 3GPP SCME C (Spatial Channel Model Extension C) quasi-static Rayleigh fading with mobile speed of 3 km/h [11] – we assume the channel is constant during the duration of a block;
- antenna configurations: 2 transmit and 2 receive antennas;
- data modulation: 16-QAM for 1st stream and QPSK for 2nd stream;
- channel coding: 1/3-rate turbo code;
- we use linear MMSE equalizer described in Equation (6.11);
- we assume no feedback error and perfect channel estimation at the receiver.

6.4.1 Impact of Imperfect Feedback: Precoder Quantization/ Averaging

We directly quantize the 2×2 precoding matrix V_k in the form of Jacobi rotation matrix, which is a unitary matrix [12]. We use the following matrix to quantize V_k:

$$\hat{V}_k = \begin{bmatrix} \cos\hat{\theta}_k & -\sin\hat{\theta}_k \cdot e^{j\hat{\phi}_k} \\ \sin\hat{\theta}_k \cdot e^{j\hat{\phi}_k} & \cos\hat{\theta}_k \end{bmatrix} \tag{6.12}$$

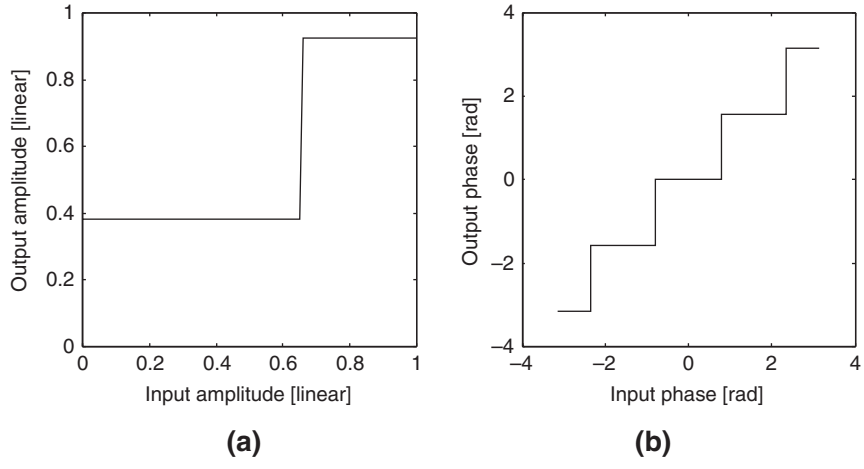

Figure 6.4 Input-output characteristics of the quantizers: (a) amplitude quantizer (1 bit); (b) phase quantizer (2 bits)

where for B_{amp} bits to quantize the amplitude component,

$$\hat{\theta}_k \in \left\{ (2l-1)\frac{\pi}{4 \cdot 2^{B_{amp}}};\ l = 1, \cdots,\ 2^{B_{amp}} \right\} \tag{6.13}$$

and for B_{phase} bits to quantize the phase component,

$$\hat{\phi}_k \in \left\{ \frac{2\pi}{2^{B_{phase}}} l - \pi;\ l = 1, \cdots,\ 2^{B_{phase}} \right\} \tag{6.14}$$

Figure 6.4 shows the input-output quantization characteristics. For phase quantization, we use the first antenna as a reference and normalize the phase of the second antenna element with respect to that of first antenna element. To reduce the overhead of the feedback, $\{V_k\}$s are averaged over either 12 or 25 contiguous subcarriers.

Figure 6.5 shows the Monte Carlo simulation results for frame error rate (FER) performance of the 2×2 SC-FDMA unitary precoded TxBF system. We can see that the performance loss at 1 % FER with regards to no averaging and no quantization case is 1.3 dB for the worst case (25-subcarrier averaging and 2-bit phase-only quantization).

Figure 6.6(a) shows the effect of different quantization bit resolutions (no averaging) and Figure 6.6(b) shows the effect of different averaging sizes (1-bit amplitude and 2-bit phase quantization). As we use more bits and smaller averaging size, we see less performance degradation.

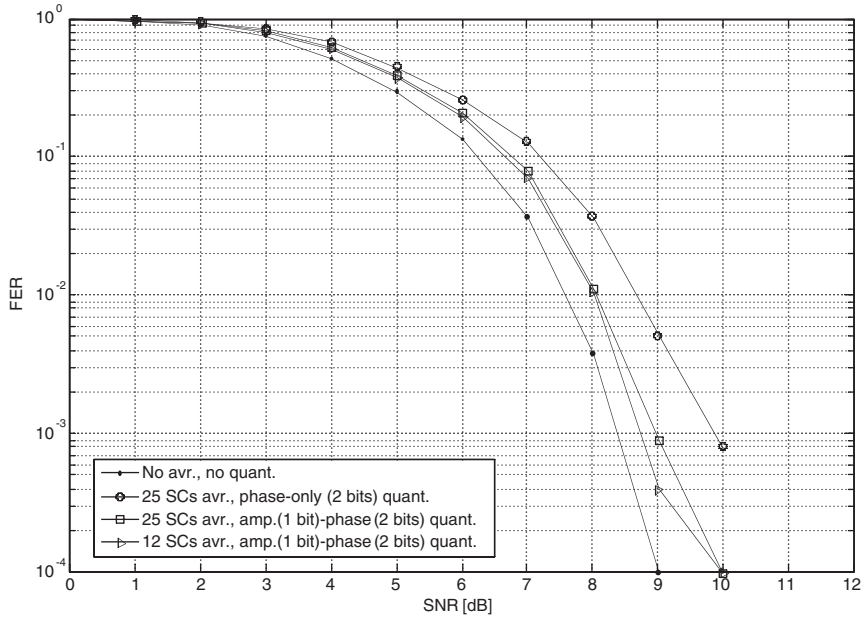

Figure 6.5 FER performance of a 2×2 SC-FDMA unitary precoded TxBF system with feedback averaging and quantization

Table 6.1 summarizes the tradeoff between feedback overhead and performance loss based on the results in Figure 6.5. Performance loss is the SNR level increase at 1 % FER point with regards to that of no averaging and no quantization result. As we increase the feedback overhead, that is, increase the amount of precoding information, there is less performance loss.

6.4.2 Impact of Imperfect Feedback: Feedback Delay

Delay is inevitable in any realistic feedback system. When the channel is changing fast due to the user's motion or change of the environment, the precoder may be outdated and it will affect the receiver performance. Figure 6.7 shows the impact of feedback delay for different user speeds. We consider feedback delays of 2, 4, and 6 TTIs with no feedback quantization or averaging.

We can see from Figure 6.7(a) that at a low speed of 3 km/h, there is only a trivial loss of performance even for the longest delay of 6 TTIs. But as the user speed becomes faster, we can see the performance degradation becomes more severe as illustrated in Figure 6.7(b). Clearly, in high mobility

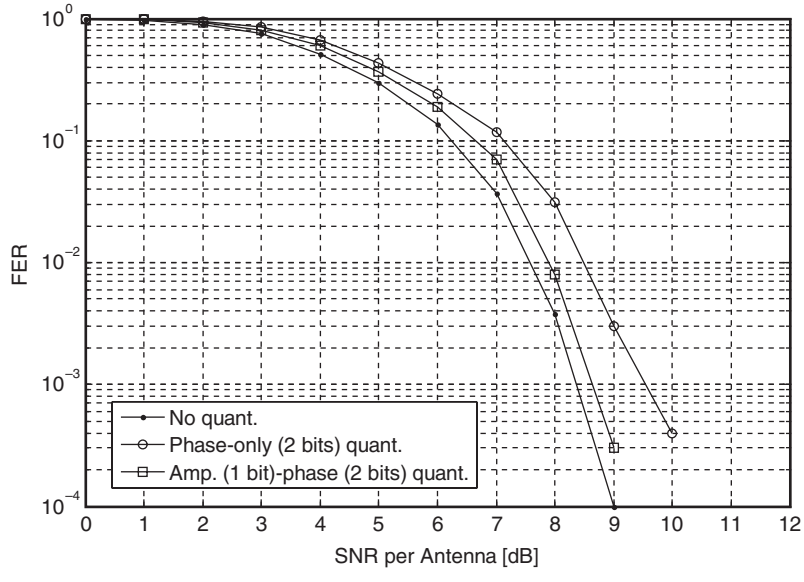

(a)

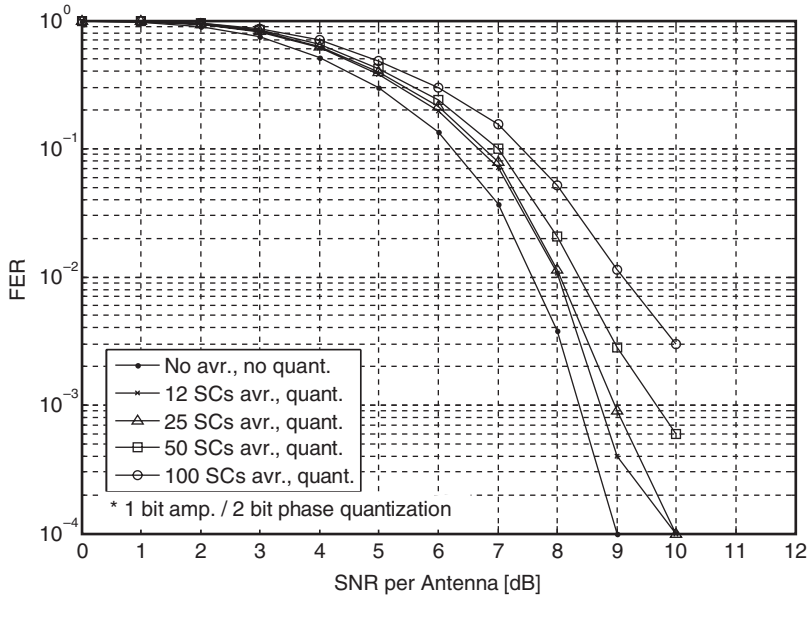

(b)

Figure 6.6 FER performance: (a) with different quantization bit resolutions (no averaging); (b) with different averaging sizes (1-bit amplitude and 2-bit phase quantization)

Table 6.1 Summary of feedback overhead versus performance loss

Averaging size (subcarriers per block)	No. of blocks	Quantization resolution (bits)	Feedback overhead	Performance loss
25	12	Phase: 2, Amp.: none	2 bits × 12 = 24 bits	1.3 dB
25	12	Phase: 2, Amp.: 1	3 bits × 12 = 36 bits	0.6 dB
12	25	Phase: 2, Amp.: none	2 bits × 25 = 50 bits	1 dB
12	25	Phase: 2, Amp.: 1	3 bits × 25 = 75 bits	0.5 dB

and long feedback delay situations, TxBF with unitary precoding does not perform well at all.

6.5 SC-FDMA Spatial Diversity

The transmit diversity scheme is one of the well-known techniques to achieve spatial diversity. In this scheme, signals are transmitted from multiple spatially separated antennas. With careful mapping of the signals into the multiple transit antennas, a gain equal to maximal ratio combining (MRC) can be achieved. For two transmit antennas, the Alamouti diversity scheme is a simple and elegant method to achieve efficiently the spatial diversity gain [3]. Figure 6.8 shows the single carrier narrowband transmitter with the Alamouti scheme for two transmit antennas.

Space-time block coding (STBC) and space-frequency block coding (SFBC) are transmit diversity schemes that are well-suited for wideband multi-carrier systems such as OFDM [13], [14]. Similarly, with spatial multiplexing, we can use spatial diversity techniques in SC-FDMA by applying the spatial processing on a subcarrier-by-subcarrier basis in the frequency domain after DFT. Figures 6.9 and 6.10 show examples of SC-FDMA STBC and SFBC implementations for two transmit antennas, respectively [15].

6.6 Summary

The MIMO technique utilizes multiple antenna elements on the transmitter and the receiver to improve communication link quality and/or communication capacity, and it has two aspects in terms of performance improvement: spatial diversity and spatial multiplexing. Spatial diversity improves

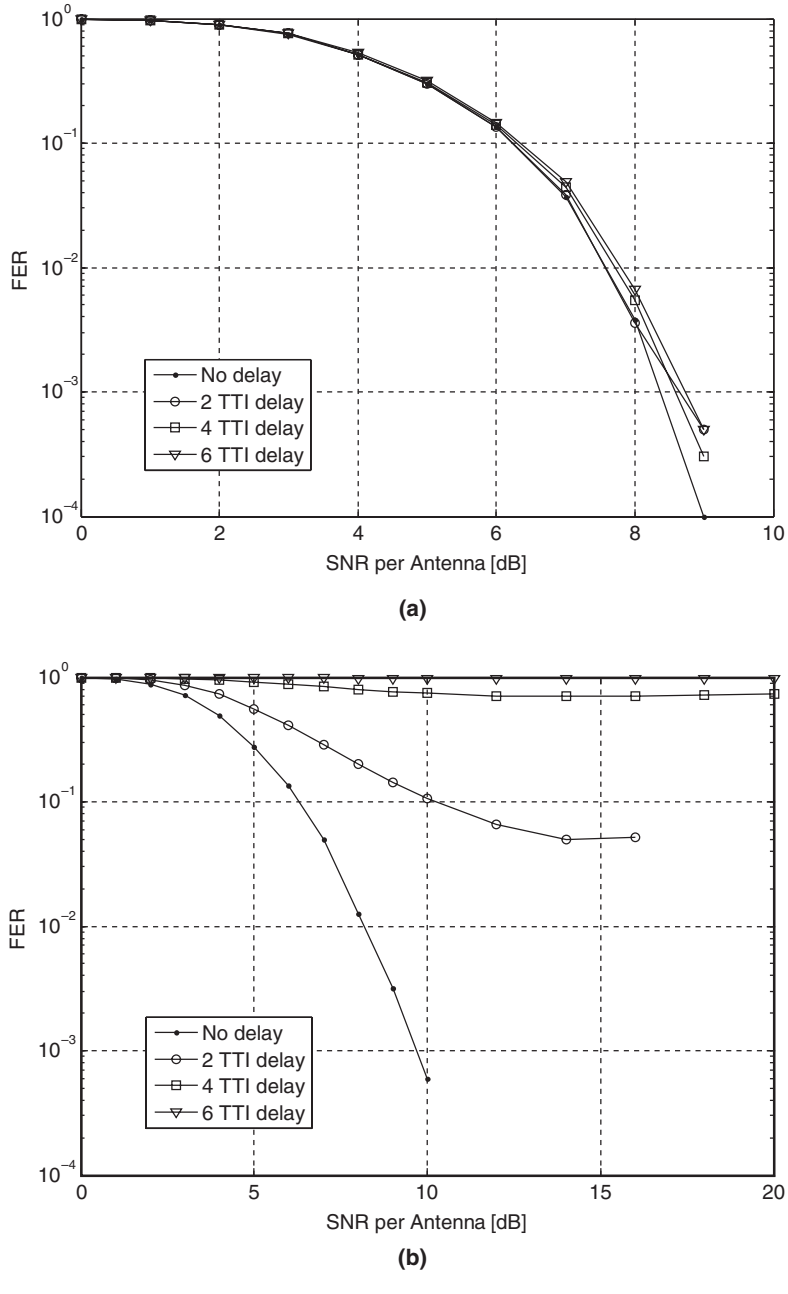

Figure 6.7 FER performance of a 2 × 2 SC-FDMA unitary precoded TxBF system with feedback delays of 2, 4, and 6 TTIs: (a) user speed of 3 km/h; (b) user speed of 150 km/h

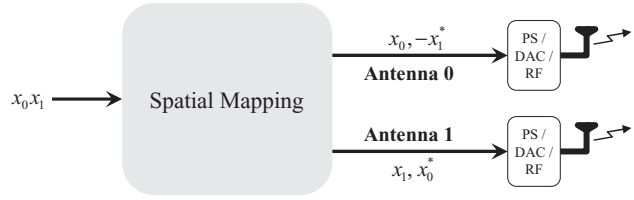

Figure 6.8 Single carrier narrowband transmitter with the Alamouti scheme for two transmit antennas

the reliability of communication in fading channels and spatial multiplexing increases the capacity by sending multiple streams of data in parallel through multiple spatial channels.

Transmit eigen-beamforming (TxBF) with unitary precoding is a spatial multiplexing technique that utilizes the eigen-structure of the channel to generate independent spatial channels. Practical considerations of TxBF that affect the performance and the overhead of the system are precoder quantization/averaging and feedback delay. Quantizing and averaging the

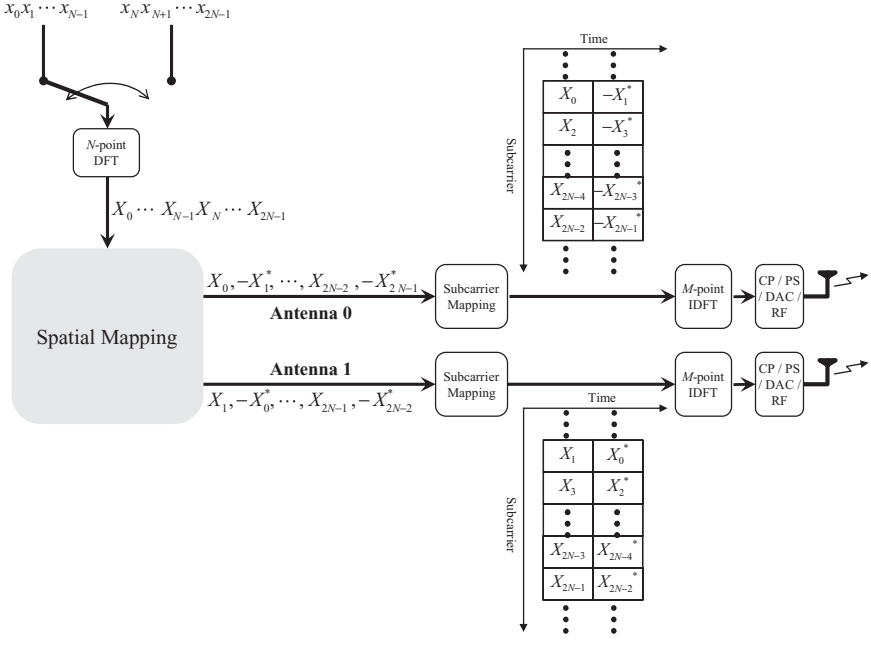

Figure 6.9 Implementation of SC-FDMA STBC transmitter for two transmit antenna

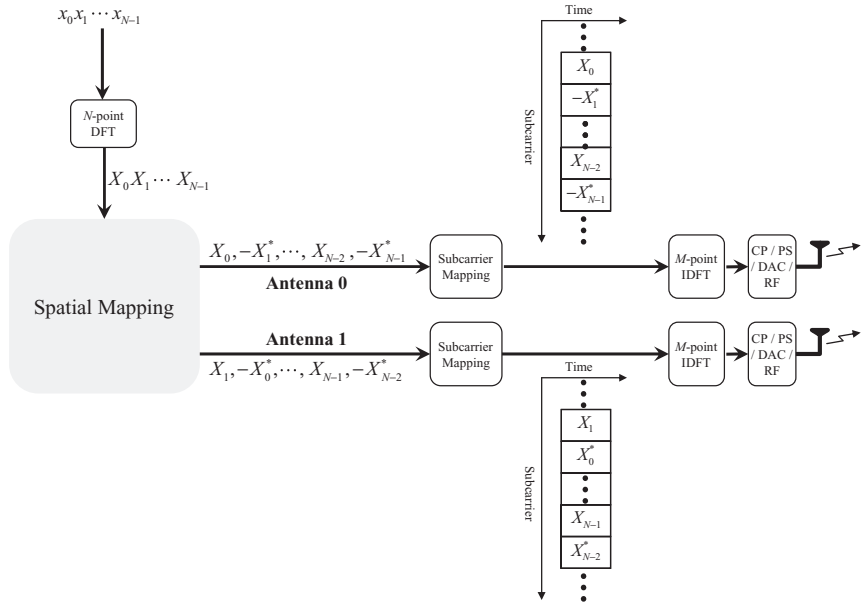

Figure 6.10 Implementation of SC-FDMA SFBC transmitter for two transmit antenna

precoding matrix reduces the feedback overhead but the link performance suffers.

In this chapter, we gave an overview of the realization of MIMO spatial multiplexing and spatial diversity in SC-FDMA. We specifically analyzed the unitary precoded TxBF technique on an SC-FDMA system. We showed with numerical simulations that there is a tradeoff between the feedback overhead and the link performance loss. We also showed that feedback delay is another impairment that degrades the performance especially for the high-speed mobile users.

References

[1] Paulraj, A., Nabar, R., and Gore, D., *Introduction to Space-Time Wireless Communications*, Cambridge University Press, May 2003.

[2] Chryssomallis, M., "Smart Antennas," *IEEE Antennas and Propagation Mag.*, vol. **42**, no. 3, June 2000, pp. 129–136.

[3] Alamouti, S., "A Simple Transmit Diversity Technique for Wireless Communications," *IEEE J. Select. Areas Commun.*, vol. **16**, Oct. 1998, pp. 1451–1458.

[4] Tarokh, V., Seshadri, N., and Calderbank, A.R., "Space-Time Codes for High Data Rate Wireless Communication: Performance Criterion and Code Construction," *IEEE Trans. Inform. Theory*, vol. **44**, Mar. 1998, pp. 744–765.

[5] Foschini, G.J., "Layered Space-Time Architecture for Wireless Communication in a Fading Environment when using Multi-Element Antennas," *Bell Labs Tech. J.*, vol. **1**, no. 2, 1996, pp. 41–59.

[6] Telatar, I.E., "Capacity of Multi-Antenna Gaussian Channels," *Europ. Trans. Telecommu.*, vol. **10**, Nov./Dec. 1999, pp. 585–595.

[7] Zheng, L. and Tse, D.N.C., "Diversity and Multiplexing: A Fundamental Tradeoff in Multiple-Antenna Channels," *IEEE Trans. Info. Theory*, vol. **49**, no. 5, May 2003, pp. 1073–1096.

[8] Stüber, G.L., Barry, J.R., McLaughlin, S.W., *et al.*, "Broadband MIMO-OFDM Wireless Communications," *Proceedings of the IEEE*, Feb. 2004, vol. **92**, no. 2, pp. 271–294.

[9] Hammerschmidt, J.S., Brunner, C., and Drewes, C., "Eigenbeamforming - A Novel Concept in Array Signal Processing," *Proc. European Wireless Conference 2000*, Dresden, Germany, Sep. 2000.

[10] InterDigital, "Extension of Uplink MIMO SC-FDMA with Preliminary Simulation Results," Technical Document R1-060365, *3GPP TSG-RAN WG1 #44*, Feb. 2006.

[11] Ericsson, Elektrobit, Nokia, Motorola, and Siemens, "LTE Channel Models and Simulations," Technical Document R4-060334, *3GPP TSG-RAN WG4 #38*, Feb. 2006.

[12] Golub, G.H. and Van Loan, C.F., *Matrix Computations*, Johns Hopkins University Press, 2nd edition, 1989.

[13] Lee, K.F. and Williams, D.B., "A Space-Frequency Transmitter Diversity Technique for OFDM Systems," *Proc. IEEE GLOBECOM '00*, vol. **3**, San Francisco, CA, Nov. 2000, pp. 1473–1477.

[14] Bauch, G., "Space-Time Block Codes Versus Space-Frequency Block Codes," *Proc. IEEE 57th Veh. Technol. Conf. (VTC '03-Spring)*, vol. **1**, Apr. 2003, pp. 567–571.

[15] Alcatel, "Effect of Different ST/SF Coding and Mapping Schemes on the PAPR of the SC-FDMA in E-UTRA Uplink," Technical Document R1-061123, *3GPP TSG-RAN WG1 #45*, May 2006.

7

Peak Power Characteristics of a SC-FDMA Signal

7.1 Introduction

Peak-to-average-power ratio (PAPR) is a performance measurement that is indicative of the power efficiency of the transmitter. In the case of an ideal linear power amplifier where we achieve linear amplification up to the saturation point, we reach the maximum power efficiency when the amplifier is operating at the saturation point. A positive PAPR in dB means that we need a power backoff to operate in the linear region of the power amplifier. We can express the theoretical relationship between PAPR [dB] and transmit power efficiency as follows [1]:

$$\eta = \eta_{\max} \cdot 10^{-\frac{PAPR}{20}} \tag{7.1}$$

where η is the power efficiency and $\eta_{\max}$ is the maximum power efficiency. For class A power amplifier, $\eta_{\max}$ is 50 % and for class B, 78.5 % [2]. Figure 7.1 shows the relationship graphically and it is evident from the figure that high PAPR degrades the transmit power efficiency performance.

A salient advantage of SC-FDMA over OFDMA is the lower PAPR because of its inherent single carrier structure. The lower PAPR is greatly beneficial in the uplink communications where the mobile terminal is the transmitter. As we showed in Section 3.4, time domain samples of the SC-FDMA modulated signals are different depending on the subcarrier mapping scheme and we can expect different PAPR characteristics for different subcarrier mapping schemes.

Single Carrier FDMA: A New Air Interface for Long Term Evolution Hyung G. Myung and David J. Goodman
 ISBN: 978-0-470-72449-1

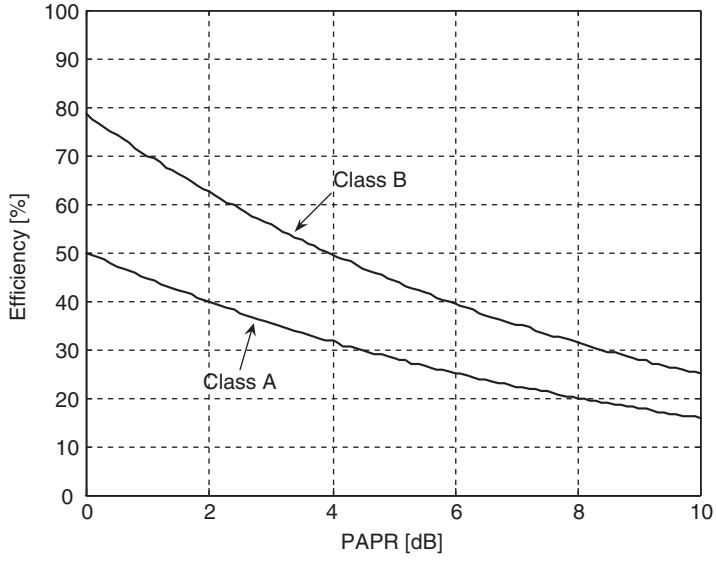

Figure 7.1 A theoretical relationship between PAPR and transmit power efficiency for ideal class A and B amplifiers

In this chapter, we first present an analytical analysis of peak power characteristics for a conventional single carrier modulated signal. In Section 7.3, we characterize the PAPR for single antenna transmission of SC-FDMA and investigate the PAPR properties for different subcarrier mapping schemes. In Section 7.4, we analyze the PAPR characteristics for multiple antenna transmission. Specifically, we numerically analyze the complementary cumulative distribution function (CCDF) of PAPR for the 2×2 unitary precoded transmit eigen-beamforming (TxBF) SC-FDMA system described in Chapter 6. In Section 7.5, we describe a symbol amplitude clipping method to reduce peak power. We show the link level performance and frequency domain aspects of the proposed clipping method.

7.2 Peak Power Characteristics of a Single Carrier Signal

The peak power of any signal $x(t)$ is the maximum of its squared envelope $|x(t)|^2$. However, for a continuous random process, $\max |x(t)|^2$ could be unbounded. Even for a random process with discrete values where $\max |x(t)|^2$ is bounded, it may occur at very low probability. The distribution of $|x(t)|^2$ is a more useful performance indicator and we describe it with the complementary cut-off probability. For a given w, cut-off

probability is defined as $\Pr\{|x(t)|^2 \leq w\} = F_{|x(t)|^2}(w)$, where $F_{|x(t)|^2}(w)$ is the cumulative distribution function (CDF) of $|x(t)|^2$, and the complementary cut-off probability is $\Pr\{|x(t)|^2 \geq w\} = 1 - F_{|x(t)|^2}(w)$. $\Pr\{|x(t)|^2 \geq w\}$ is also referred to as the complementary cumulative distribution function (CCDF).

In [3], Wulich and Goldfeld showed that the amplitude of a single carrier (SC) modulated signal does not have a Gaussian distribution and that it is difficult to derive analytically the exact form of the distribution. As an alternative, they explained a way to derive an upper bound for the complementary distribution of the instantaneous power using the Chernoff bound. We follow their derivation to characterize the peak power analytically for the conventional single carrier modulated signal.

We consider a baseband representation of the conventional SC modulated signal

$$x(t, \underline{s}) = \sum_{k=-\infty}^{\infty} s_k p(t - kT) \tag{7.2}$$

where $\{s_k\}_{k=-\infty}^{\infty}$ are transmitted symbols, $\underline{s} = [\ldots, s_{-1}, s_0, s_1, \ldots]$, $p(t)$ is the pulse shaping filter, and T is the symbol duration. s_k belongs to a modulation constellation set C of size B, that is, $s_k \in C = \{c_b : 0 \leq b \leq B - 1\}$ and it is uniformly distributed. We assume that $\{s_k\}$s are independent of each other.

Let us define a random variable Z for a given $t_0 \in [0, T)$ as follows:

$$Z \triangleq x(t_0, \underline{s}) = \sum_{k=-\infty}^{\infty} s_k p(t_0 - kT) = \sum_{k=-\infty}^{\infty} a_k \tag{7.3}$$

where $a_k = s_k p(t_0 - kT)$. $\{a_k\}$s are also mutually independent since $\{s_k\}$s are mutually independent.

Since s_k is uniformly distributed over C and from Equation (7.3),

$$\Pr[a_k = c_b p(t_0 - kT)] = \Pr[s_k = c_b] = \frac{1}{B} \tag{7.4}$$

where $0 \leq b \leq B - 1$.

Our goal is to characterize the following CCDF:

$$\Pr\left[\left|x(t_0, \underline{s})\right|^2 \geq w\right] = \Pr\left[|Z|^2 \geq w\right] = \Pr[|Z| \geq \delta] \tag{7.5}$$

where $w \geq 0$ and $\delta = \sqrt{w}$.

Let us assume the modulation constellation set C is real and its constellation points are symmetric around zero. Then,

$$\begin{aligned}\Pr[|Z| \geq \delta] &= \Pr[Z \geq \delta] + \Pr[Z \leq -\delta] \\ &= 2\Pr[Z \geq \delta]\end{aligned} \tag{7.6}$$

Using the Chernoff bound, the following inequality holds [4]:

$$\Pr[Z \geq \delta] \leq e^{-\hat{\nu}\delta} E\left\{e^{\hat{\nu}Z}\right\} \tag{7.7}$$

where $\hat{\nu}$ is a solution of the following equation:

$$E\left\{Ze^{\nu Z}\right\} - \delta \cdot E\left\{e^{\nu Z}\right\} = 0 \tag{7.8}$$

By expanding $E\{Ze^{\nu Z}\}$ and $E\{e^{\nu Z}\}$, Equation (7.8) becomes

$$\sum_{k=-\infty}^{\infty} \frac{E\left\{a_k e^{\hat{\nu}a_k}\right\}}{E\left\{e^{\hat{\nu}a_k}\right\}} = \delta \tag{7.9}$$

for $\nu = \hat{\nu}$. By solving Equation (7.9), we obtain $\hat{\nu}$ for a given δ. Since Equation (7.9) is not in a closed form, we evaluate the solution numerically.

We can upper-bound the CCDF $\Pr[|x(t_0, \underline{s})|^2 \geq w]$ as follows from Equations (7.5), (7.6), and (7.7).

$$\Pr\left[\left|x(t_0, \underline{s})\right|^2 \geq w\right] \leq 2e^{-\hat{\nu}\delta} \prod_{k=-\infty}^{\infty} E\left\{e^{\hat{\nu}a_k}\right\} \triangleq P_{ub,SC} \tag{7.10}$$

To make Equations (7.9) and (7.10) tractable for numerical evaluation, we limit the span by only considering $-K_{\max} \leq k \leq K_{\max}$. In the case of IFDMA, as long as its input block size N is larger than $K_{\max}$, the instantaneous power distribution of the IFDMA signal will have the same upper bound as the conventional SC signal because the input symbols are mutually independent within the span of $-K_{\max} \leq k \leq K_{\max}$.

Let us consider BPSK modulation. For BPSK, we use the following constellation set:

$$C_{BPSK} = \{-1, 1\} \tag{7.11}$$

Also, we consider the following raised-cosine pulse in Equation (3.5):

$$p(t) = \frac{\sin(\pi t/T)}{\pi t/T} \cdot \frac{\cos(\pi \alpha t/T)}{1 - 4\alpha^2 t^2/T^2} \tag{7.12}$$

where $0 \leq \alpha \leq 1$ is the roll-off factor.

Then, Equation (7.9) becomes

$$\sum_{k=-K_{\max}}^{K_{\max}} \frac{\frac{1}{2}p(t_0-kT)e^{\hat{\nu}p(t_0-kT)} - \frac{1}{2}p(t_0-kT)e^{-\hat{\nu}p(t_0-kT)}}{\frac{1}{2}e^{\hat{\nu}p(t_0-kT)} + \frac{1}{2}e^{-\hat{\nu}p(t_0-kT)}} = \delta \qquad (7.13)$$

After we determine $\hat{\nu}$ from Equation (7.13), the upper bound in Equation (7.10) becomes

$$P_{ub,SC}^{(BPSK)} \triangleq e^{-\hat{\nu}\delta}\left(\frac{1}{2}\right)^{2K_{\max}} \prod_{k=-K_{\max}}^{K_{\max}} \left(e^{\hat{\nu}p(t_0-kT)} + e^{-\hat{\nu}p(t_0-kT)}\right) \qquad (7.14)$$

and we upper-bound the CCDF as

$$\Pr\left[\left|x^{(BPSK)}(t_0, \underline{s})\right|^2 \geq w\right] \leq P_{ub,SC}^{(BPSK)} \qquad (7.15)$$

Detailed derivations of Equations (7.9), (7.10), (7.13), and (7.14) are provided in Appendix B at the end of the book.

Figure 7.2 shows $P_{ub,SC}^{(BPSK)}$ for $K_{\max} = 8$, $T = 1$, and $t_0 = T/2 = 0.5$ along with the empirical results using Monte Carlo simulation. We considered roll-off factor α of 0, 0.2, 0.4, and 0.6. For the Monte Carlo simulation, we generated 1000 random BPSK-modulated blocks with each block having 64 symbols, and produced a histogram. We can see that the upper bound we derived in Equation (7.14) is valid compared to the empirical results and that the bound is rather tight in the tail region of the distribution in which we are most interested. Another interesting observation is the fact that the peak power at a given probability increases as the roll-off factor of the raised-cosine filter becomes closer to zero ($a = 0$ corresponds to an ideal bandpass filter).

In case of an OFDM multi-carrier signal, we can simply express the CCDF of the PAPR for N subcarriers with Nyquist rate sampling as follows [5]:

$$\Pr\{PAPR \geq w\} = 1 - \left(1 - e^{-w}\right)^N \qquad (7.16)$$

It should be noted that if oversampling is applied or the number of subcarriers is small, this expression is not accurate. More accurate derivations can be found in [6] and [7].

Figure 7.3 compares the analytical upper bounds of CCDF for single carrier modulated signals with the theoretical CCDF for OFDM. For single carrier signals, we consider a roll-off factor of 0, 0.2, and 0.4. For OFDM, the numbers of occupied subcarriers N are 32, 128, and 512, and we do not apply a pulse-shaping filter. We consider the case of BPSK modulation. We can see that single carrier signals indeed have lower peak power at a given probability than that of OFDM.

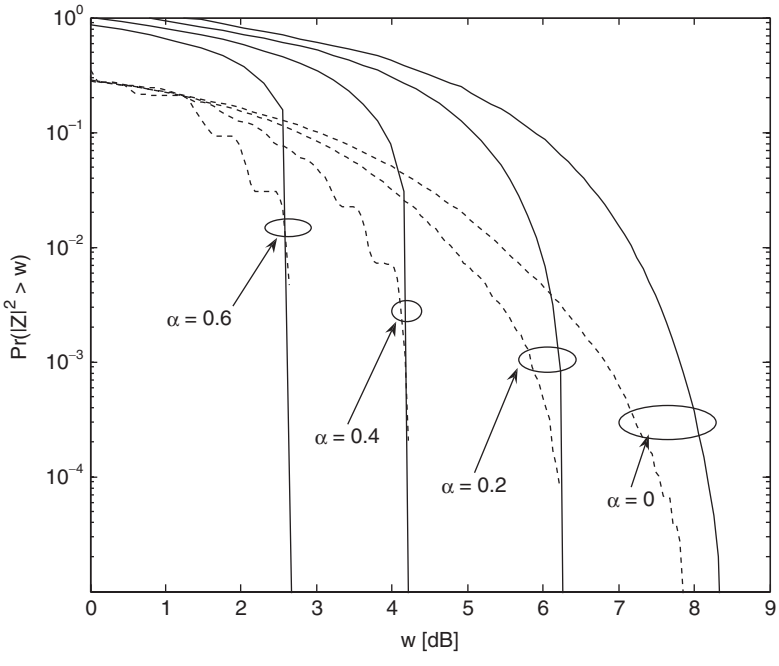

Figure 7.2 CCDF of instantaneous power for BPSK modulation and different values of roll-off factor α; dotted lines are empirical results and solid lines are the upper bounds

7.3 PAPR of Single Antenna Transmission Signals

In this section, we analyze the PAPR of the SC-FDMA signal for each subcarrier mapping mode. We follow the notations in Figure 3.2 of Chapter 3.

Let $\{x_m : m = 0,\ 1, \ldots,\ M-1\}$ be data symbols to be modulated. Then, $\{X_k : k = 0,\ 1, \ldots,\ M-1\}$ are frequency domain samples after DFT of $\{x_m : m = 0,\ 1, \ldots,\ M-1\}$, $\{\tilde{X}_l : l = 0,\ 1, \ldots,\ N-1\}$ are frequency domain samples after subcarrier mapping, and $\{\tilde{x}_n : n = 0,\ 1, \ldots,\ N-1\}$ are time symbols after IDFT of $\{\tilde{X}_l : l = 0,\ 1, \ldots,\ N-1\}$. We represent the complex passband transmit signal of SC-FDMA $x(t)$ for a block of data as

$$x(t) = e^{j\omega_c t} \sum_{n=0}^{N-1} \tilde{x}_n p(t - n\tilde{T}) \tag{7.17}$$

where ω_c is the carrier frequency of the system, $p(t)$ is the baseband pulse, and $\tilde{T}$ is the symbol duration of the transmitted symbol $\tilde{x}_n$. We consider a raised-cosine (RC) pulse and a square-root raised-cosine (RRC)

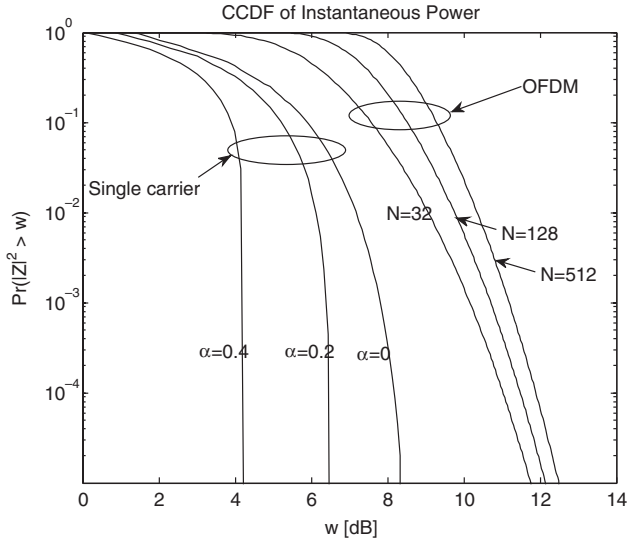

Figure 7.3 CCDF of instantaneous power for single carrier and OFDM signals with BPSK data constellations based on analytical formula: for single carrier signals, we consider a roll-off factor of 0, 0.2, and 0.4; for OFDM, the numbers for occupied subcarriers N are 32, 128, and 512

pulse, which are widely used pulse shapes in wireless communications. The following are the time and frequency expressions for the two pulse shapes:

$$P_{RC}(f) = \begin{cases} \tilde{T}, & 0 \le |f| \le \dfrac{1-\alpha}{2\tilde{T}} \\ \dfrac{\tilde{T}}{2}\left\{1+\cos\left[\dfrac{\pi\tilde{T}}{\alpha}\left(|f|-\dfrac{1-\alpha}{2\tilde{T}}\right)\right]\right\}, & \dfrac{1-\alpha}{2\tilde{T}} \le |f| \le \dfrac{1+\alpha}{2\tilde{T}} \\ 0, & |f| \ge \dfrac{1+\alpha}{2\tilde{T}} \end{cases} \tag{7.18}$$

$$p_{RC}(t) = \frac{\sin\left(\dfrac{\pi t}{\tilde{T}}\right)\cdot\cos\left(\dfrac{\pi\alpha t}{\tilde{T}}\right)}{\dfrac{\pi t}{\tilde{T}}\cdot\left(1-\dfrac{4\alpha^2 t^2}{\tilde{T}^2}\right)} \tag{7.19}$$

$$P_{RRC}(f) = \sqrt{P_{RC}(f)} \tag{7.20}$$

$$p_{RRC}(t) = \frac{\sin\left(\dfrac{\pi t}{\tilde{T}}(1-\alpha)\right)+4\alpha\dfrac{t}{\tilde{T}}\cdot\cos\left(\dfrac{\pi t}{\tilde{T}}(1+\alpha)\right)}{\dfrac{\pi t}{\tilde{T}}\cdot\left(1-\dfrac{16\alpha^2 t^2}{\tilde{T}^2}\right)} \tag{7.21}$$

We define the PAPR as follows for transmit signal $x(t)$:

$$\text{PAPR} = \frac{\text{peak power of } x(t)}{\text{average power of } x(t)} = \frac{\max\limits_{0 \le t \le N\tilde{T}} |x(t)|^2}{\frac{1}{N\tilde{T}} \int_0^{N\tilde{T}} |x(t)|^2 \, dt} \tag{7.22}$$

Without pulse shaping, symbol rate sampling will give the same PAPR as the continuous case because SC-FDMA signal is modulated over a single carrier. Thus, we express the PAPR without pulse shaping with symbol rate sampling as follows:

$$\text{PAPR} = \frac{\max\limits_{n=0,1,\ldots,N-1} |\tilde{x}_n|^2}{\frac{1}{N} \sum\limits_{n=0}^{N-1} |\tilde{x}_n|^2} \tag{7.23}$$

As mentioned earlier, the amplitude of a single carrier modulated signal does not have a Gaussian distribution unlike OFDM signals and it is difficult to derive analytically the exact form of the distribution. In this book, we resort to numerical analysis to investigate the PAPR properties for SC-FDMA signals.

Using Monte Carlo simulation, we calculate the CCDF (Complementary Cumulative Distribution Function) of PAPR, which is the probability that PAPR is higher than a certain PAPR value PAPR_0 ($\Pr\{PAPR > PAPR_0\}$). We evaluate and compare the CCDFs of PAPR for IFDMA, DFDMA, LFDMA, and OFDMA. The simulation setup and assumptions are as follows:

- We generate 10^4 uniformly random data blocks to acquire the CCDF of PAPR.
- We consider QPSK and 16-QAM symbol constellations.
- We truncate the baseband pulse $p(t)$ from $-6\tilde{T}$ to $6\tilde{T}$ time periods, we oversample it by 8 times, and we use transmission bandwidth of 5 MHz.
- We consider consecutive chunks for LFDMA.
- We do not apply any pulse shaping in the case OFDMA.

Figure 7.4 contains the plots of CCDF of PAPR for IFDMA, DFDMA, LFDMA, and OFDMA for total number of subcarriers $N = 512$, number of input symbols $M = 128$, IFDMA spreading factor $Q = 4$, and DFDMA spreading factor $\tilde{Q} = 2$. We compare the PAPR value that is exceeded with the probability less than 0.1 % ($\Pr\{PAPR > PAPR_0\} = 10^{-3}$), or 99.9-percentile PAPR. We denote 99.9-percentile PAPR as $\text{PAPR}_{99.9\%}$. Table 7.1 summarizes the 99.9-percentile PAPR for each subcarrier mapping.

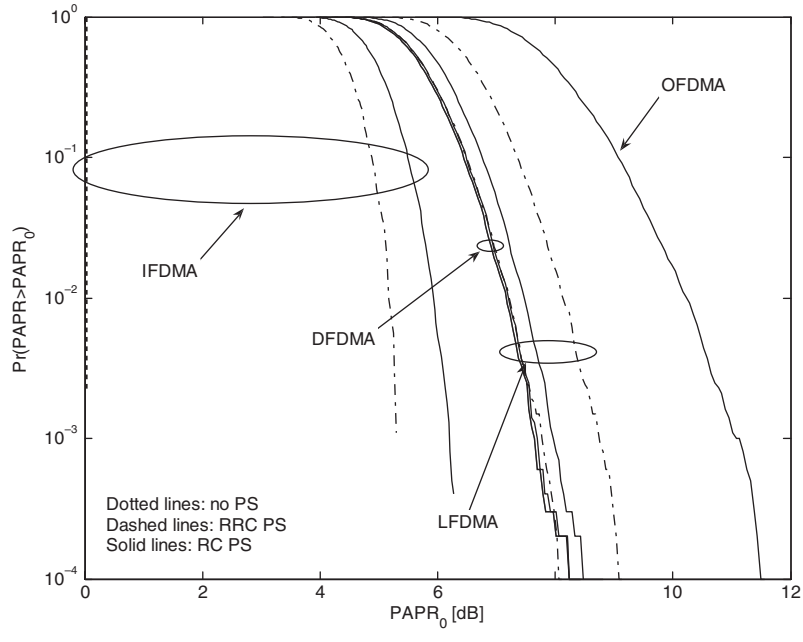

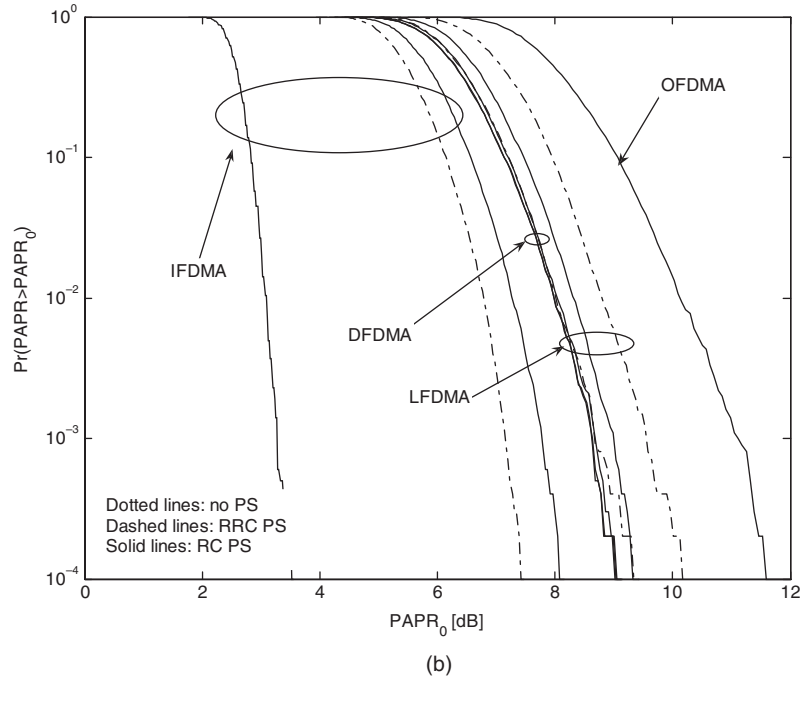

Figure 7.4 Comparison of CCDF of PAPR for IFDMA, DFDMA, LFDMA, and OFDMA with total number of subcarriers $N = 512$, number of input symbols $M = 128$, IFDMA spreading factor $Q = 4$, DFDMA spreading factor $\tilde{Q} = 2$, and α (roll-off factor) $= 0.22$: (a) QPSK; (b) 16-QAM

Table 7.1 99.9-percentile PAPR for IFDMA, DFDMA, LFDMA, and OFDMA

Modulation	Pulse shaping	IFDMA (dB)	DFDMA (dB)	LFDMA (dB)	OFDMA (dB)
QPSK	None	0	7.7	7.7	11.1
	RC	6.2	7.7	8.0	N/A
	RRC	5.3	7.8	8.7	N/A
16-QAM	None	3.2	8.7	8.7	11.1
	RC	7.8	8.7	9.0	N/A
	RRC	7.2	8.7	9.5	N/A

RC: raised-cosine pulse shaping; RRC: squared-root raised-cosine pulse shaping; rolloff factor = 0.22

We can see that all the cases for SC-FDMA have indeed lower PAPR than that of OFDMA. Also, IFDMA has the lowest PAPR, and DFDMA and LFDMA have very similar levels of PAPR.

Figure 7.5 shows the impact of the roll-off factor α on the PAPR when using raised-cosine pulse shaping for $N = 256$, $M = 64$, and $Q = 4$. We can see that this impact is more obvious in the case of IFDMA. As the roll-off factor decreases from 1 to 0, PAPR increases significantly for IFDMA. This implies that there is a tradeoff between PAPR performance and out-of-band radiation because out-of-band radiation increases with increasing roll-off factor.

7.4 PAPR of Multiple Antenna Transmission Signals

In this section, we analyze the PAPR characteristics of multiple antenna transmission for an SC-FDMA system. Specifically, we investigate unitary precoded transmit eigen-beamforming (TxBF) for two transmit antennas, which we described in Section 6.4 of Chapter 6. Since it is difficult to derive the PAPR analytically, we resort to numerical analysis using Monte Carlo simulation to investigate the PAPR properties of our MIMO SC-FDMA system. We use the parameters in Section 6.4 for the simulations in this section.

As described in Section 6.4, we apply unitary precoding in the frequency domain after DFT. Precoding in the frequency domain is convolution (filtering) and summation in the time domain as shown in Figure 7.6. Thus we expect to see an increase in the peak power because of the filtering and summation.

Figure 7.7 shows the CCDF of the PAPR for 2×2 unitary precoded TxBF. To verify that the filtering aspect of the precoding is the dominant

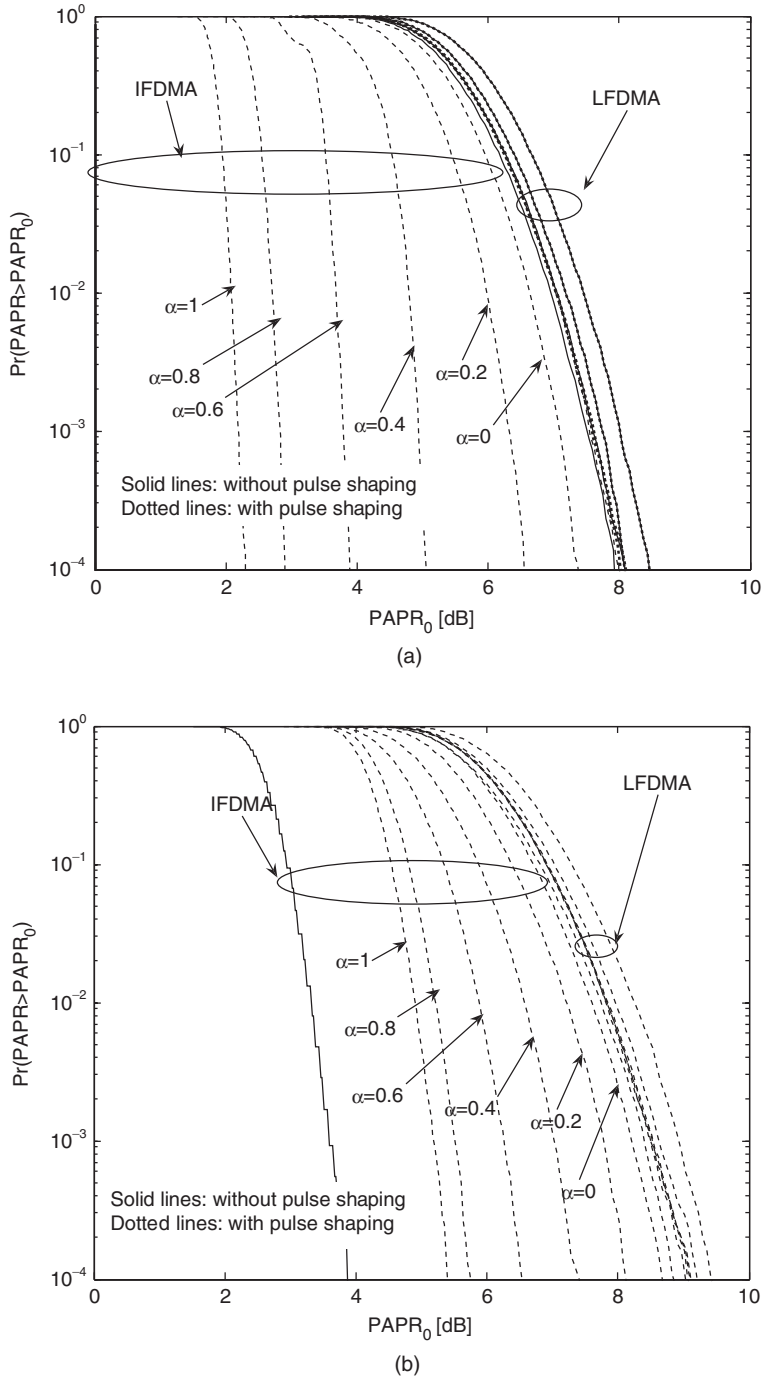

Figure 7.5 Comparison of CCDF of PAPR for IFDMA and LFDMA with total number of subcarriers $N = 256$, number of input symbols $M = 64$, spreading factor $Q = 4$, and α (roll-off factor) of 0, 0.2, 0.4, 0.6, 0.8, and 1: (a) QPSK; (b) 16-QAM

$$V_k = \begin{pmatrix} V_{11,k} & V_{12,k} \\ V_{21,k} & V_{22,k} \end{pmatrix}, S_k = \begin{pmatrix} S_{1,k} \\ S_{2,k} \end{pmatrix}$$

$$X_k = V_k \cdot S_k$$

$$= \begin{pmatrix} V_{11,k} & V_{12,k} \\ V_{21,k} & V_{22,k} \end{pmatrix} \cdot \begin{pmatrix} S_{1,k} \\ S_{2,k} \end{pmatrix}$$

$$= \begin{pmatrix} V_{11,k} \cdot S_{1,k} + V_{12,k} \cdot S_{2,k} \\ V_{21,k} \cdot S_{1,k} + V_{22,k} \cdot S_{2,k} \end{pmatrix} \quad \longleftrightarrow \quad \underline{x} = \begin{pmatrix} \underline{v_{11}} * \underline{s_1} + \underline{v_{12}} * \underline{s_2} \\ \underline{v_{21}} * \underline{s_1} + \underline{v_{22}} * \underline{s_2} \end{pmatrix}$$

$$\underline{V_{ij}} = \{V_{ij,0}, V_{ij,1}, \cdots, V_{1ij,M-}\}$$

$$\underline{S_l} = \{S_{l,0}, S_{l,1}, \cdots, S_{l,M-1}\}$$

$$\underline{v_{ij}} = IDFT\{\underline{V_{ij}}\} \quad , \underline{s_l} = IDFT\{\underline{S_l}\}$$

Frequency domain Time domain

Figure 7.6 Precoding in the frequency domain is convolution and summation in the time domain. Subscript k refers to the subcarrier number

factor in increasing the PAPR, we also show results for the case when there is only filtering by intentionally setting the 2nd antenna signal to zero, that is, $\underline{s_2} = 0$ (the graph labeled "2nd stream zero"), and for the case when there is only summation by intentionally replacing the convolution with a scalar multiplication of the first element of $\underline{v_{ij}}$ (the graph labeled "Only summation"). With precoding, we can see that there is an increase of 1.6 dB for the 1st antenna and 2.6 dB for the 2nd antenna in the 99.9-percentile

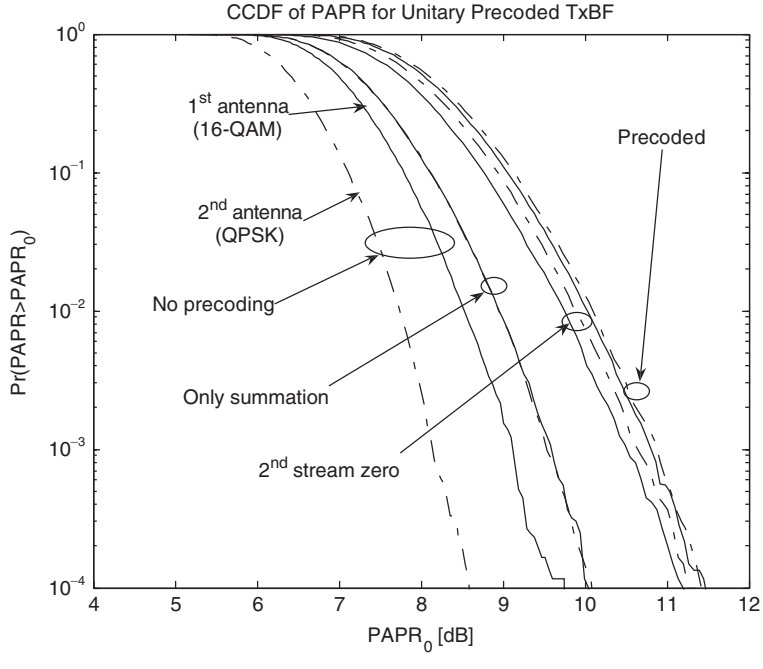

Figure 7.7 CCDF of PAPR for 2 × 2 unitary precoded TxBF

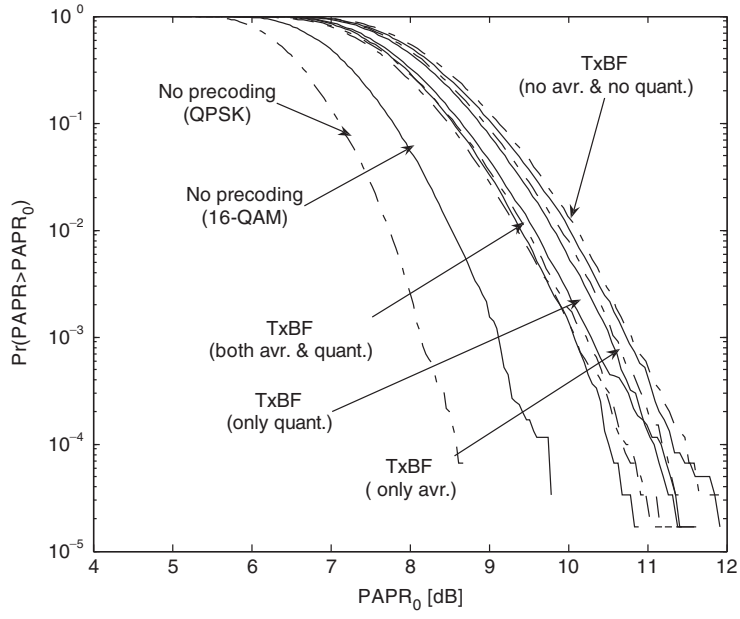

Figure 7.8 Impact of quantization and averaging of the precoding matrix on PAPR

PAPR. We can also observe that the filtering aspect is the main contributor to the increase of PAPR for precoding.

Figure 7.8 illustrates the impact of quantization and averaging of the precoding matrix on the PAPR characteristics. We use the quantization and averaging process described in Section 6.4.1 of Chapter 6. We average the channel H over 25 continuous subcarriers and perform direct quantization of the precoder matrix V using 3 bits (1 bit for amplitude and 2 bits for phase information).

Without averaging of channel and quantization of precoding matrix, the MIMO TxBF signal has 1.6 ∼2.6 dB higher $\text{PAPR}_{99.9\%}$ with respect to single antenna transmission. When we apply both averaging and quantization, $\text{PAPR}_{99.9\%}$ decreases by 0.7 dB. This is due to the fact that the averaging and quantization of the precoding matrix smoothes the time filtering, and thus reduces the peak power.

Figure 7.9 compares the CCDF of the PAPR for unitary precoded TxBF with those of different MIMO schemes. We consider space-frequency block coding (SFBC) and nonprecoded spatial multiplexing (SM) for comparison. Since the spatial multiplexing that we consider does not have any precoding or spatial processing at the transmitter, it has the same PAPR

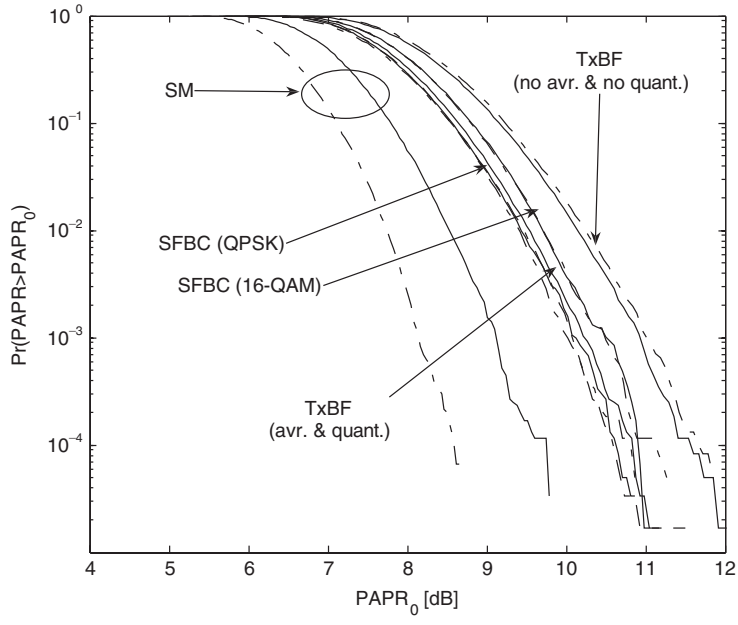

Figure 7.9 PAPR comparison with other MIMO schemes

as the case of single antenna transmission. Without quantization/averaging of precoding matrix, TxBF has higher $\text{PAPR}_{99.9\%}$ than that of SFBC by $0.5 \sim 1$ dB. However, TxBF and SFBC have similar PAPR when we have quantization/averaging of the precoding matrix.

7.5 Peak Power Reduction by Symbol Amplitude Clipping

One way to reduce PAPR is to limit or clip the peak power of the transmitted symbols. Depending on the smoothness of the limiter, we can define three types of limiter: *hard*, *soft*, and *smooth* [8]. The input-out relationship of each type of amplitude limiter for a complex symbol is as follows. Note that we leave the phase of the symbol as is, and modify only the amplitude part:

Hard limiter:

$$y_m = g_{hard}(x_m) = A_{\max} e^{j\angle x_m} \tag{7.24}$$

Soft limiter:

$$y_m = g_{soft}(x_m) = \begin{cases} x_m, & |x_m| \le A_{\max} \\ A_{\max} e^{j\angle x_m}, & |x_m| > A_{\max} \end{cases} \tag{7.25}$$

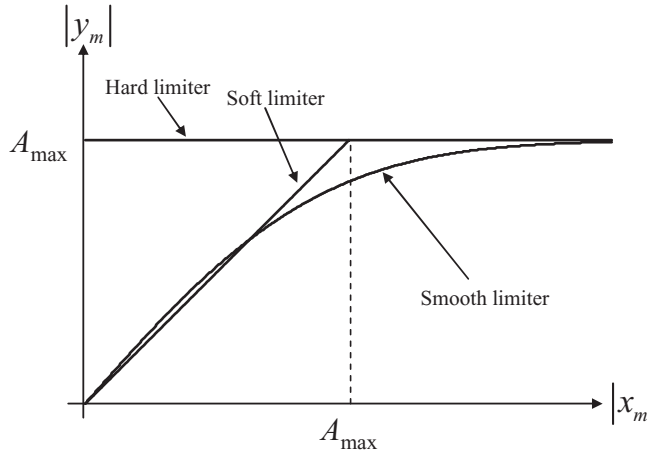

Figure 7.10 Three types of amplitude limiter

Smooth limiter:

$$y_m = g_{smooth}(x_m) = A_{\max}\text{erf}(|x_m| / A_{\max})\, e^{j\angle x_m} \tag{7.26}$$

where x_m is the input symbol to the limiter, $\angle x_m$ is the phase component of x_m, y_m is the output symbol of the limiter, $A_{\max} > 0$, and $\text{erf}(x) = \frac{2}{\sqrt{\pi}} \int_0^x e^{-t^2} dt$. Figure 7.10 graphically illustrates the input amplitude-output amplitude relationship of each limiter. In the subsequent analysis, we use the soft limiter for clipping.

The problems associated with clipping are in-band signal distortion and generation of out-of-band signal. Because SC-FDMA modulation spreads the information data across all the modulated symbols, in-band signal distortion is mitigated when an SC-FDMA symbol is clipped.

To analyze the impact of symbol amplitude clipping on the link level performance, we apply clipping to the unitary precoded TxBF MIMO system that we described in Chapter 6 and show numerical simulation results. We use the parameters and assumptions in Section 6.4 for the simulations in this section.

Figure 7.11 shows the block diagram of a symbol amplitude clipping method for spatial multiplexing SC-FDMA MIMO transmission. In our current analysis, we apply the clipping after baseband pulse shaping. We can also consider other sophisticated clipping methods, such as iterative clipping.

Figure 7.12 shows the CCDF of symbol power with clipping at various levels. With 7 dB-max clipping, less than 1 % of the symbols are clipped.

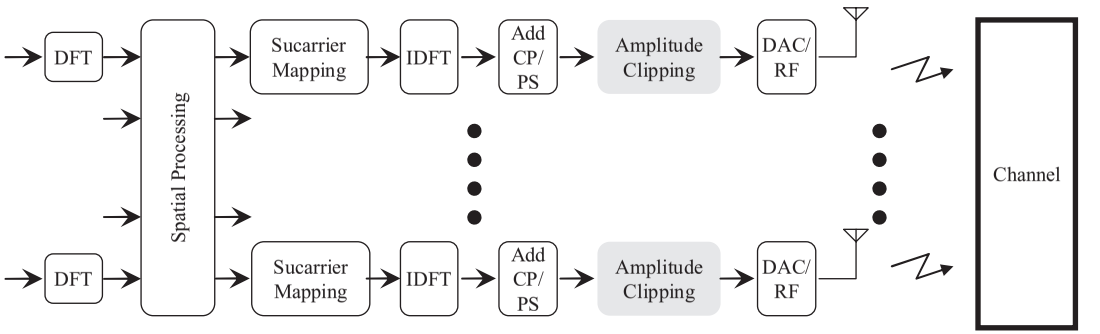

Figure 7.11 Block diagram of a symbol amplitude clipping method for SC-FDMA MIMO transmission

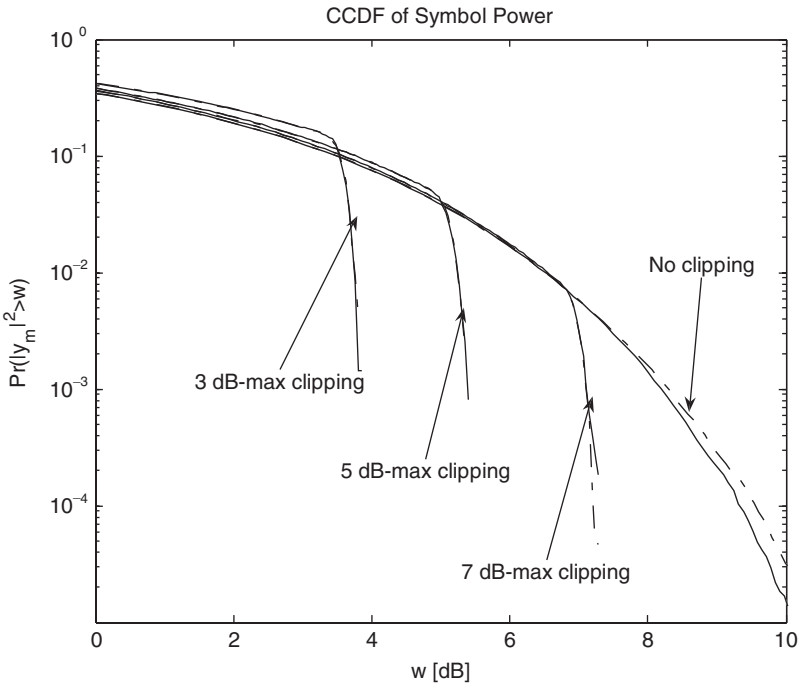

Figure 7.12 CCDF of symbol power after clipping. y_m represents the baseband symbol. Solid line represents CCDF for antenna 1 and dashed line represents CCDF for antenna 2

Note that even with as much as 3 dB-max PAPR clipping, only about 10 % of the modulated symbols are clipped.

Figure 7.13 shows the uncoded bit error rate (BER) and coded frame error rate (FER) performances when we apply symbol amplitude clipping. We can observe that the performance degradation due to clipping is almost none for 7 dB-max clipping. The performance degrades slightly more when we apply 5 or 3 dB-max clipping. For 3 dB-max clipping, an error floor starts to appear in the high signal-to noise ratio (SNR) region for uncoded BER. But when we incorporate forward error correction coding, it mitigates this effect. Thus, we can use a modest amount of amplitude clipping to limit the increase in the PAPR for unitary precoded TxBF with SC-FDMA without compromising the link level performance.

Clipping, consequently, will generate both in-band and out-of-band frequency components. Figure 7.14 shows the power spectral density (PSD) of the clipped signals. For PSD calculation, we use Hanning window with 1/4 of window overlapping. For 7 dB-max clipping, the spectrum is

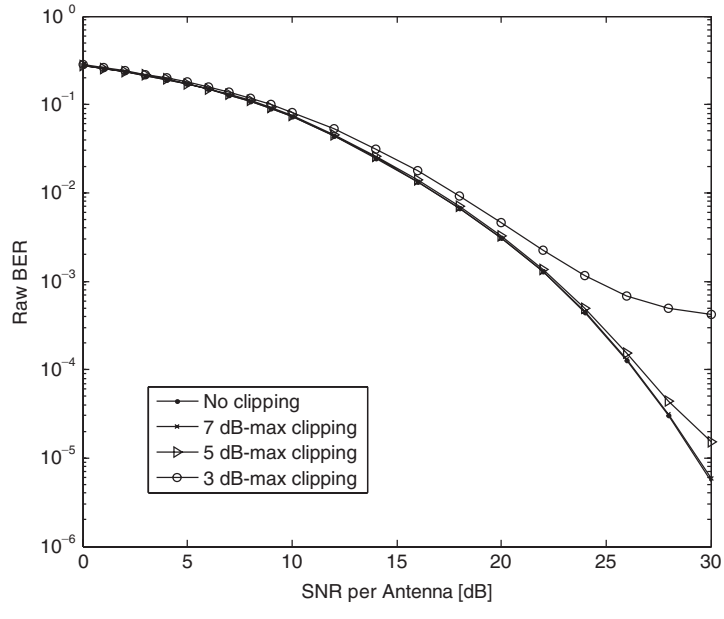

(a)

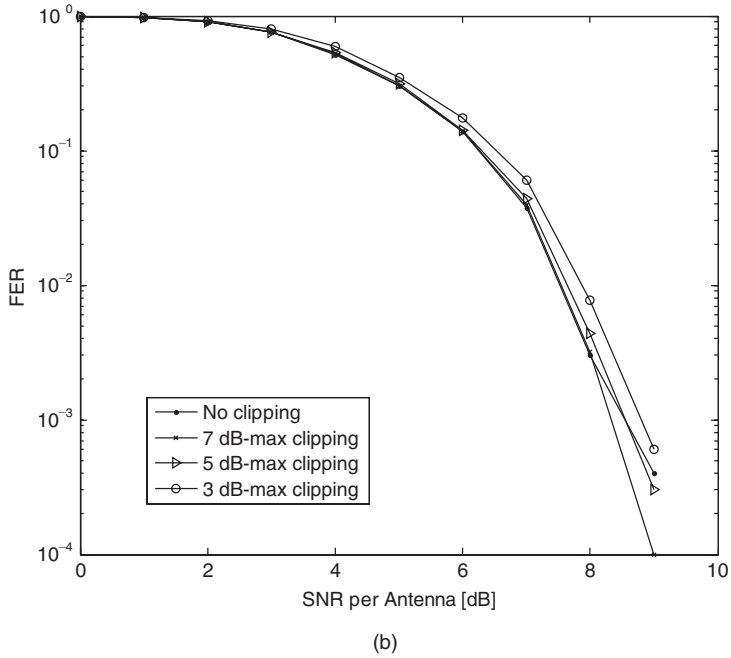

(b)

Figure 7.13 Link level performance for clipping: (a) uncoded BER; (b) coded FER

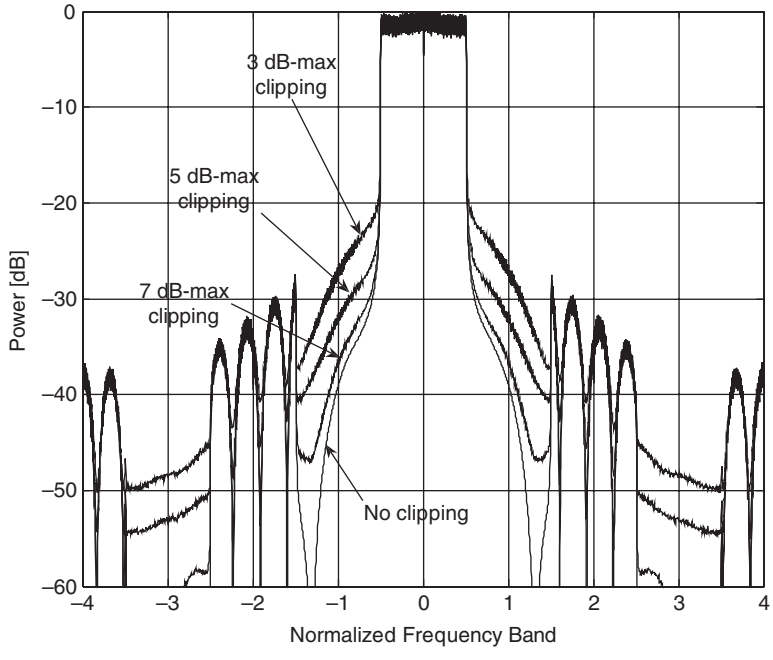

Figure 7.14 PSD of the clipped signals

almost the same as that of the original signal. More pronounced out-of-band components arise when we use 5 or 3 dB-max clipping. Thus, we should control the amount of clipping depending on the out-of-band radiation requirements.

7.6 Summary

In this chapter, we analyzed the PAPR of SC-FDMA signals for single and multiple antenna transmissions using numerical simulations. We showed that SC-FDMA signals do indeed have lower PAPR compared to OFDMA signals. Also, we have shown that DFDMA and LFDMA incur higher PAPR compared to IFDMA but compared to OFDMA, it is still lower, though not significantly. Another noticeable fact is that pulse shaping increases PAPR, thus degrading the power efficiency, and that the roll-off factor in the case of raised-cosine pulse shaping has a significant impact on PAPR of IFDMA. A pulse-shaping filter should be designed carefully in order to reduce the PAPR without degrading the system performance.

For multiple antenna transmission, we observed that the unitary precoding TxBF scheme increases the PAPR because of its filtering aspect. It was

interesting to discover that averaging and quantization of the precoder matrix actually reduces the PAPR.

In order to reduce the peak power in an SC-FDMA system, we examined a symbol amplitude clipping method and applied it to the 2×2 unitary precoded TxBF system. Numerical simulation results showed that moderate clipping does not affect the link level performance. But out-of-band radiation is a concern when we use clipping.

References

[1] Miller, S.L. and O'Dea, R.J., "Peak Power and Bandwidth Efficient Linear Modulation," *IEEE Trans. Commun.*, vol. **46**, no. 12, Dec. 1998, pp. 1639–1648.

[2] Cripps, S.C., *RF Power Amplifiers for Wireless Communications*, Artech House, 1999.

[3] Wulich, D. and Goldfeld, L., "Bound of the Distribution of Instantaneous Power in Single Carrier Modulation," *IEEE Trans. Wireless Commun.*, vol. **4**, no. 4, July 2005, pp. 1773–1778.

[4] Yates, R.D. and Goodman, D.J., *Probability and Stochastic Processes: A Friendly Introduction for Electrical and Computer Engineers*, John Wiley & Sons Ltd, 2nd edition, 2005.

[5] Han, S.H. and Lee, J.H., "An Overview of Peak-to-Average Power Ratio Reduction Techniques for Multicarrier Transmission," *IEEE Wireless Commun.*, vol. **12**, no. 2, Apr. 2005, pp. 56–65.

[6] Ochiai, H. and Imai, H., "On the Distribution of the Peak-to-Average Power Ratio in OFDM Signals," *IEEE Trans. Commun.*, vol. **49**, no. 2, Feb. 2001, pp. 282–289.

[7] Sharif, M., Gharavi-Alkhansari, M., and Khalaj, B.H., "On the Peak-to-Average Power of OFDM Signals Based on Oversampling," *IEEE Trans. Commun.*, vol. **51**, no. 1, Jan. 2003, pp. 72–78.

[8] Shi, Q., "OFDM in Bandpass Nonlinearity," *IEEE Trans. Consumer Electron.*, vol. **42**, no. 3, Aug. 1996, pp. 253–258.

8

Simulation of a SC-FDMA System Using MATLAB®

8.1 Introduction

In this chapter, we illustrate a simple yet insightful link level simulation method for SC-FDMA systems. Section 8.2 will focus on simulating the single carrier with a frequency domain equalization (SC/FDE) system and Section 8.3 on simulating an SC-FDMA system.

For the multipath channel, we consider ITU Pedestrian A and ITU Vehicular A channels [1] with additive white Gaussian noise (AWGN). The delay profiles of the two channels are described in Table 8.1.

As you can see from Table 8.1, the Pedestrian A channel has relatively short channel delay whereas the Vehicular A channel has much longer delay. Consequently, the Vehicular A channel has much more severe frequency selectivity in the frequency domain, which is illustrated in Figure 8.1.

Table 8.2 summarizes the simulation assumptions and parameters that were used throughout this chapter. Since the system sampling rate is set to 5 mega-samples per second, the channel delay was quantized to the nearest multiples of 200 nsec ($= 1/(5 \times 10^6)$). Also, the length of the cyclic prefix (CP) is chosen as 4 μs (20 samples) considering the maximum channel delay of the Vehicular A channel, which is 2.51 μs.

8.2 Link Level Simulation of SC/FDE

Figures 8.2 and 8.3 show the flow of the link level simulations for SC/FDE and OFDM, respectively. As mentioned in Chapter 2, we can see the

Single Carrier FDMA: A New Air Interface for Long Term Evolution Hyung G. Myung and David J. Goodman
 ISBN: 978-0-470-72449-1

Table 8.1 Channel delay profiles of ITU Pedestrian A and Vehicular A channels [1]

Channel model		Path 1	Path 2	Path 3	Path 4	Path 5	Path 6
Ped. A	Delay (nsec)	0	110	190	410	–	–
	Power (dB)	0	−9.7	−19.2	−22.8	–	–
Veh. A	Delay (nsec)	0	310	710	1090	1730	2510
	Power (dB)	0	−1.0	−9.0	−10.0	−15.0	−20.0

similarity between the two systems; they both use the same signal processing blocks. The Matlab codes for the simulations are provided in the Appendix at the end of this chapter. Figures 8.4, 8.5, and 8.6 are simulation results using the simulators described in Figures 8.2 and 8.3. The simulation calculates symbol error rate (SER) for performance measurement.

Figure 8.4 shows the SER performance of the SC/FDE system with different types of channel equalization method. We can see that MMSE equalization gives better performance because of its robustness against noise during the equalization processing. Other advanced equalization methods, such as decision feedback equalization (DFE) and turbo equalization, should give performance approaching the AWGN channel.

Figure 8.5 compares the SER performance between SC/FDE and OFDM. For the AWGN channel, we can see that they essentially have the

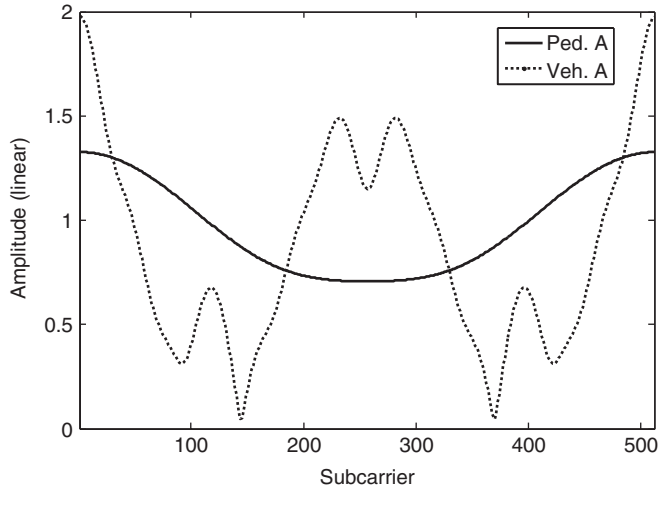

Figure 8.1 Frequency domain channel responses of ITU Pedestrian A and Vehicular A channels

Table 8.2 Simulation assumptions and parameters

System bandwidth	5 MHz
Sampling rate	5 mega-samples per second
Data modulation format	QPSK
Pulse shaping	None
Cyclic prefix	20 samples (4 μs)
Transmitter IFFT size	512
Subcarrier (tone) spacing	9.765625 kHz (= 5 MHz/512)
SC-FDMA input block size	16 symbols
SC-FDMA input FFT size	16
Channel estimation	Perfect
Equalization	Zero forcing or minimum mean square error (MMSE)
Channel coding	None
Detection	Hard decision
Number of iterations	$> 10^4$

same performance. With multipath channels, we can see that SC/FDE outperforms OFDM because of the inherent frequency diversity. This is more evident in the Vehicular A channel simulation results where the frequency-selectivity is severe. As mentioned in Chapter 2, an OFDM system needs a good channel coding or channel adaptive modulation scheme to overcome this limitation.

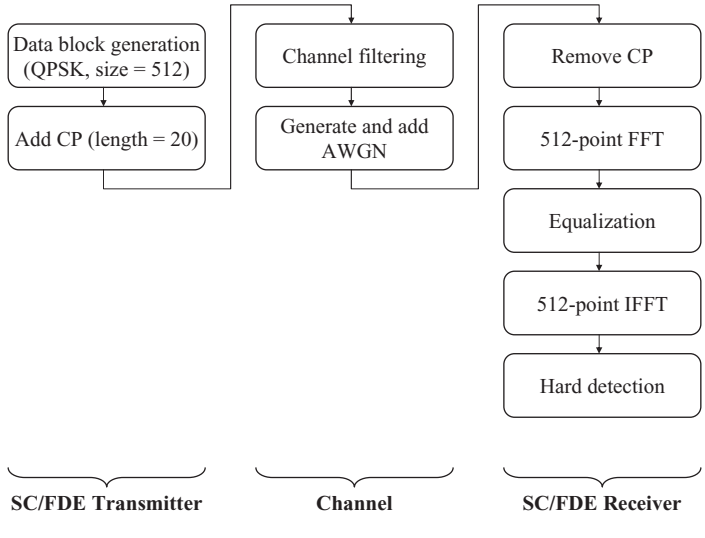

Figure 8.2 Block diagram of SC/FDE link level simulator

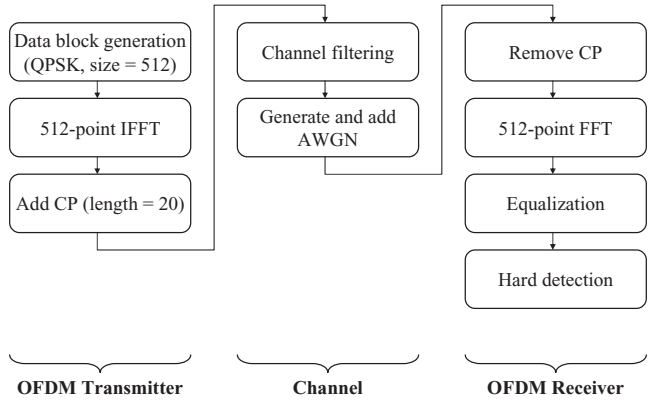

Figure 8.3 Block diagram of OFDM link level simulator

Figure 8.6 shows the effect of not using the CP. In both cases of SC/FDE and OFDM, the performance degrades significantly in the high SNR regime when the length of the CP is zero. This illustrates the critical role of CP in the presence of a multipath channel.

8.3 Link Level Simulation of SC-FDMA

Figure 8.7 shows the flow of the link level simulation for SC-FDMA. In the simulations, we consider interleaved FDMA (IFDMA), which is a

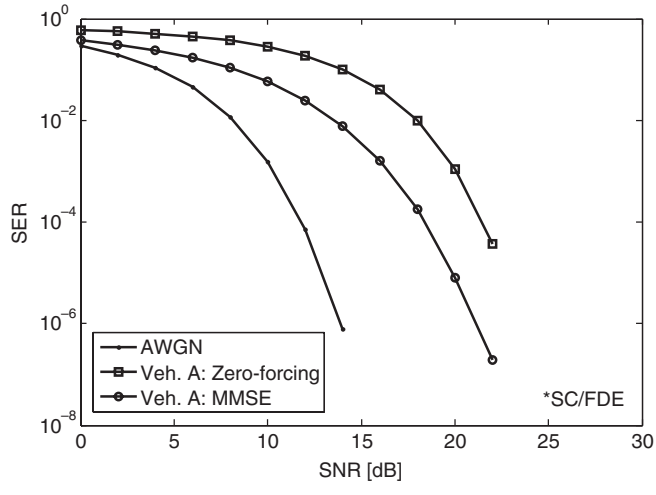

Figure 8.4 Symbol error rate performance of SC/FDE system with different types of equalization method; Vehicular A channel was used

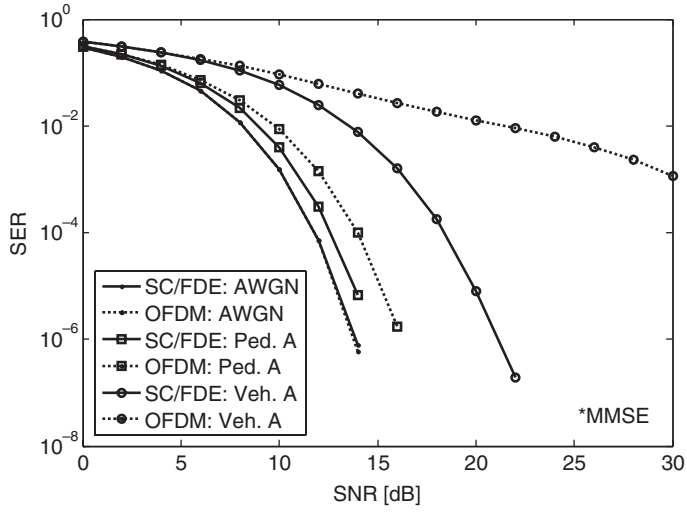

Figure 8.5 Symbol error rate performance comparison between SC/FDE and OFDM; MMSE equalization was used

distributed subcarrier mapping scheme, and localized FDMA (LFDMA) with static scheduling (i.e., no channel-dependent scheduling or subband hopping). The Matlab codes for the simulation are provided in the Appendix at the end of this chapter. Figure 8.8 illustrates the location of the chunk, or subband, considered in the localized subcarrier mapping.

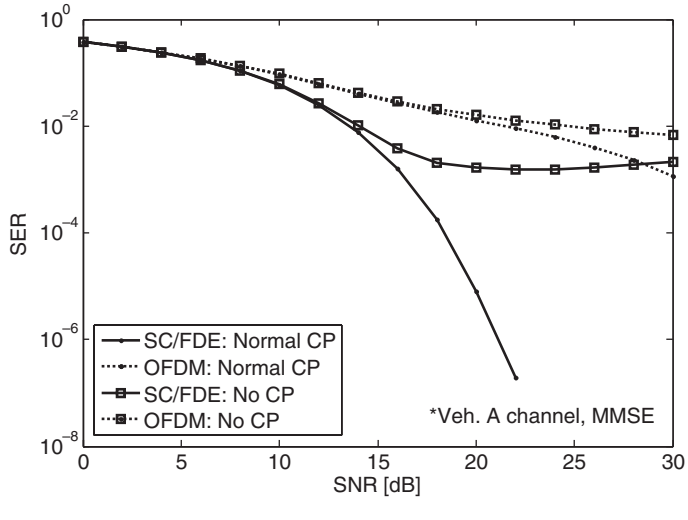

Figure 8.6 Symbol error rate performance without CP; Vehicular A channel and MMSE equalization were used

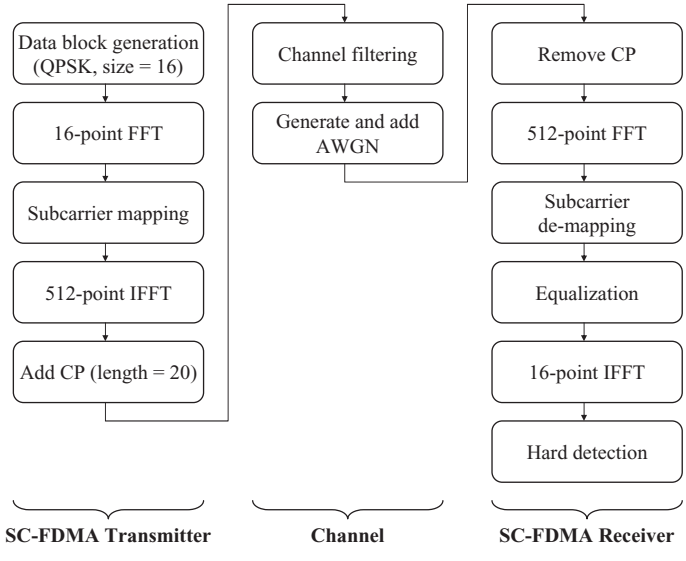

Figure 8.7 Block diagram of SC-FDMA link level simulator

Figure 8.9 shows the simulation results using the simulators described in Figure 8.7. The simulation calculates symbol error rate (SER) for performance measurement.

Figure 8.9 shows the SER performance of the SC-FDMA system for the two different subcarrier mapping schemes. For AWGN channel,

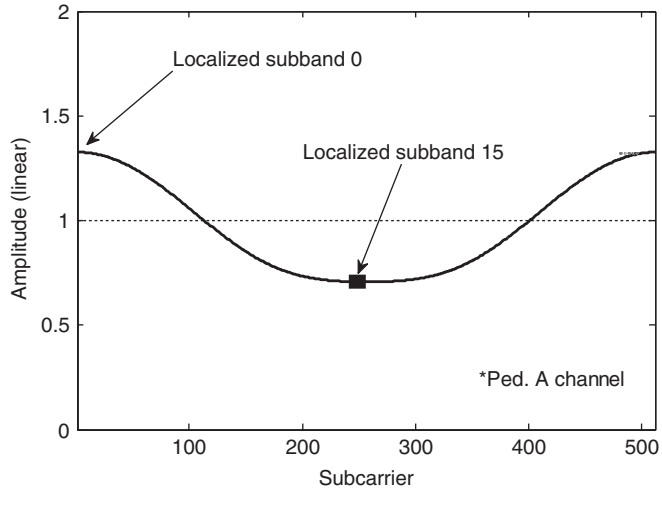

Figure 8.8 Localized subband illustration for ITU Pedestrian A channel

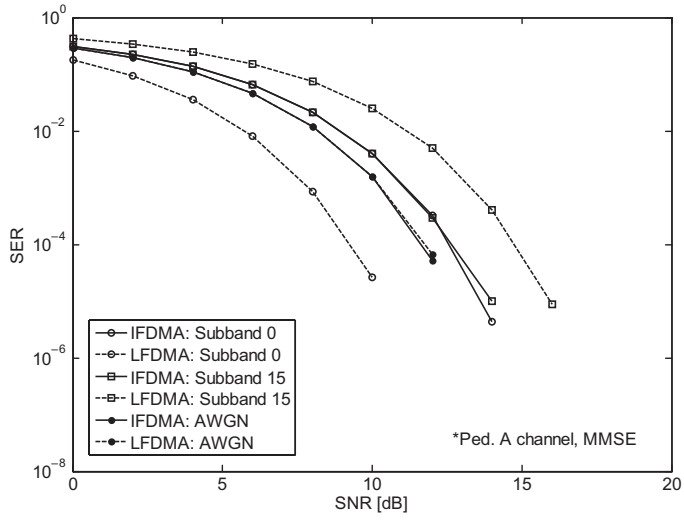

Figure 8.9 Symbol error rate performance of SC-FDMA with different subcarrier mapping schemes

we can see that both subcarrier mapping schemes essentially have the same performance. With multipath channels, the performance of IFDMA (distributed subcarrier mapping) does not depend on the location of the subband because of the inherent frequency diversity. For LFDMA (localized subcarrier mapping), the performance varies depending on which part of the spectrum it occupies. In localized subband 0, the channel gain is higher than the average and accordingly the SER performance is much better. In localized subband 15, the channel gain is lower, and the performance is worse accordingly. As mentioned in Chapter 3, localized subcarrier mapping lacks frequency diversity and it should either use channel-dependent scheduling or subband hopping to overcome this limitation.

8.4 Peak-to-Average Power Ratio Simulation of SC-FDMA

Figures 8.10 and 8.11 show the flow of the PAPR simulations for SC-FDMA and OFDMA, respectively. For OFDMA, windowing or pulse shaping is not considered and the data occupy the first localized chunk of the band. The simulation results using these PAPR simulators are in Figures 7.4 and 7.5 in Chapter 7.

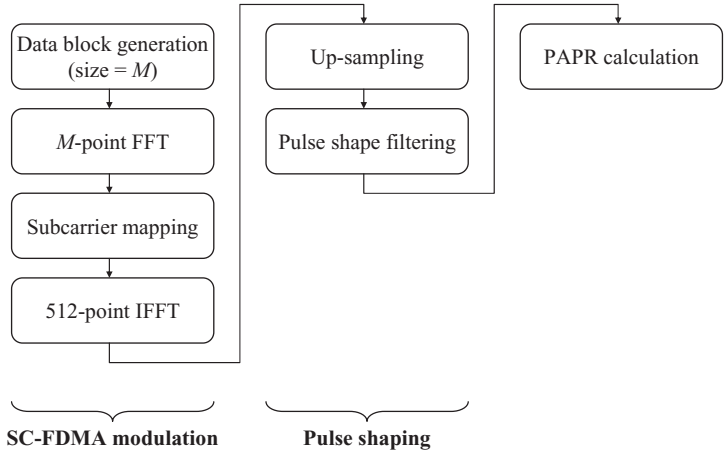

Figure 8.10 Block diagram of PAPR simulator for SC-FDMA

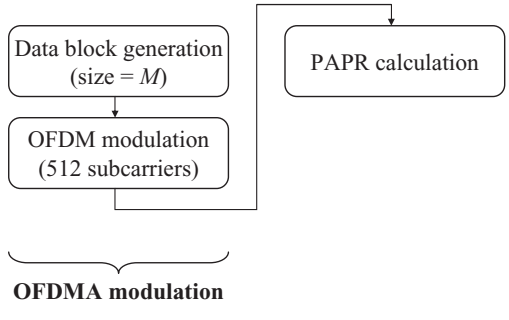

Figure 8.11 Block diagram of PAPR simulator for OFDMA

8.5 Summary

In this chapter, we have illustrated methods to simulate single carrier with frequency domain equalization (SC/FDE) and SC-FDMA systems. The Matlab codes for the simulations are provided in the Appendix at the end of this chapter.

References

[1] 3rd Generation Partnership Project, 3GPP TS 25.101 – *Technical Specification Group Radio Access Network; User Equipment (UE) Radio Transmission and Reception (FDD) (Release 7)*, Sep. 2007, Section B.2.2.

Appendix – Simulation Codes

Matlab Simulation Codes for SC/FDE

```
%=====================================================
%This is the main run routine for SC/FDE. The
%parameters for the simulation are set here and the
%simulation functions are called.
%=====================================================
function runSimSCFDE()

SP.FFTsize = 512; % The size of the FFT and IFFT.
SP.CPsize = 20; % CP length.

SP.SNR = [0:2:30]; % Simulated SNR range is from 0 dB
                     to 30 dB.
SP.numRun = 10^4; % The number of simulation
                    iterations is 10^4.

% Channels based on 3GPP TS 25.104.
pedAchannel = [1 10^(-9.7/20) 10^(-22.8/20)];
pedAchannel = pedAchannel/sqrt(sum(pedAchannel.^2));
               % Normalize the channel.

vehAchannel = [1 0 10^(-1/20) 0 10^(-9/20) 10^(-10/20)
              0 0 0 10^(-15/20) 0 0 0 10^(-20/20)];
vehAchannel = vehAchannel/sqrt(sum(vehAchannel.^2));
              % Normalize the channel.

idenChannel = 1; % This is identity channel for
                   AWGN simulation.

% Set the type of the channel.
SP.channel = pedAchannel;

% Set the equalization type. Either "ZERO" or "MMSE".
SP.equalizerType ='MMSE';

% Run the simulation for SC/FDE.
SER_scfde = scfde(SP);

% Run the simulation for OFDM.
SER_ofdm = ofdm(SP);

% Save the data.
save scfde
```

```
%==================================
% This is the simulator for SC/FDE.
%==================================
function SER = scfde(SP)

numSymbols = SP.FFTsize; % The size of the data block
                           is equal to the FFT size.

% Frequency domain version of the channel response.
H_channel = fft(SP.channel,SP.FFTsize);

for n = 1:length(SP.SNR),
  errCount = 0; % Initialize the error count.

  for k = 1:SP.numRun,

    % Generate random data block.
    tmp = round(rand(2,numSymbols));
    tmp = tmp*2 - 1;
    inputSymbols = (tmp(1,:) + i*tmp(2,:))/sqrt(2);

    % Add CP.
    TxSymbols = [inputSymbols(numSymbols-SP.CPsize+1:
                 numSymbols) inputSymbols];

    % Propagate through multi-path channel.
    RxSymbols = filter(SP.channel, 1, TxSymbols);

    % Generate AWGN with appropriate noise power.
    tmp = randn(2, numSymbols+SP.CPsize);
    complexNoise = (tmp(1,:) + i*tmp(2,:))/sqrt(2);
    noisePower = 10^(-SP.SNR(n)/10);

    % Add AWGN to the transmitted signal.
    RxSymbols = RxSymbols + sqrt(noisePower)
                *complexNoise;

    % Remove CP.
    EstSymbols = RxSymbols(SP.CPsize+1:numSymbols+SP.
                 CPsize);

    % Convert the received signal into frequency
      domain.
    Y = fft(EstSymbols, SP.FFTsize);
```

```
    % Perform channel equalization in the
      frequency domain.
    if SP.equalizerType == 'ZERO'
       Y = Y./H_channel;
    elseif SP.equalizerType == 'MMSE'
       C = conj(H_channel)./(conj(H_channel).*H_channel
           + 10^(-SP.SNR(n)/10));
       Y = Y.*C;
    end

    % Convert the signal back to time domain.
    EstSymbols = ifft(Y);

    % Perform hard decision detection.
    EstSymbols = sign(real(EstSymbols))
                 + i*sign(imag(EstSymbols));
    EstSymbols = EstSymbols/sqrt(2);

    % Check whether there is error.
    I = find((inputSymbols-EstSymbols) == 0);

    % Count the number of errors.
    errCount = errCount + (numSymbols-length(I));
  end

  % Calculate the symbol error rate (SER).
  SER(n,:) = errCount / (numSymbols*SP.numRun);

end

%================================
% This is the simulator for OFDM.
%================================

function SER = ofdm(SP)

numSymbols = SP.FFTsize; % The size of the data block
                           is equal to the FFT size.

% Frequency domain version of the channel response.
H_channel = fft(SP.channel,SP.FFTsize);

for n = 1:length(SP.SNR),
   errCount = 0; % Initialize the error count.
```

```
for k = 1:SP.numRun,
    % Generate random data block.
    tmp = round(rand(2,numSymbols));
    tmp = tmp*2 - 1;
    inputSymbols = (tmp(1,:) + i*tmp(2,:))/sqrt(2);

    % Perform OFDM modulation using IFFT.
    TxSamples = sqrt(SP.FFTsize)*ifft(inputSymbols);

    % Add CP.
    ofdmSymbol = [TxSamples(numSymbols-SP.
                  CPsize+1:numSymbols) TxSamples];

    % Propagate through multi-path channel.
    RxSamples = filter(SP.channel, 1, ofdmSymbol);

    % Generate AWGN with appropriate noise power.
    tmp = randn(2, numSymbols+SP.CPsize);
    complexNoise = (tmp(1,:) + i*tmp(2,:))/sqrt(2);
    noisePower = 10^(-SP.SNR(n)/10);

    % Add AWGN to the transmitted signal.
    RxSamples = RxSamples + sqrt(noisePower)
                *complexNoise;

    % Remove CP.
    EstSymbols = RxSamples(SP.CPsize+1:numSymbols
                 +SP.CPsize);

    % Convert the received signal into frequency
      domain.
    Y = fft(EstSymbols, SP.FFTsize);

    % Perform channel equalization in the frequency
      domain.
    if SP.equalizerType == 'ZERO'
       Y = Y./H_channel;
    elseif SP.equalizerType == 'MMSE'
       C = conj(H_channel)./(conj(H_channel).*H_channel
           + 10^(-SP.SNR(n)/10));
       Y = Y.*C;
    end

    % Perform hard decision detection.
```

```
    EstSymbols = Y;
    EstSymbols = sign(real(EstSymbols))
                 + i*sign(imag(EstSymbols));
    EstSymbols = EstSymbols/sqrt(2);

    % Check whether there is error.
    I = find((inputSymbols-EstSymbols) == 0);

    % Count the number of errors.
    errCount = errCount + (numSymbols-length(I));
  end

  % Calculate the symbol error rate (SER).
  SER(n,:) = errCount / (numSymbols*SP.numRun);
end
```

Matlab Simulation Codes for SC-FDMA (Link Level)

```
%==========================
% This is the main run routine for SC-FDMA. The
  parameters for the simulation
% are set here and the simulation function is called.
%==============================================

function runSimSCFDMA()

SP.FFTsize = 512; % The size of the transmitter
                    IFFT and the receiver FFT.
SP.inputBlockSize = 16; % Input data block size.
SP.CPsize = 20; % CP length.
SP.subband = 0; % Set the subband location.

SP.SNR = [0:2:30]; % Simulated SNR range is from
                     0 dB to 30 dB.
SP.numRun = 10^5; % The number of simulation
                    iterations is 10^5.

% Channels based on 3GPP TS 25.104.
pedAchannel = [1 10^(-9.7/20) 10^(-22.8/20)];
pedAchannel = pedAchannel/sqrt(sum(pedAchannel.^2));
              % Normalize the channel.

vehAchannel = [1 0 10^(-1/20) 0 10^(-9/20) 10^(-10/20)
             0 0 0 10^(-15/20) 0 0 0 10^(-20/20)];
```

```
vehAchannel = vehAchannel/sqrt(sum(vehAchannel.^2));
              % Normalize the channel.

idenChannel = 1; % This is identity channel for AWGN
                   simulation.

% Set the type of the channel.
SP.channel = pedAchannel;

% Set the equalization type. Either "ZERO" or "MMSE".
SP.equalizerType ='MMSE';

% Run the simulation for SC-FDMA.
[SER_ifdma SER_lfdma] = scfdma(SP);

% Save the data.
save scfdma

%===================================
% This is the simulator for SC-FDMA.
%===================================
function [SER_ifdma SER_lfdma] = scfdma(SP)

numSymbols = SP.FFTsize; % The number of transmitted
                           SC-FDMA symbols.
Q = numSymbols/SP.inputBlockSize; % The bandwidth
                                    spreading factor.

% Frequency domain version of the channel response.
H_channel = fft(SP.channel,SP.FFTsize);

for n = 1:length(SP.SNR),
    % Initialize the error count.
    errCount_ifdma = 0;
    errCount_lfdma = 0;

    for k = 1:SP.numRun,
    % Generate random data block.
    tmp = round(rand(2,SP.inputBlockSize));
    tmp = tmp*2 - 1;
    inputSymbols = (tmp(1,:) + i*tmp(2,:))/sqrt(2);

    % DFT-precoding.
    inputSymbols_freq = fft(inputSymbols);
```

```
% Initialize the output subcarriers.
inputSamples_ifdma = zeros(1,numSymbols);
inputSamples_lfdma = zeros(1,numSymbols);

% Subcarrier mapping.
% Interleaved (distributed) mapping.
inputSamples_ifdma(1+SP.subband:Q:numSymbols) =
 inputSymbols_freq;
% Localized mapping.
inputSamples_lfdma([1:SP.inputBlockSize]
 +SP.inputBlockSize*SP.subband) =
 inputSymbols_freq;

% Convert the signal back to time domain.
inputSamples_ifdma = ifft(inputSamples_ifdma);
inputSamples_lfdma = ifft(inputSamples_lfdma);

% Add CP.
TxSamples_ifdma = [inputSamples_ifdma
               (numSymbols - SP.CPsize+
               1:numSymbols) inputSamples_ifdma];
TxSamples_lfdma = [inputSamples_lfdma
               (numSymbols - SP.CPsize+
               1:numSymbols) inputSamples_lfdma];

% Propagate through multi-path channel.
RxSamples_ifdma = filter(SP.channel, 1,
                  TxSamples_ifdma);
RxSamples_lfdma = filter(SP.channel, 1,
                  TxSamples_lfdma);

% Generate AWGN with appropriate noise power.
tmp = randn(2, numSymbols+SP.CPsize);
complexNoise = (tmp(1,:) + i*tmp(2,:))/sqrt(2);
noisePower = 10^(-SP.SNR(n)/10);

% Add AWGN to the transmitted signal.
RxSamples_ifdma = RxSamples_ifdma +
                  sqrt(noisePower/Q)*complexNoise;
RxSamples_lfdma = RxSamples_lfdma +
                  sqrt(noisePower/Q)*complexNoise;

% Remove CP.
```

```
RxSamples_ifdma = RxSamples_ifdma(SP.CPsize+1:
                  numSymbols+SP.CPsize);
RxSamples_lfdma = RxSamples_lfdma(SP.CPsize+1:
                  numSymbols+SP.CPsize);

% Convert the received signal into frequency
domain.
Y_ifdma = fft(RxSamples_ifdma, SP.FFTsize);
Y_lfdma = fft(RxSamples_lfdma, SP.FFTsize);

% Subcarrier de-mapping.
Y_ifdma = Y_ifdma(1+SP.subband:Q:numSymbols);
Y_lfdma = Y_lfdma([1:SP.inputBlockSize]
          +SP.inputBlockSize*SP.subband);

% Find the channel response for the interleaved
subcarriers.
H_eff = H_channel(1+SP.subband:Q:numSymbols);

% Perform channel equalization in the frequency
domain.
if SP.equalizerType == 'ZERO'
   Y_ifdma = Y_ifdma./H_eff;
elseif SP.equalizerType == 'MMSE'
   C = conj(H_eff)./(conj(H_eff).*H_eff
      + 10^(-SP.SNR(n)/10));
   Y_ifdma = Y_ifdma.*C;
end

% Find the channel response for the localized
subcarriers.
H_eff = H_channel([1:SP.inputBlockSize]
         +SP.inputBlockSize*SP.subband);

% Perform channel equalization in the frequency
domain.
if SP.equalizerType == 'ZERO'
   Y_lfdma = Y_lfdma./H_eff;
elseif SP.equalizerType == 'MMSE'
   C = conj(H_eff)./(conj(H_eff).*H_eff
      + 10^(-SP.SNR(n)/10));
   Y_lfdma = Y_lfdma.*C;
end
```

```
    % Convert the signal back to time domain.
    EstSymbols_ifdma = ifft(Y_ifdma);
    EstSymbols_lfdma = ifft(Y_lfdma);

    % Perform hard decision detection.
    EstSymbols_ifdma = sign(real(EstSymbols_ifdma)) +
                       i*sign(imag(EstSymbols_ifdma));
    EstSymbols_ifdma = EstSymbols_ifdma/sqrt(2);
    EstSymbols_lfdma = sign(real(EstSymbols_lfdma)) +
                       i*sign(imag(EstSymbols_lfdma));
    EstSymbols_lfdma = EstSymbols_lfdma/sqrt(2);

    % Find and count errors.
    I_ifdma = find((inputSymbols-EstSymbols_ifdma)
            == 0);
    errCount_ifdma = errCount_ifdma +
                  (SP.inputBlockSize-length(I_ifdma));
    I_lfdma = find((inputSymbols-EstSymbols_lfdma)
            == 0);
    errCount_lfdma = errCount_lfdma +
                 (SP.inputBlockSize-length(I_lfdma));
  end

  % Calculate the symbol error rate (SER).
  SER_ifdma(n,:) = errCount_ifdma /
                   (SP.inputBlockSize*SP.numRun);
  SER_lfdma(n,:) = errCount_lfdma /
                  (SP.inputBlockSize*SP.numRun);
end
```

Matlab Simulation Codes for SC-FDMA and OFDMA (PAPR)

```
%=======================================
% This is the PAPR simulator for SC-FDMA.
%=======================================
function paprSCFDMA()

dataType = 'Q-PSK'; % Modulation format.
totalSubcarriers = 512; % Number of total subcarriers.
numSymbols = 16; % Data block size.

Q = totalSubcarriers/numSymbols; % Bandwidth spreading
                                 factor of IFDMA.
```

```
Q_tilda = 31; % Bandwidth spreading factor of DFDMA.
                Q_tilda < Q.
subcarrierMapping = 'IFDMA'; % Subcarrier mapping
                                scheme.
pulseShaping = 1; % Whether to do pulse shaping
                    or not.
filterType = 'rc'; % Type of pulse shaping filter.
rolloffFactor = 0.0999999999; % Rolloff factor for
                     the raised-cosine filter.
                    % To prevent divide-by-zero, for
                    example, use
                    % 0.099999999 instead of 0.1.

Fs = 5e6; % System bandwidth.
Ts = 1/Fs; % System sampling rate.
Nos = 4; % Oversampling factor.

if filterType == 'rc' % Raised-cosine filter.
    psFilter = rcPulse(Ts, Nos, rolloffFactor);
elseif filterType == 'rr' % Root raised-cosine filter.
    psFilter = rrcPulse(Ts, Nos, rolloffFactor);
end
numRuns = 1e4; % Number of iterations.

papr = zeros(1,numRuns); % Initialize the PAPR
                           results.

for n = 1:numRuns,
    % Generate random data.
    if dataType == 'Q-PSK'
       tmp = round(rand(numSymbols,2));
       tmp = tmp*2 - 1;
       data = (tmp(:,1) + j*tmp(:,2))/sqrt(2);
    elseif dataType == '16QAM'
        dataSet = [-3+3i -1+3i 1+3i 3+3i ...
            -3+i -1+i 1+i 3+i ...
            -3-i -1-i 1-i 3-i ...
            -3-3i -1-3i 1-3i 3-3i];
        dataSet = dataSet/sqrt(mean(abs(dataSet).^2));
        tmp = ceil(rand(numSymbols,1)*16);
        for k = 1:numSymbols,
            if tmp(k) == 0
                tmp(k) = 1;
            end
```

```
            data(k) = dataSet(tmp(k));
        end
        data = data.';
    end

    % Convert data to frequency domain.
    X = fft(data);

    % Initialize the subcarriers.
    Y = zeros(totalSubcarriers,1);

    % Subcarrier mapping.
    if subcarrierMapping == 'IFDMA'
        Y(1:Q:totalSubcarriers) = X;
    elseif subcarrierMapping == 'LFDMA'
        Y(1:numSymbols) = X;
    elseif subcarrierMapping == 'DFDMA'
        Y(1:Q_tilda:Q_tilda*numSymbols) = X;
    end

    % Convert data back to time domain.
    y = ifft(Y);

    % Perform pulse shaping.
    if pulseShaping == 1
        % Up-sample the symbols.
        y_oversampled(1:Nos:Nos*totalSubcarriers) = y;
        % Perform filtering.
        y_result = filter(psFilter, 1, y_oversampled);
    else
        y_result = y;
    end

    % Calculate the PAPR.
    papr(n) = 10*log10(max(abs(y_result).^2)/
              mean(abs(y_result).^2));
end

% Plot CCDF.
[N,X] = hist(papr, 100);
semilogy(X,1-cumsum(N)/max(cumsum(N)),'b')

% Save data.
save paprSCFDMA
```

```
%====================================
% Raised-cosine pulse shaping filter.
%====================================
function r = rcPulse(Ts, Nos, alpha)

% Set the time range.
t1 = [-6*Ts:Ts/Nos:-Ts/Nos];
t2 = [Ts/Nos:Ts/Nos:6*Ts];

% Calculate the filter values.
r1 = (sin(pi*t1/Ts)./(pi*t1)).*(cos(pi*alpha
      *t1/Ts)./(1-(4*alpha*t1/Ts).^2);
r2 = (sin(pi*t2/Ts)./(pi*t2)).*(cos(pi*alpha
      *t2/Ts)./(1-(4*alpha*t2/Ts).^2);
r = [r1 1/Ts r2];

%========================================
% Root raised-cosine pulse shaping filter.
%========================================
function r = rrcPulse(Ts, Nos, alpha)

% Set the time range.
t1 = [-6*Ts:Ts/Nos:-Ts/Nos];
t2 = [Ts/Nos:Ts/Nos:6*Ts];

% Calculate the filter values.
r1 = (4*alpha/(pi*sqrt(Ts))) ...
     *(cos((1+alpha)*pi*t1/Ts)+(Ts./(4*alpha*t1)) ...
     .*sin((1-alpha)*pi*t1/Ts))./(1-(4*alpha*t1/Ts).^2);
r2 = (4*alpha/(pi*sqrt(Ts))) ...
    *(cos((1+alpha)*pi*t2/Ts)+(Ts./(4*alpha*t2)) ...
    .*sin((1-alpha)*pi*t2/Ts))./(1-(4*alpha*t2/Ts).^2);

r = [r1 (4*alpha/(pi*sqrt(Ts))+(1-alpha)/
     sqrt(Ts)) r2];

%====================================

% This is the PAPR simulator for OFDMA.
%====================================
function paprOFDMA()

dataType = 'Q-PSK'; % Modulation format.
totalSubcarriers = 512; % Number of total subcarriers.
```

```
numSymbols = 16; % Data block size.
Fs = 5e6; % System bandwidth.
Ts = 1/Fs; % System sampling rate.
Nos = 4; % Oversampling factor.

Nsub = totalSubcarriers;
Fsub = [0:Nsub-1]*Fs/Nsub; % Subcarrier spacing.
numRuns = 1e4; % Number of runs.

papr = zeros(1,numRuns); % Initialize the PAPR
                           results.

for n = 1:numRuns,
    % Generate random data.
    if dataType == 'Q-PSK'
       tmp = round(rand(numSymbols,2));
       tmp = tmp*2 - 1;
       data = (tmp(:,1) + j*tmp(:,2))/sqrt(2);
    elseif dataType == '16QAM'
        dataSet = [-3+3i -1+3i 1+3i 3+3i ...
            -3+i -1+i 1+i 3+i ...
            -3-i -1-i 1-i 3-i ...
            -3-3i -1-3i 1-3i 3-3i];
        dataSet = dataSet/sqrt(mean(abs(dataSet).^2));
        tmp = ceil(rand(numSymbols,1)*16);
        for k = 1:numSymbols,
            if tmp(k) == 0
                tmp(k) = 1;
            end
            data(k) = dataSet(tmp(k));
        end
        data = data.';
    end

    % Time range of the OFDM symbol.
    t = [0:Ts/Nos:Nsub*Ts];

    % OFDM modulation.
    y = 0;
    for k = 1:numSymbols,
        y= y + data(k)*exp(j*2*pi*Fsub(k)*t);
    end

    % Calculate PAPR.
```

```
    papr(n) = 10*log10(max(abs(y).^2)/mean(abs(y).^2));
end

% Plot CCDF.
[N,X] = hist(papr, 100);
semilogy(X,1-cumsum(N)/max(cumsum(N)),'b')

% Save data.
save paprOFDMA
```

Appendix A

Derivation of Time Domain Symbols of Localized FDMA and Distributed FDMA

In this appendix, we use the symbol notations described in Figure A.1: x_m $(m = 0, 1, \ldots, M-1)$ represents modulated source symbols and X_k $(k = 0, 1, \ldots, M-1)$ represents M samples of the DFT of x_m; Y_l $(l = 0, 1, \ldots, N-1)$ represents the frequency domain samples after subcarrier mapping and y_n $(n = 0, 1, \ldots, N-1)$ represents the transmitted time domain channel symbols that are obtained from the inverse DFT (IDFT) of Y_n.

A.1 Time Domain Symbols of LFDMA

For LFDMA, the frequency samples after subcarrier mapping $\{Y_l\}$ can be described as follows:

$$Y_l = \begin{cases} X_l, & 0 \le l \le M-1 \\ 0, & M \le l \le N-1 \end{cases} \tag{A.1}$$

Let $n = Q \cdot m + q$, where $0 \le m \le M-1$, $0 \le q \le Q-1$, and $N = Q \cdot M$. Then

$$y_n = y_{Qm+q} = \frac{1}{N} \sum_{l=0}^{N-1} Y_l e^{j2\pi \frac{n}{N} l} = \frac{1}{Q} \cdot \frac{1}{M} \sum_{l=0}^{M-1} X_l e^{j2\pi \frac{Qm+q}{QM} l} \tag{A.2}$$

If $q = 0$, then

Single Carrier FDMA: A New Air Interface for Long Term Evolution Hyung G. Myung and David J. Goodman
 ISBN: 978-0-470-72449-1

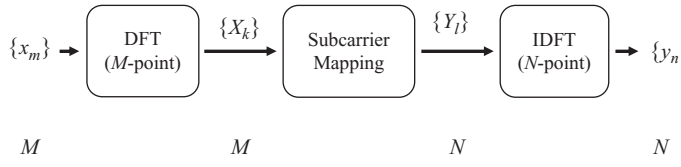

*M, N: number of data symbols

Figure A.1 Symbol notations for SC-FDMA modulations

$$\begin{aligned} y_n = y_{Qm} &= \frac{1}{Q} \cdot \frac{1}{M} \sum_{l=0}^{M-1} X_l e^{j2\pi \frac{Qm}{QM} l} \\ &= \frac{1}{Q} \cdot \frac{1}{M} \sum_{l=0}^{M-1} X_l e^{j2\pi \frac{m}{M} l} \\ &= \frac{1}{Q} x_m \\ &= \frac{1}{Q} x_{(n) \bmod M} \end{aligned} \tag{A.3}$$

If $q \neq 0$, since $X_l = \sum_{p=0}^{M-1} x_p e^{-j2\pi \frac{p}{M} l}$, then Equation (A.2) can be expressed as follows:

$$\begin{aligned} y_n &= y_{Q \cdot m+q} \\ &= \frac{1}{Q} \cdot \frac{1}{M} \sum_{l=0}^{M-1} X_l e^{j2\pi \frac{Q \cdot m+q}{Q \cdot M} l} \\ &= \frac{1}{Q} \cdot \frac{1}{M} \sum_{l=0}^{M-1} \left(\sum_{p=0}^{M-1} x_p e^{-j2\pi \frac{p}{M} l} \right) e^{j2\pi \frac{Q \cdot m+q}{Q \cdot M} l} \\ &= \frac{1}{Q} \cdot \frac{1}{M} \sum_{l=0}^{M-1} \sum_{p=0}^{M-1} x_p e^{j2\pi \left\{ \frac{(m-p)}{M} + \frac{q}{Q \cdot M} \right\} l} \\ &= \frac{1}{Q} \cdot \frac{1}{M} \sum_{p=0}^{M-1} x_p \left(\sum_{l=0}^{M-1} e^{j2\pi \left\{ \frac{(m-p)}{N} + \frac{q}{Q \cdot M} \right\} l} \right) \end{aligned}$$

$$
\begin{aligned}
&= \frac{1}{Q} \cdot \frac{1}{M} \sum_{p=0}^{M-1} x_p \frac{1 - e^{j2\pi(m-p)} e^{j2\pi \frac{q}{Q}}}{1 - e^{j2\pi \left\{ \frac{(m-p)}{M} + \frac{q}{Q \cdot M} \right\}}} \\
&= \frac{1}{Q} \cdot \frac{1}{M} \sum_{p=0}^{M-1} x_p \frac{1 - e^{j2\pi \frac{q}{Q}}}{1 - e^{j2\pi \left\{ \frac{(m-p)}{M} + \frac{q}{Q \cdot M} \right\}}} \\
&= \frac{1}{Q} \cdot \left(1 - e^{j2\pi \frac{q}{Q}} \right) \cdot \frac{1}{M} \sum_{p=0}^{M-1} \frac{x_p}{1 - e^{j2\pi \left\{ \frac{(m-p)}{M} + \frac{q}{Q \cdot M} \right\}}}
\end{aligned} \tag{A.4}
$$

Thus,

$$
\begin{aligned}
&\therefore y_n = y_{Q \cdot m + q} \\
&= \begin{cases} \dfrac{1}{Q} x_{(n) \bmod M}, & q = 0 \\ \dfrac{1}{Q} \cdot \left(1 - e^{j2\pi \frac{q}{Q}} \right) \cdot \dfrac{1}{M} \displaystyle\sum_{p=0}^{M-1} \dfrac{x_p}{1 - e^{j2\pi \left\{ \frac{(m-p)}{M} + \frac{q}{QM} \right\}}}, & q \neq 0 \end{cases}
\end{aligned} \tag{A.5}
$$

A.2 Time Domain Symbols of DFDMA

For DFDMA, the frequency samples after subcarrier mapping $\{Y_l\}$ can be described as follows:

$$
Y_l = \begin{cases} X_{l/\tilde{Q}}, l = \tilde{Q} \cdot k & (0 \leq k \leq M - 1) \\ 0, \quad \text{otherwise} \end{cases} \tag{A.6}
$$

where $0 \leq l \leq N - 1$, $N = Q \cdot M$, and $1 \leq \tilde{Q} < Q$. Let $n = Q \cdot m + q$ $(0 \leq m \leq M - 1, 0 \leq q \leq Q - 1)$.
Then

$$
\begin{aligned}
y_n &= y_{Q \cdot m + q} \\
&= \frac{1}{N} \cdot \sum_{l=0}^{N-1} Y_l e^{j2\pi \frac{n}{N} l} \\
&= \frac{1}{Q} \frac{1}{M} \cdot \sum_{k=0}^{M-1} X_k e^{j2\pi \frac{Qm+q}{QM} \tilde{Q} k}
\end{aligned} \tag{A.7}
$$

If $q = 0$, then

$$
y_n = y_{Q \cdot m}
$$

$$
\begin{aligned}
&= \frac{1}{Q}\frac{1}{M} \cdot \sum_{k=0}^{M-1} X_k e^{j2\pi \frac{Qm}{QM}\tilde{Q}k} \\
&= \frac{1}{Q}\frac{1}{M} \cdot \sum_{k=0}^{M-1} X_k e^{j2\pi \frac{m}{M}\tilde{Q}k} \\
&= \frac{1}{Q}\frac{1}{M} \cdot \sum_{k=0}^{M-1} X_k e^{j2\pi \frac{\tilde{Q}\cdot m}{M}k} \\
&= \frac{1}{Q}\left(\frac{1}{M} \cdot \sum_{k=0}^{M-1} X_k e^{j2\pi \frac{(\tilde{Q}\cdot m)_{\bmod M}}{M}k}\right) \\
&= \frac{1}{Q} \cdot x_{(\tilde{Q}\cdot m)_{\bmod M}} \\
&= \frac{1}{Q} \cdot x_{(\tilde{Q}(n)_{\bmod M})_{\bmod M}}
\end{aligned} \tag{A.8}
$$

If $q \neq 0$, since $X_k = \sum_{p=0}^{M-1} x_p e^{-j2\pi \frac{p}{M}k}$, then

$$
\begin{aligned}
y_n &= y_{Q\cdot m+q} \\
&= \frac{1}{Q}\frac{1}{M} \cdot \sum_{k=0}^{M-1} X_k e^{j2\pi \frac{Qm+q}{QM}\tilde{Q}k} \\
&= \frac{1}{Q}\frac{1}{M} \cdot \sum_{k=0}^{M-1} \left(\sum_{p=0}^{M-1} x_p e^{-j2\pi \frac{p}{M}k}\right) e^{j2\pi \frac{Qm+q}{QM}\tilde{Q}k} \\
&= \frac{1}{Q}\frac{1}{M} \cdot \sum_{k=0}^{M-1}\sum_{p=0}^{M-1} x_p e^{j2\pi\left\{\frac{(\tilde{Q}m-p)}{M}+\frac{\tilde{Q}q}{QM}\right\}k} \\
&= \frac{1}{Q}\frac{1}{M} \cdot \sum_{p=0}^{M-1} x_p \left(\sum_{k=0}^{M-1} e^{j2\pi\left\{\frac{(\tilde{Q}m-p)}{M}+\frac{\tilde{Q}q}{QM}\right\}k}\right) \\
&= \frac{1}{Q}\frac{1}{M} \cdot \sum_{p=0}^{M-1} x_p \frac{1-e^{j2\pi(\tilde{Q}m-p)}e^{j2\pi\frac{\tilde{Q}q}{Q}}}{1-e^{j2\pi\left\{\frac{(\tilde{Q}m-p)}{M}+\frac{\tilde{Q}q}{QM}\right\}}} \\
&= \frac{1}{Q}\frac{1}{M} \cdot \sum_{p=0}^{M-1} x_p \frac{1-e^{j2\pi\frac{\tilde{Q}q}{Q}}}{1-e^{j2\pi\left\{\frac{(\tilde{Q}m-p)}{M}+\frac{\tilde{Q}q}{QM}\right\}}}
\end{aligned}
$$

$$= \frac{1}{Q}\left(1 - e^{j2\pi\frac{\tilde{Q}}{Q}q}\right) \cdot \frac{1}{M}\sum_{p=0}^{M-1}\frac{x_p}{1 - e^{j2\pi\left\{\frac{(\tilde{Q}m-p)}{M} + \frac{\tilde{Q}q}{QM}\right\}}} \tag{A.9}$$

Thus,

$$\begin{aligned}
&\therefore y_n = y_{Q\cdot m+q} \\
&= \begin{cases} \dfrac{1}{Q} \cdot x_{\left(\tilde{Q}(n)_{\bmod M}\right)_{\bmod M}}, & q = 0 \\ \dfrac{1}{Q}\left(1 - e^{j2\pi\frac{\tilde{Q}}{Q}q}\right) \cdot \dfrac{1}{M}\displaystyle\sum_{p=0}^{M-1}\frac{x_p}{1 - e^{j2\pi\left\{\frac{(\tilde{Q}m-p)}{M} + \frac{\tilde{Q}q}{QM}\right\}}}, & q \neq 0 \end{cases}
\end{aligned} \tag{A.10}$$

Appendix B

Derivations of the Upper Bounds in Chapter 7

B.1 Derivation of Equations (7.9) and (7.10) in Chapter 7

We can expand $E\left\{Ze^{\nu Z}\right\}$ as follows:

$$\begin{aligned} E\left\{Ze^{\nu Z}\right\} &= E\left\{\sum_{k=-\infty}^{\infty} a_k \exp\left(\nu \sum_{l=-\infty}^{\infty} a_l\right)\right\} \\ &= \sum_{k=-\infty}^{\infty} E\left\{a_k \prod_{l=-\infty}^{\infty} e^{\nu a_l}\right\} \\ &= \sum_{k=-\infty}^{\infty} E\left\{a_k e^{\nu a_k} \prod_{\substack{l=-\infty \\ l\neq k}}^{\infty} e^{\nu a_l}\right\} \\ &= \sum_{k=-\infty}^{\infty} E\left\{a_k e^{\nu a_k}\right\} \prod_{\substack{l=-\infty \\ l\neq k}}^{\infty} E\left\{e^{\nu a_l}\right\} \end{aligned} \tag{B.1}$$

We can also expand $E\left\{e^{\nu Z}\right\}$ similarly as follows:

$$\begin{aligned} E\left\{e^{\nu Z}\right\} &= E\left\{\exp\left(\nu \sum_{l=-\infty}^{\infty} a_l\right)\right\} \\ &= E\left\{\prod_{l=-\infty}^{\infty} e^{\nu a_l}\right\} \end{aligned}$$

Single Carrier FDMA: A New Air Interface for Long Term Evolution Hyung G. Myung and David J. Goodman
© 2008 John Wiley & Sons, Ltd. ISBN: 978-0-470-72449-1

$$= \prod_{l=-\infty}^{\infty} E\left\{e^{\nu a_l}\right\} \tag{B.2}$$

By applying (B.1) and (B.2) to Equation (7.7) in Chapter 7 for $\nu = \hat{\nu}$, we get the following:

$$\sum_{k=-\infty}^{\infty} E\left\{a_k e^{\hat{\nu} a_k}\right\} \prod_{\substack{l=-\infty \\ l\neq k}}^{\infty} E\left\{e^{\hat{\nu} a_l}\right\} - \delta \cdot \prod_{l=-\infty}^{\infty} E\left\{e^{\hat{\nu} a_l}\right\} = 0$$

$$\sum_{k=-\infty}^{\infty} E\left\{a_k e^{\hat{\nu} a_k}\right\} \prod_{\substack{l=-\infty \\ l\neq k}}^{\infty} E\left\{e^{\hat{\nu} a_l}\right\} = \delta \cdot \prod_{l=-\infty}^{\infty} E\left\{e^{\hat{\nu} a_l}\right\} \tag{B.3}$$

By dividing each side with $\prod_{l=-\infty}^{\infty} E\left\{e^{\hat{\nu} a_l}\right\}$, we obtain

$$\sum_{k=-\infty}^{\infty} \frac{E\left\{a_k e^{\hat{\nu} a_k}\right\}}{E\left\{e^{\hat{\nu} a_k}\right\}} = \delta \tag{B.4}$$

Using (B.2), Equation (7.6) in Chapter 7 becomes

$$\Pr\{Z \geq \delta\} \leq e^{-\hat{\nu}\delta} \prod_{k=-\infty}^{\infty} E\left\{e^{\hat{\nu} a_k}\right\} \tag{B.5}$$

B.2 Derivations of Equations (7.13) and (7.14) in Chapter 7

From Equation (7.11) in Chapter 7,

$$\begin{aligned} &s_k \in C_{BPSK} \\ &a_k \in \{-p(t_0 - kT),\, p(t_0 - kT)\} \end{aligned} \tag{B.6}$$

Also,

$$\begin{aligned} P\{s_k = -1\} = P\{s_k = 1\} &= \frac{1}{2} \\ P\{a_k = -p(t_0 - kT)\} = P\{a_k = p(t_0 - kT)\} &= \frac{1}{2} \end{aligned} \tag{B.7}$$

Using (B.6) and (B.7), Equation (7.8) in Chapter 7 becomes

$$\sum_{k=-K_{\max}}^{K_{\max}} \frac{\frac{1}{2}p(t_0-kT)e^{\hat{\nu}p(t_0-kT)} - \frac{1}{2}p(t_0-kT)e^{-\hat{\nu}p(t_0-kT)}}{\frac{1}{2}e^{\hat{\nu}p(t_0-kT)} + \frac{1}{2}e^{-\hat{\nu}p(t_0-kT)}} = \delta \quad \text{(B.8)}$$

After we determine $\hat{\nu}$ from (B.8), the upper bound in Equation (7.10) from Chapter 7 becomes

$$\begin{aligned} P_{ub,SC}^{(BPSK)} &\triangleq 2e^{-\hat{\nu}\delta} \prod_{k=-K_{\max}}^{K_{\max}} E\left\{e^{\hat{\nu}a_k}\right\} \\ &= 2e^{-\hat{\nu}\delta} \prod_{k=-K_{\max}}^{K_{\max}} \left(\frac{1}{2}e^{\hat{\nu}p(t_0-kT)} + \frac{1}{2}e^{-\hat{\nu}p(t_0-kT)}\right) \\ &= 2e^{-\hat{\nu}\delta}\left(\frac{1}{2}\right)^{2K_{\max}+1} \prod_{k=-K_{\max}}^{K_{\max}} \left(e^{\hat{\nu}p(t_0-kT)} + e^{-\hat{\nu}p(t_0-kT)}\right) \\ &= e^{-\hat{\nu}\delta}\left(\frac{1}{2}\right)^{2K_{\max}} \prod_{k=-K_{\max}}^{K_{\max}} \left(e^{\hat{\nu}p(t_0-kT)} + e^{-\hat{\nu}p(t_0-kT)}\right) \end{aligned} \quad \text{(B.9)}$$

and we upper-bound the CCDF as

$$\Pr\left[\left|x^{(BPSK)}(t_0, S)\right|^2 \geq w\right] \leq P_{ub,SC}^{(BPSK)} \quad \text{(B.10)}$$

Appendix C

Deciphering the 3GPP LTE Specifications

Unless you are really familiar with the LTE standardization process, it is rather difficult to understand how things actually work just by reading through the specifications. Since a technical specification is merely a description of a guideline for interoperability, it does not necessarily explain any rationale or background information for choice of the specific methodologies or parameters.

One way to find a more detailed description of the specific methodology or parameter in the specification is to go through the contribution papers (called technical documents, or tdocs) that 3GPP uploads on their meeting website. 3GPP has different work groups working on different aspects of the radio interface and network architecture. The Technical Specification Group Radio Access Networks (TSG RAN) is where all the radio air interface specifications are handled and it has five working groups (WG) as described in Table C.1.

Table C.2 highlights the LTE specifications and their corresponding working groups.

Most of the physical layer and MAC layer components are discussed in RAN1 meetings and the meeting information is at http://www.3gpp.org/ftp/Specs/html-info/Meetings-R1.htm. Figure C.1 is a screenshot of the website.

If you go to this site, there is a column called "First & Last tdoc" (tdoc = technical document) as shown in Figure C.1. This is the paper number that identifies each contribution paper. If you click on the link, it directs you to the ftp site where you can access all the tdocs of the particular meeting.

Single Carrier FDMA: A New Air Interface for Long Term Evolution Hyung G. Myung and David J. Goodman
 ISBN: 978-0-470-72449-1

Table C.1 TSG RAN work groups

RAN WG1 (RAN1)	Layer 1 (Physical layer) specification
RAN WG2 (RAN2)	Layer 2 (MAC, RLC) and layer 3 specification
RAN WG3 (RAN3)	Overall UTRAN architecture.
RAN WG4 (RAN4)	Radio performance and protocol aspects
RAN WG5 (RAN5)	Mobile terminal conformance testing

Since the tdocs are uploaded in zip files without any title (only the tdoc numbers are specified in the file name), you would have to look at the excel spreadsheet of the tdoc list (provided at the bottom of the list) to know which is which. Tdoc numbers are in the form of R*x*-*yyzzzz* where *x* is the RAN work group number, *yy* is the year of the meeting, and *zzzz* is the cumulative number assigned to the document. For example, R1-081165 refers to the document 1165 of RAN1 meeting in the year 2008.

It may be daunting to go through each tdoc list spreadsheet for each meeting because the list is usually very long list ($300 \sim 400$) and not organized by subject. What you can do is first read the meeting summary report that summarizes the discussions and decisions from the meeting by subject. You can find the meeting report by following "Files" link and then "Report" link. From the meeting report, you can find out about the decisions made and the relevant tdocs. Once you know the tdoc number, you can locate the link from the "First & last tdoc" column and access it from there.

Table C.2 LTE specifications and their corresponding working groups

Document number	Working group
36.1xx	RAN4
36.2xx	RAN1
36.3xx	RAN2
36.4xx	RAN3
36.5xx	RAN5
36.8xx	RAN4
36.902	RAN3
36.913	RAN
36.938	RAN4
36.942	RAN4
36.956	RAN4

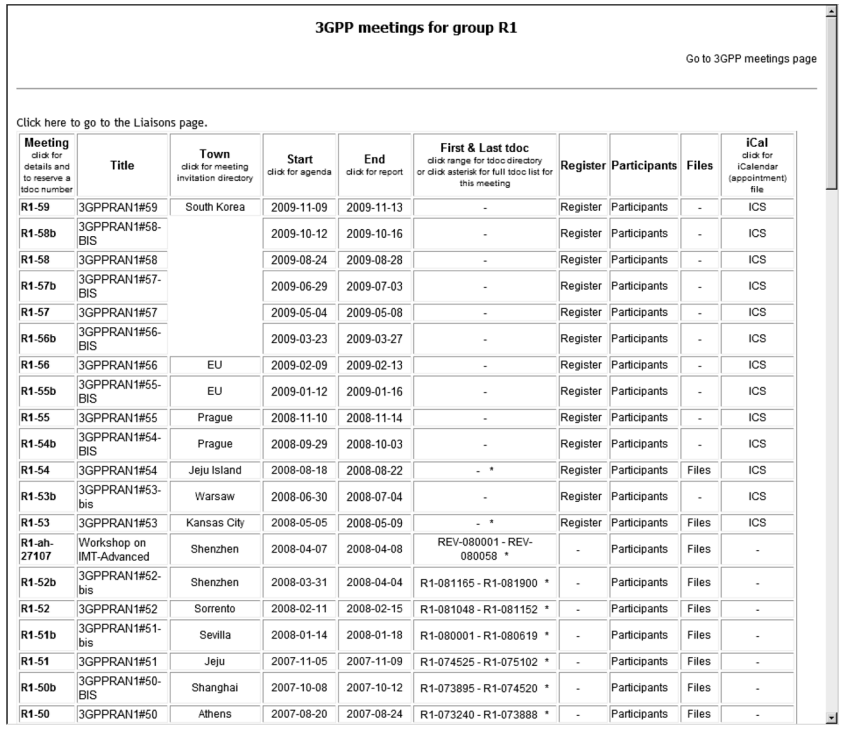

3GPP meetings for group R1

Go to 3GPP meetings page

Click here to go to the Liaisons page.

Meeting click for details and to reserve a tdoc number	Title	Town click for meeting invitation directory	Start click for agenda	End click for report	First & Last tdoc click range for tdoc directory or click asterisk for full tdoc list for this meeting	Register	Participants	Files	iCal click for iCalendar (appointment) file
R1-59	3GPPRAN1#59	South Korea	2009-11-09	2009-11-13	-	Register	Participants	-	ICS
R1-58b	3GPPRAN1#58-BIS		2009-10-12	2009-10-16	-	Register	Participants	-	ICS
R1-58	3GPPRAN1#58		2009-08-24	2009-08-28	-	Register	Participants	-	ICS
R1-57b	3GPPRAN1#57-BIS		2009-06-29	2009-07-03	-	Register	Participants	-	ICS
R1-57	3GPPRAN1#57		2009-05-04	2009-05-08	-	Register	Participants	-	ICS
R1-56b	3GPPRAN1#56-BIS		2009-03-23	2009-03-27	-	Register	Participants	-	ICS
R1-56	3GPPRAN1#56	EU	2009-02-09	2009-02-13	-	Register	Participants	-	ICS
R1-55b	3GPPRAN1#55-BIS	EU	2009-01-12	2009-01-16	-	Register	Participants	-	ICS
R1-55	3GPPRAN1#55	Prague	2008-11-10	2008-11-14	-	Register	Participants	-	ICS
R1-54b	3GPPRAN1#54-BIS	Prague	2008-09-29	2008-10-03	-	Register	Participants	-	ICS
R1-54	3GPPRAN1#54	Jeju Island	2008-08-18	2008-08-22	- *	Register	Participants	Files	ICS
R1-53b	3GPPRAN1#53-bis	Warsaw	2008-06-30	2008-07-04	-	Register	Participants	-	ICS
R1-53	3GPPRAN1#53	Kansas City	2008-05-05	2008-05-09	- *	Register	Participants	Files	ICS
R1-ah-27107	Workshop on IMT-Advanced	Shenzhen	2008-04-07	2008-04-08	REV-080001 - REV-080058 *	-	Participants	Files	-
R1-52b	3GPPRAN1#52-bis	Shenzhen	2008-03-31	2008-04-04	R1-081165 - R1-081900 *	-	Participants	Files	-
R1-52	3GPPRAN1#52	Sorrento	2008-02-11	2008-02-15	R1-081048 - R1-081152 *	-	Participants	Files	-
R1-51b	3GPPRAN1#51-bis	Sevilla	2008-01-14	2008-01-18	R1-080001 - R1-080619 *	-	Participants	Files	-
R1-51	3GPPRAN1#51	Jeju	2007-11-05	2007-11-09	R1-074525 - R1-075102 *	-	Participants	Files	-
R1-50b	3GPPRAN1#50-BIS	Shanghai	2007-10-08	2007-10-12	R1-073895 - R1-074520 *	-	Participants	Files	-
R1-50	3GPPRAN1#50	Athens	2007-08-20	2007-08-24	R1-073240 - R1-073888 *	-	Participants	Files	-

Figure C.1 Screenshot of the 3GPP RAN1 meeting information website at http://www.3gpp.org/ftp/Specs/html-info/Meetings-R1.htm

For example, the channel coding scheme specified in TS 36.212 uses quadratic permutation polynomial (QPP) interleaver. Let's say we want to find more details of the QPP interleaver. By searching through the meeting reports, we can find that there was a decision to adopt the QPP interleaver in RAN1 meeting #47b. The document that proposes this method is R1-070483 and other related documents are listed as well in the meeting report. By looking at the listed documents, we can understand more about the QPP interleaver that is new in LTE channel coding.

Appendix D

Abbreviations

3GPP	3rd Generation Partnership Project
ADC	Analog-to-Digital Conversion
AES	Advanced Encryption Standard
AMC	Adaptive Modulation and Coding
ARQ	Automatic Repeat reQuest
AWGN	Additive White Gaussian Noise
BCCH	Broadcast Control Channel
BCH	Broadcast Channel
BER	Bit Error Rate
BLAST	Bell Labs Layered Space-Time
BPSK	Binary Phase Shift Keying
b/s	Bits per second
BSS	Base Station System
BTS	Base Transceiver System
BWA	Broadband Wireless Access
CAZAC	Constant Amplitude Zero Auto-Correlation
CCCH	Common Control Channel
CCD	Cyclic Delay Diversity
CCDF	Complementary Cumulative Distribution Function
CCM	Counter with Ciphering block chaining Message
CDM	Code Division Multiplexing
CDMA	Code Division Multiple Access
CDS	Channel Dependent Scheduling
CN	Core Network
CP	Cyclic Prefix
CQI	Channel Quality Indicator

Single Carrier FDMA: A New Air Interface for Long Term Evolution Hyung G. Myung and David J. Goodman
 ISBN: 978-0-470-72449-1

CSI	Channel State Information
DAC	Digital-to-Analog Conversion
DCCH	Dedicated Control Channel
DFDMA	Distributed Frequency Division Multiple Access
DFT	Discrete Fourier Transform
DL-SCH	Downlink Shared Channel
DSP	Digital Signal Processor
DTCH	Dedicated Traffic Channel
DwPTS	Downlink Pilot Time Slot
EAP	Extensible Authentication Protocol
E-MBMS	Enhanced Multimedia Broadcast/Multicast Service
E-UTRA	Evolved Universal Terrestrial Radio Access
E-UTRAN	Evolved Universal Terrestrial Radio Access Network
FDD	Frequency Division Duplex
FDE	Frequency Domain Equalization
FDM	Frequency Division Multiplexing
FDMA	Frequency Division Multiple Access
FER	Frame Error Rate
FFT	Fast Fourier Transform
GP	Guard Period
GSM	Global System for Mobile
HARQ	Hybrid Automatic Repeat reQuest
HSDPA	High Speed Downlink Packet Access
HSUPA	High Speed Uplink Packet Access
IBI	Inter-Block Interference
ICI	Inter-Carrier Interference
IDFT	Inverse Discrete Fourier Transform
IEEE	Institute of Electrical and Electronic Engineers
IFDMA	Interleaved Frequency Division Multiple Access
IFFT	Inverse Fast Fourier Transform
IMS	IP Multimedia Subsystem
IMT-2000	International Mobile Telecommunications-2000
IP	Internet Protocol
ISI	Inter-Symbol Interference
ITU	International Telecommunication Union
LFDMA	Localized Frequency Division Multiple Access
LMMSE	Linear Minimum Mean Square Error
LTE	Long Term Evolution
MAC	Medium Access Control
MBMS	Multimedia Broadcast/Multicast Service
MBS	Multicast and Broadcast Service

MCCH	Multicast Control Channel
MCH	Multicast Channel
MIMO	Multiple Input Multiple Output
MMSE	Minimum Mean Square Error
MS	Mobile Station
MTCH	Multicast Traffic Channel
OFDM	Orthogonal Frequency Division Multiplexing
OFDMA	Orthogonal Frequency Division Multiple Access
PAPR	Peak-to-Average-Power Ratio
PBCH	Physical Broadcast Channel
PCCH	Paging Control Channel
PCFICH	Physical Control Format Indicator Channel
PCH	Paging Channel
PDCCH	Physical Downlink Control Channel
PDSCH	Physical Downlink Shared Channel
PHICH	Physical Hybrid ARQ Channel
PHY	Physical
PLMN	Public Land Mobile Network
PMCH	Physical Multicast Channel
PRACH	Physical Random Access Channel
PS	Pulse Shaping
PSD	Power Spectral Density
PSR	Packet Success Rate
PUCCH	Physical Uplink Control Channel
PUSCH	Physical Uplink Shared Channel
QAM	Quadrature Amplitude Modulation
QoS	Quality of Service
QPSK	Quaternary Phase Shift Keying
RACH	Random Access Channel
RAN	Radio Access Network
RB	Resource Block
RF	Radio Frequency
RLC	Radio Link Control
RNC	Radio Network Controller
RNS	Radio Network System
RRC	Radio Resource Control
RS	Reference Signal
SC	Single Carrier
SC/FDE	Single Carrier with Frequency Domain Equalization
SC-CFDMA	Single Carrier Code-Frequency Division Multiple Access
SC-FDMA	Single Carrier Frequency Division Multiple Access

SDMA	Spatial Division Multiple Access
SER	Symbol Error Rate
SFBC	Space-Frequency Block Coding
SIM	Subscriber Identity Module
SM	Spatial Multiplexing
SNR	Signal-to-Noise Ratio
STBC	Space-Time Block Coding
SVD	Singular Value Decomposition
TDD	Time Division Duplex
TDM	Time Division Multiplexing
TDMA	Time Division Multiple Access
TR	Technical Report
TS	Technical Specification
TSG	Technical Specification Group
TTI	Transmission Time Interval
TU6	Typical Urban 6-path
TxBF	Transmit Eigen-Beamforming
UE	User Equipment
UL-SCH	Uplink Shared Channel
UMB	Ultra Mobile Broadband
UMTS	Universal Mobile Telecommunications System
UpPTS	Uplink Pilot Time Slot
USIM	UMTS Subscriber Identity Module
UTRA	Universal Terrestrial Radio Access
UTRAN	Universal Terrestrial Radio Access Network
VoIP	Voice over Internet Protocol
WCDMA	Wideband Code Division Multiple Access
WG	Workgroup
WiMAX	Worldwide Interoperability for Microwave Access
WLAN	Wireless Local Area Network
WMAN	Wireless Metropolitan Area Network
WSSUS	Wide-Sense Stationary Uncorrelated Scattering

Index

Single Carrier FDMA: A New Air Interface for Long Term Evolution Hyung G. Myung and David J. Goodman
 ISBN: 978-0-470-72449-1